Bed height and material density effects on fluidized bed hydrodynamics

by

David Escudero Guevara

A thesis submitted to the graduate faculty
in partial fulfillment of the requirements for the degree of
MASTER OF SCIENCE

Major: Biorenewable Resources and Technology

Program of Study Committee:
Theodore J. Heindel, Major Professor
Michael Olsen
D. Raj Raman

Iowa State University
Ames, Iowa
2010

Copyright © David Escudero Guevara, 2010. All rights reserved.

Table of Contents

Table of Contents……ii

List of Figures…….....v

List of Tables……viii

Acknowledgments……...ix

Abstract……x

Chapter 1: Introduction……..1

1.1 Motivation……...1

1.2 Objectives……2

Chapter 2: Literature Review……4

2.1 Fluidization……..4

2.1.1 Fluidized Beds……..4

2.1.2 Fluidization Regimes……7

2.1.3 Gas Holdup……...9

2.1.4 Minimum Fluidization Velocity……...9

2.1.5 Bed height effects in the minimum fluidization velocity……...11

2.1.6 Biomass Fluidization……..15

2.1.6.1 Material properties effects on fluidization……...18

2.1.6.2 Methods to improve biomass fluidization……20

2.1.6.2.1 Binary Mixtures……20

2.1.6.2.2 Acoustic Fluidized Beds……...23

2.2 Fluidized Bed Hydrodynamics: Measurement Techniques……...26

2.2.1 Invasive Techniques……...26

2.2.2 Noninvasive Techniques……28

2.2.3 Noninvasive X-ray techniques..……30

2.2.3.1 X-Ray Radiography..…….....30

2.2.3.2 X- Ray Stereography…….31

2.2.3.3 X-Ray Computed Tomography…….33

2.3 Summary…….36

Chapter 3: Experimental Setup…….....38

3.1 Equipment……38

3.1.1 Fluidized Bed Reactor……..38

3.1.2 Air Flow and Pressure Measurement……39

3.2 Bed Material……41

3.2.1 Material Selection and Preparation……...42

3.3 Identifying the Minimum Fluidization Velocity…….....44

3.4 X-ray Facility……46

3.4.1 X-ray Equipment……46

3.4.2 X-ray Computed Tomography……48

3.4.2.1 Experimental Procedures……48

3.4.2.2 Calibrations……..50

3.4.2.2.1 Pixel Normalization……..51

3.4.2.2.2 Beam Hardening……51

3.4.2.2.3 Volume Files Correction……...52

3.4.3 Determining Gas Holdup from CT Data……52

3.5 Summary……54

Chapter 4: Results and Discussion……...55

4.1 Minimum Fluidization Velocity……55

4.2 Gas Holdup……62

4.2.1 Height to Diameter ratio effects on Local Gas Holdup……..63

4.2.2 Bed Material Density effects on Local Gas Holdup……...92

4.3 Summary……98

Chapter 5: Conclusions and Recommendations…….....99

5.1 Conclusions……99

5.2 Recommendations……...102

References……103

List of Figures

Figure 2.1: Fluidized bed schematic…….5

Figure 2.2: Fluidization regimes in a gas-solid fluidized bed……..8

Figure 2.3: Minimum spouting fluidization velocity as a function of bed height using mung beans……...13

Figure 2.4: Minimum fluidization velocity as a function of bed heights of glass beads……...14

Figure 2.5: Minimum fluidization velocity for cotton stalk and corn stalk as a function of biomass length-to-diameter ratio……...19

Figure 2.6: Effect of the fluidization media diameter on U_{mf} of the mixture……...22

Figure 2.7: Effect of the fluidization media density on U_{mf} of the mixture……...22

Figure 2.8: Effect of sound frequency on U_{mf} of a quartz sand-biomass mixture…….24

Figure 2.9: Minimum fluidization velocity at different sound pressure levels: quartz sand and a) sawdust or b) wheat stalk……...25

Figure 2.10: Invasive techniques classification……27

Figure 2.11: X-ray radiography schematic……...31

Figure 2.12: X-ray stereography schematic……..32

Figure 2.13: X-ray computed tomography schematic……..34

Figure 3.1: Fluidized bed reactor schematic (not to scale)……39

Figure 3.2: Schematic of the air flow system……40

Figure 3.3: Material selection based on Geldart's classification……43

Figure 3.4: Sample minimum fluidization plot for glass beads with H/D = 1……....46

Figure 3.5: CT imaging planes……...50

Figure 4.1: Bed pressure drop as a function of gas velocity for glass beads……..56

Figure 4.2: Minimum fluidization velocity as a function of height-to-diameter ratio (H/D)…….57

Figure 4.3: Bed pressure force/bed weight as a function of superficial gas velocity for glass beads……58

Figure 4.4: Bed pressure force/bed weight as a function of superficial gas velocity for ground corncob……59

Figure 4.5: Bed pressure force/bed weight as a function of superficial gas velocity for ground walnut shell……..60

Figure 4.6: Bed pressure drop as a function of gas velocity for glass beads, ground corncob and ground walnut shell for H/D =1……...61

Figure 4.7: Effect of material density on fluidization force balance for H/D = 1..……62

Figure 4.8: Glass beads gas holdup y- and z- slices for $U_g = 1.25U_{mf}$ at different H/ D ratios……65

Figure 4.9: Glass beads gas holdup y- and z- slices for $U_g = 1.5U_{mf}$ at different H/ D ratios……66

Figure 4.10: Glass beads gas holdup y- and z- slices for $U_g = 1.75U_{mf}$ at different H/ D ratios……67

Figure 4.11: Glass beads gas holdup y- and z- slices for $U_g = 2U_{mf}$ at different H/ D ratios……68

Figure 4.12: Glass beads gas holdup y- and z- slices for $U_g = 3U_{mf}$ at different H/ D ratios……69

Figure 4.13: Ground corncob holdup y- and z- slices for $U_g = 1.25U_{mf}$ at different H/ D ratios……72

Figure 4.14: Ground corncob holdup y- and z- slices for $U_g = 3U_{mf}$ at different H/ D ratios……73

Figure 4.15: Ground walnut shell holdup y- and z- slices for $U_g = 1.25U_{mf}$ at different H/ D ratios……75

Figure 4.16: Ground walnut shell holdup y- and z- slices for $U_g = 3U_{mf}$ at different H/ D ratios……76

Figure 4.17: Effect of superficial gas velocity on horizontal-average and time-average gas holdup for different U_g values at H/D = 1...……78

Figure 4.18: Effect of superficial gas velocity on horizontal-average and time-average gas holdup for different U_g values at H/D = 1.5...……79

Figure 4.19: Gas holdup as a function of height for glass beads for different H/D ratios at $U_g = 1.25U_{mf}$ 80

Figure 4.20: Gas holdup as a function of height for glass beads for different H/D ratios and $U_g = 3U_{mf}$……..81

Figure 4.21: Gas holdup as a function of height for ground corncob for different H/D ratios at $U_g = 1.25U_{mf}$……82

Figure 4.22: Gas holdup as a function of height for ground walnut shell for different H/D ratios at $U_g = 1.25U_{mf}$……83

Figure 4.23: Gas holdup as a function of height for ground walnut shell for different H/D ratios at $U_g = 3U_{mf}$……84

Figure 4.24: Y-slice local gas holdup as a function of location at h = 0.25D for glass beads……85

Figure 4.25: X- slice local gas holdup as a function of location at h = 0.25D for glass beads……86

Figure 4.26: Y-slice local gas holdup as a function of location at h = 0.5D for glass beads……..87

Figure 4.27: X-slice local gas holdup as a function of location at h = 0.5D for glass beads……..88

Figure 4.28: Y-slice local gas holdup as a function of location at h = 0.5D for ground corncob……...89

Figure 4.29: Y-slice local gas holdup as a function of location at h = 0.75D for ground corncob……...90

Figure 4.30: Y-slice local gas holdup as a function of location at h = 0.5D for ground walnut shell……91

Figure 4.31: Y-slice local gas holdup as a function of location at h = 0.75D for ground walnut shell……92

Figure 4.32: Gas holdup y-slice for all materials at $U_g = 1.25U_{mf}$ for different H/D ratio……93

Figure 4.33: Gas holdup y-slice for all materials at $U_g = 3U_{mf}$ for different H/D ratio……94

Figure 4.34: Gas holdup as a function of height for all materials at H/D = 1 and $U_g = 1.5U_{mf}$…...……...……...97

List of Tables

Table 2.1: Experimental conditions and results of Sau et al. (2007)……12

Table 2.2: Material properties used by Zhong et al. (2006)……..13

Table 2.3: Different thermochemical processes and products……..16

Table 2.4: Materials used by Abdullah et al. (2003)…….20

Table 3.1: Summary of bed characteristics……...44

Table 4.1: Minimum fluidization velocity results…….57

Table 4.2: Experimental conditions……..63

Acknowledgements

I would especially like to thank my family for being always there with me, for their constant support, advice and more than anything for all the love they have given me in these years. Also, for teaching me that anything is possible in life if you work hard to accomplish your goals, and for reminding me that it is important to take advantage of the opportunities presented to us in life.

I would like to thank my major professor Dr. Ted Heindel for all the support, guidance and advice. Also, for giving me the opportunity to be part of his research group and immersing me into the multiphase flow area.

I also want to thank the Fulbright Commission for the funding and for the opportunity they gave me to come to Iowa State University and complete this Master's degree.

Special thanks to Dr. Raj Raman and Dr. Michael Olsen for being part of my committee and reviewing this thesis.

Thanks to my workmates at the laboratory for their help and assistance in many instances of this research.

The X-ray facility used in this research was funded by the National Science Foundation under award number CTS-0216367.

Abstract

Fluidized bed reactors are important assets of many industrial applications. Understanding how a fluidized bed as a multiphase flow system operates will improve its capabilities and operations. Minimum fluidization velocity and local gas holdup are important parameters used to characterize the hydrodynamic behavior of a material inside the fluidized bed. Due to the opaque nature of a fluidized bed system, noninvasive X-ray techniques are often used to visualize and obtain valuable data regarding the internal flow structures of the fluidized material.

This research determines how fluidized bed hydrodynamics are influenced by different experimental conditions. X-ray computed tomography imaging is applied to fluidized beds of glass beads, ground corncob, and ground walnut shell to obtain qualitative and quantitative data for the respective analysis. Minimum fluidization velocity is determined for the three materials at different bed height and flow conditions. Computed tomography data are used to measure the local time-average gas holdup for each material. Finally, the effects in the fluidization behavior and flow hydrodynamics caused by changes in bed height, bed material, and superficial gas velocity are explained.

Results show different bed heights do not produce any significant change on the minimum fluidization velocity and these results corroborate data presented in the literature. Conversely, the density difference between the three materials influenced the minimum fluidization velocity. A denser material required a higher superficial gas velocity to start fluidization. Therefore, the minimum fluidization velocity increased when the density of the material increased; also corroborate data presented in the literature.

It was also found that as superficial gas velocity increased, the overall gas holdup increased for every bed height studied. Flow behavior was also affected with the increase in superficial gas velocity. Increasing bed height, particularly at the higher gas flow rates, enhanced bubble coalescence creating slugs that flow thorough the center of the bed, producing regions of low gas holdup near the walls of the fluidized bed. Also, the effects of bed height observed in the time-average local gas holdup vary depending of the bed material tested

Finally, as material density decreases, gas holdup increases. Glass beads have lower gas holdup than both ground walnut shell and ground corncob, while ground corncob exhibit the largest gas holdup of all three materials in this study. Ground corncob exhibits a better distribution of gas holdup along the entire bed, therefore providing more uniform fluidization.

Chapter 1: Introduction

1.1 Motivation

Fluidization is the phenomenon of imparting the properties of a fluid to a bed of particulate solids by passing a fluid (liquid or gas) through the material. Fluidized beds are reactors in which fluidization of particulate solids takes place. Fluidized beds are an important asset in many industrial processes because they present several advantages that include a high rate of heat and mass transfer, low pressure drops, and uniform temperature distribution.

Fluidized bed hydrodynamic behavior is very complex and must be understood to improve fluidized bed operations. Several parameters are used to understand the behavior of a material the moment it is fluidized. Therefore, studying several materials of different characteristics will help to establish common and different behaviors. Glass beads, for example, provide a uniform fluidizing bed. Fluidizing biomass particles, on the other hand, is challenging due to their irregular size, shape, and density. Most of the studies available in the literature focus on the effects of different materials to the flow structure in a fluidized bed, but do not address the effects that bed height has on the same flow structure. Understanding the influence of these particular characteristics on the fluidized bed hydrodynamics is important.

One of the most important parameters to characterize fluidized bed conditions is the minimum fluidization velocity (U_{mf}), which quantifies the drag force needed to attain solid suspension in the gas phase. The minimum fluidization velocity also constitutes a reference for evaluating fluidization intensity when the bed is operated at higher gas velocities (Zhong et al., 2008). In general, U_{mf} is a function of particle properties/geometry, fluid properties, and bed geometry. Gas holdup is another very

important parameter that characterizes the fluidization quality, mixing, and process efficiency in a fluidization system, and is defined as the volume fraction of gas present within the bed.

Noninvasive measurement techniques are valuable because they provide insight into the flow behavior and general hydrodynamic characteristics of multiphase flow and opaque systems (Yates et al., 2002). Noninvasive X-ray techniques such, as X-ray computed tomography (CT), generate a 3D image of the object of interest. X-rays pass through the object and the intensity values are recorded at several projections by an imaging device. X-ray computed tomography provided a high spatial resolution, this characteristic can be used to measure the time-average local gas holdup in a very efficient way and can be used to quantify the flow hydrodynamics.

1.2 Objectives

The goal of this study is to improve the understanding of fluidized bed hydrodynamics by determining the effects of bed height and material density on the time-average gas holdup in a cylindrical fluidized bed using X-ray CT imaging. To accomplish this goal, this research will complete the following objectives.

1. Review the literature regarding fluidization, bed height, and material density effects on fluidized beds hydrodynamics, and noninvasive X-ray techniques for visualization of multiphase flow systems.
2. Determine the effects of bed height on the minimum fluidization velocity.
3. Compare the effects of material density on the minimum fluidization velocity.
4. Acquire X-ray CT images and determine time-average local gas holdup information for the fluidized bed.
5. Evaluate the effects of bed height on the time-average local gas holdup.

6. Determine the material density effects on the time-average local gas holdup.

The following work presents the research performed to accomplish these objectives. Chapter 2 reviews selected literature on fluidized beds and techniques to characterize fluidized beds hydrodynamics. Chapter 3 describes the experimental procedures, equipment, and methods used to collect data for the analysis of the fluidized bed hydrodynamic behavior. Chapter 4 presents the results of the analysis for minimum fluidization velocity and time-average local gas holdup. Chapter 5 provides the conclusions of this study and recommendations for future work. Finally, the references used in this study are listed.

Chapter 2: Literature Review

This chapter provides a review of two topics necessary to understand the concepts applied in this research. Section 2.1 will overview fluidization concepts like fluidization regimes, fluidized beds, minimum fluidization velocity, bed height effects in fluidization, fluidization of certain types of material, and methods to improve fluidization. Section 2.2 will provide an explanation of the techniques used to characterize fluidized bed hydrodynamics. First, it will address a description of invasive and noninvasive techniques, followed by a deeper description of noninvasive X-ray techniques, such as X-ray radiography, X-ray stereography, and X-ray computed tomography. Finally, section 2.3 will provide a brief summary of this review.

2.1 Fluidization

This section overviews important principles and characteristics related to fluidization and is divided into six subsections. The first describes important features, as well as different types of fluidized beds. The next subsection provides a description of the different fluidization regimes. The third subsection briefly explains gas holdup, followed by a discussion on minimum fluidization velocity in subsection four. Subsection five overviews the bed height effects in the minimum fluidization velocity. Finally, subsection six describes unique characteristics of biomass fluidization.

2.1.1 Fluidized Beds

Fluidized beds are reactors in which fluidization of particulate solids takes place. There are several types and geometries of fluidized beds but most of them have some key components: a plenum, a distributor, a bed region, and a freeboard region. The plenum is where the fluid enters the bed. Fluid next passes through a distributor or aeration plate, which uniformly distributes the fluid at the base of the bed. The particulate solid is

located above the distributor in the bed region. Finally, located above the bed chamber is the freeboard region, which contains particles that have been ejected from the bed. Figure 2.1 shows a schematic of a typical fluidized bed.

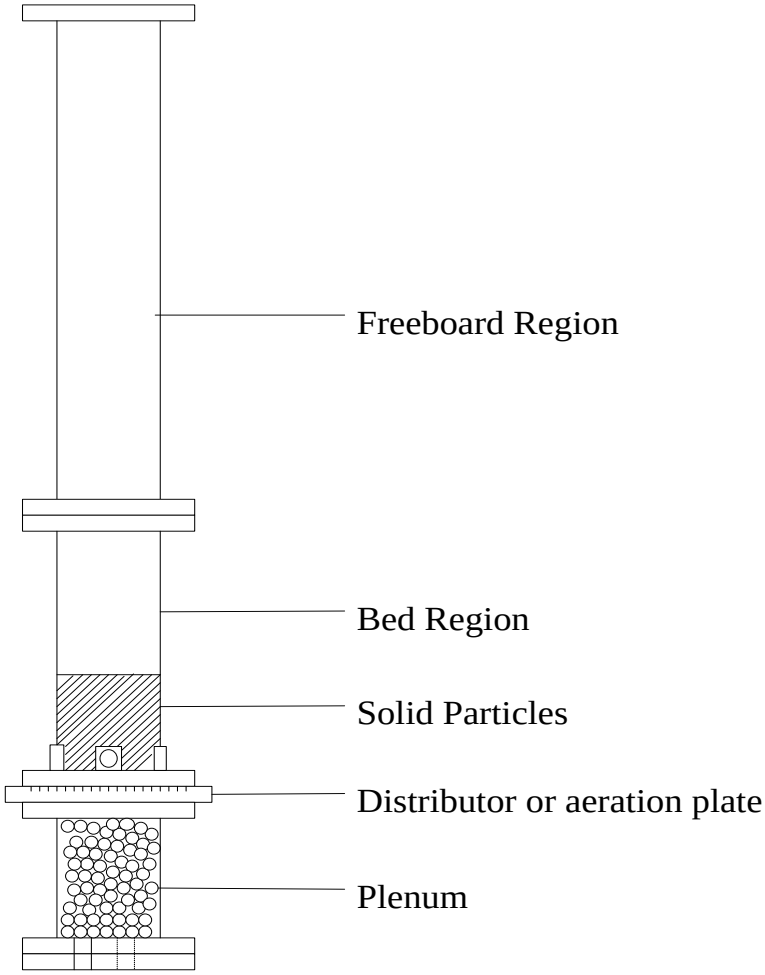

Figure 2.1: Fluidized bed schematic

Fluidized beds as chemical reactors present several advantages that include a high rate of heat and mass transfer, low pressure drops, and uniform temperature distribution. As stated before, there are several types of fluidized beds; the most common types are the Stationary Fluidized Beds (SFB) or Fixed Fluidized Beds (FFB) and Circulating Fluidized Beds (CFB). SFB or FFB refers to fluidized beds where the particles stay inside the fluidized bed. Whereas, CFB refer to fluidized beds where, due to the high velocity of

the fluid, most of the particles are entrained in the fluid flow and transported out of the bed to be recirculated back into the bed. Moreover, there are special types of fluidized beds like the spouted bed. In a spouted bed, gas (or liquid) is injected from the bottom through a central nozzle into the bottom of a normally cylindrical vessel to form a high velocity up-flow stream of gas (or liquid). The up-flowing gas carries particles in the central region (the spout) that are returned to the central bed region by a slow downward moving layer of particles between the central spout and the wall (the annulus) (Crowe, 2006).

Fluidized beds have several industrial applications depending on the type of reaction that takes place in the reactor. For a gas-solid system, which is of interested in this study, the applications can be divided into four categories described by Crowe (2006). The first category is the gas catalytic reaction. In this type of application the reactants and the products are in the same phase; however, the reaction take place on the surface of a solid catalyst. Fluid Catalytic Cracking (FCC) is one example of this type of reaction. FCC converts low value heavy components of crude oil into a variety of high value lighter products (Yang, 2003). The second category is the gas-phase reaction using solids as heat carriers. In this reaction both the reactants and the products are in the same phase (gaseous) but solids are required to produce or carry the heat needed for the reaction. The third category is the gas-solid reaction, where reactants and products are gases and solids, with the option of being gases or a combination of gas and solids. Combustion and gasification, which are going to be explained in the following subsections, are examples of processes using this type of reaction. Finally, the last category is where no chemical reactions occur. Fluidized bed drying applications are an example of this type and are used due to the fluidized bed high drying rates, high thermal efficiency and lower costs;

they are commonly used among the chemical, food, ceramic, and pharmaceutical industries.

2.1.2 Fluidization Regimes

Fluidization is the phenomenon of imparting the properties of a fluid to a bed of particulate solids by passing a fluid (liquid or gas) through the latter at a velocity which brings the fixed or stationary bed to its loosest possible state just before its transformation into a fluid-like bed (Gupta and Sathiyamoorthy, 1999). A fluid-like behavior is attained when the drag and buoyant forces surpasses the gravitational forces of the solid particles, allowing relative motion between them. Fluidization can be obtained using liquid, gas, or a liquid-gas combination, as the fluid passes through the solid material. Liquid-solid and gas-liquid-solid systems are important for several industries, but they are not of interest in this research, which is primarily focused on gas-solid systems.

Yang (2003) considered at least six different fluidization regimes for gas-solid fluidized beds: fixed bed, bubbling fluidization, slugging fluidization, turbulent fluidization, fast fluidization, and pneumatic conveying. Figure 2.2 shows a schematic of the existent fluidization regimes in as gas-solid fluidized bed. In the fixed bed regime the air flowing across the particle does not have enough velocity to move the particles. As the superficial gas velocity (U_g) increases, the system reaches the bubbling fluidization regime. In this regime, bubbles start to form and coalesce causing solid mixing; the velocity at which bubbles appeared is known as the minimum bubbling velocity (U_{mb}). Yang (2003) considered that the slugging regime appears in beds where the bed height (H) over the bed diameter (D) is larger than 2. This requirement ensures that bubbles have enough time to coalesce in bigger bubbles called slugs, when the bubbles grow to 2/3 of the bed diameter the system enters to a slugging regime.

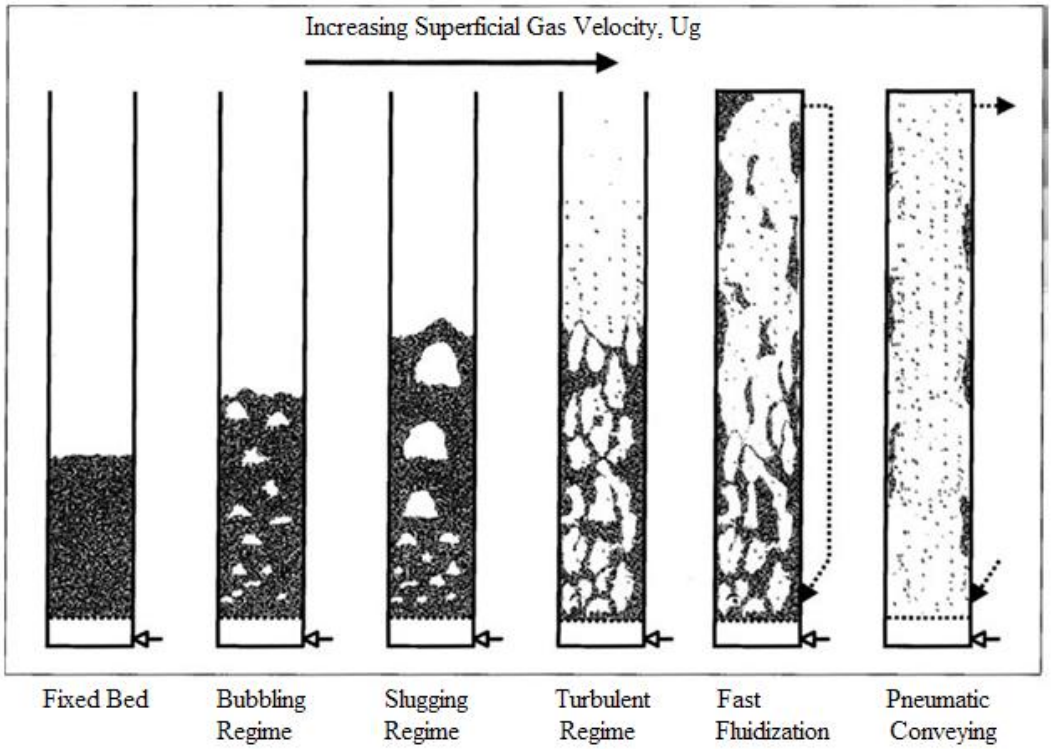

Figure 2.2: Fluidization regimes in a gas-solid fluidized bed (Crowe, 2006)

Furthermore, Crowe (2006) said that turbulent fluidization occurs when, as U_g is increased, a point is reached where the bubbles or slugs, begin to break down instead of continuing to grow. The "critical velocity," U_c, which demarcates the onset of the turbulent fluidization flow regime, is usually determined experimentally as the superficial gas velocity at which the standard deviation of pressure fluctuations reaches a maximum. If U_g increases beyond a velocity known as the transport velocity U_{tr}, a fast fluidization regime is reached. In the fast fluidization regime, solid particles are thrown outside of the bed, which makes the bed surface undistinguishable. Finally, the pneumatic conveying regime is reached when the superficial gas velocity is much higher than the transport velocity; this regime is characterized by the particle being transported out of the bed in a dilute phase.

2.1.3 Gas Holdup

Fluidized bed hydrodynamics are important to understand how fluidization behaves inside the fluidized bed. Gas holdup is one very important parameter that characterizes the fluidization quality, homogenous mixing, and process efficiency in a fluidization system, and is defined as the volume fraction of gas present within the bed material. Using an optical probe, Zhu et al. (2008) determined the solid concentration (the inverse of gas holdup) in a gas-solid system for bubbling and turbulent fluidization regimes. Results show that the turbulent regime solid concentrations are not uniform in the axial and radial direction, showing a nonuniformity of the flow structure. In the bubbling regime, the nonuniformity increases as the superficial gas velocity also increases. Moreover, Zhu et al. (2008) studied the effects that changing the static bed height have on the solid concentration. Results showed that increasing the static bed height produced an increase in the solid concentrations mainly in the central region of the bed, while the wall region had no significant changes. This phenomenon is attributed to the increased presence of bubbles in the material as the bed height is increased.

Du et al. (2003) measured the solid concentration for a turbulent fluidized bed. Results show that at high gas velocities, especially in the turbulent regime, the cross-sectional solids holdup exhibits a radial symmetric distribution, while this is not the case for the bubbling regime. At low gas velocities in the bubbling regime, dispersed bubbles yield a lower solids concentration in the center of the bed. The asymmetric distribution of solids concentration is due to the spiral motion of bubbles in the bed.

2.1.4 Minimum Fluidization Velocity

The minimum fluidization velocity (U_{mf}) is the point of transition between a fixed bed regime and a bubbling regime in a fluidized bed. Minimum fluidization velocity is one of the most important normalized parameters when characterizing the hydrodynamics in a

fluidized bed (Ramos et al., 2002). Usually, the minimum fluidization velocity is obtained experimentally, and there are several techniques reported in the literature to find the minimum fluidization velocity in a multiphase flow system. Gupta and Sathiyamoorthy (1999) described three different methods to measure U_{mf}: (i) the pressure drop method, (ii) the voidage method, and (iii) the heat transfer method. The first method measures the pressure drop across the bed as a function of the superficial gas velocity. The point of transition between a fixed bed regime and a bubbling regime is denoted by a constant pressure line in a plot of pressure vs. superficial gas velocity; this point marked the minimum fluidization velocity. In the voidage method, the minimum fluidization velocity is determined when the voidage inside the bed starts to increase due to bed expansion as the superficial gas velocity is increased. However, this method is not commonly used because it is much more complicated to locate the point where bed expansion starts. Finally, in the heat transfer method, the variation of the wall heat transfer coefficient is measured as the gas velocity increases. The point where the heat transfer coefficient increases drastically is the onset of fluidization or the minimum fluidization velocity point. This method, however, is too expensive and requires a good experimental setup to measure the heat transfer data under steady-state conditions.

Zhou et al. (2008) used the pressure drop method to find and compare the minimum fluidization velocity of a three phase system (gas-liquid-solid) between a conical and a cylindrical fluidized bed. They compared the experimental results of the minimum fluidization velocity with minimum fluidization results obtained using reported theoretical correlations, like the Ergun equation, as well as other models developed by other researchers. Results agreed when using both theoretical models and experimental procedures to obtain the minimum fluidization velocity.

The minimum fluidization velocity depends on the material properties, the bed geometry, and the fluid properties. Sau et al. (2007) determined the minimum fluidization velocity for a gas-solid system in a tapered fluidized bed (conical fluidized bed) and studied the effects that bed geometry, specifically the tapered angle, had on the minimum fluidization velocity. They used three different angles (4.61, 7.47, and 9.52 degrees) to observe their effects on minimum fluidization velocity. Results showed that as the tapered angle increased, U_{mf} also increased, which implied a dependence of the minimum fluidization velocity to the geometry of the fluidized bed. Moreover, Hilal et al. (2001) analyze the effects of bed diameter, distributor, and inserts on minimum fluidization velocity. It was shown that both the bed diameter and the type and geometry of the distributor affected U_{mf}. Minimum fluidization velocity values increased with an increase in the number of holes in the distributor plate. Furthermore, with an increase in the bed diameter, there was a decrease in the minimum fluidization velocity. Finally, insertion of tubes along the fluidized bed reduced the cross sectional area, which produced a high interstitial gas velocity causing a decrease in U_{mf}.

2.1.5 Bed height effects in the minimum fluidization velocity

Among the peer reviewed literature there are several papers that discuss the effects of bed height on the fluidized bed hydrodynamics, and more specifically, if it has an influence on the minimum fluidization velocity. Some of the results are geometry or material dependent, which must be considered when making comparisons.

Sau et al. (2007) used a gas-solid conical tapered fluidized bed to find the minimum fluidization velocity and the pressure drop across the bed. The dimensions of the fluidized bed at the bottom were 48, 42, and 50 mm, the top of the bed measured 132, 174, and 212 mm, and the column heights were 520, 504 and 483 mm, respectively. The various bed characteristics, materials, and results are summarized in Table 2.1. Sau et al. (2007)

concluded that variables such as the tapered angle affect the magnitude of the minimum fluidization velocity. Meanwhile, the bed height for this type of bed does not have a significant effect on the minimum fluidization velocity. Therefore, U_{mf} was independent of the bed height for this type of conical tapered fluidized bed.

Table 2.1: Experimental conditions and results of Sau et al. (2007).

Material	**Material Density (kg/m^3)**	**Particle Diameter (μm)**	**Tapered Angle (°)**	**Static Bed Height (m)**	**U_{mf} (m/s)**	**ΔP_{max} (Pa)**
Coal	1545	717, 1200	4.61, 9.52	0.092, 0.107, 0.13	0.19-0.34	755-2351
Sand	2638	717	9.52	0.092, 0.107, 0.13	0.26	1018-1506
Limestone	2785	500, 600, 800	4.61, 7.47, 9.52	0.092, 0.107, 0.13	0.17-0.59	850-2351
Sago	1303	1200	4.61	0.092, 0.107, 0.13	0.51	718-1018
Glass Bead	2300	1000, 2000, 3000	4.61, 7.47, 9.52	0.092, 0.107, 0.13	0.68-3.27	1134-2177
Dolomite	2785	717	9.52	0.092, 0.107, 0.13	0.32	1039-1566
Iron Ore	5025	500, 600, 800	4.61	0.092, 0.107, 0.13	0.17-0.34	1320-1910
Refractory Material	2610	717	9.52	0.092, 0.107, 0.13	0.26	1048-1495

Zhong et al. (2006) completed minimum fluidization experiments in spouted fluidized beds. Spouted fluidized beds differ from bubbling fluidized beds in the way the air is introduced into the bed chamber and in the geometry of the chamber. In a spouted fluidized bed, the bed chamber is tapered like a funnel, which creates different hydrodynamics, and the fluidization air is typically injected through a single orifice. They used a two dimensional spouted fluidized bed with dimensions 300 mm × 30 mm and a height of 2000 mm and fluidized a variety of Geldart Type-D particles (Table 2.2). Filling the bed with these materials to different heights (300-550 mm), they determined the

minimum spouting fluidization velocity, defined as the minimum superficial gas velocity at which the spout initiates in the central region and the surrounding annulus is fluidized; this is analogous to minimum fluidization velocity in a bubbling fluidized bed. They concluded that the static bed height for a spouted bed influences the minimum spouting fluidization velocity; increasing the bed height increased the spouting velocity. Figure 2.3 provides an example of these results using mung beans.

Table 2.2: Material properties used by Zhong et al. (2006).

Material	Diameter (mm)	Density (kg/m^3)
Mung Beans	3.2	1640
Polystyrene	2.8	1018
Millet	1.6	1330
Glass Beads (A)	1.3	2600
Glass Beads (B)	1.8	2600
Glass Beads (C)	2.3	2600

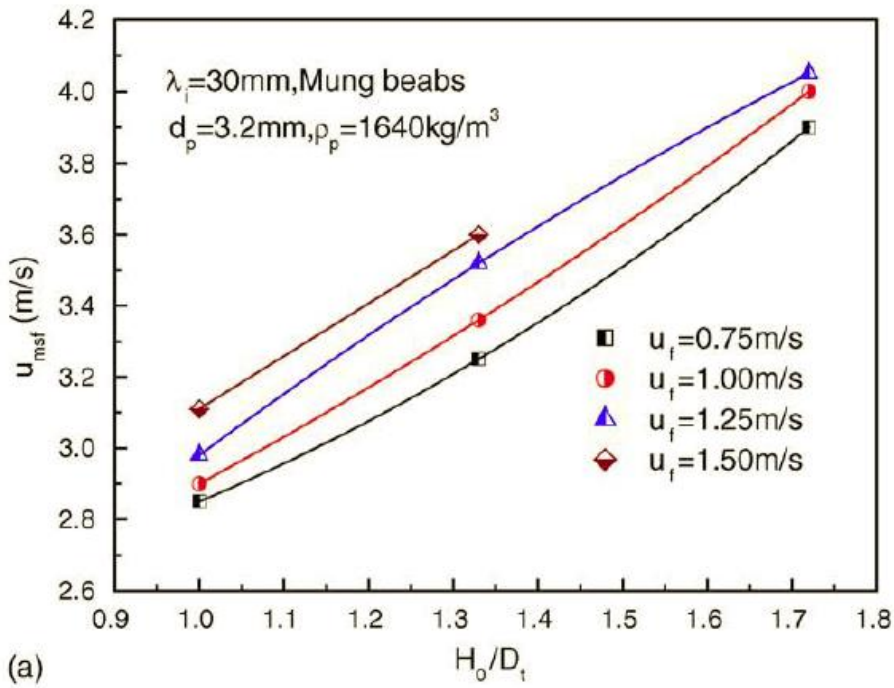

Figure 2.3: Minimum spouting fluidization velocity as a function of bed height using mung beans (Zhong et al., 2006).

Ramos et al. (2002) studied the minimum fluidization velocity for gas-solid 2D fluidized beds. They used a rectangular bed (1 × 0.2 × 0.012 m) filled with glass beads of three different diameters (160-250, 250-400, and 490-700 µm) and various bed heights (2, 4, 8, 16, 20, 40, and 60 cm). Figure 2.4 shows how bed height affected the minimum fluidization velocity when 250-400 µm glass beads were used as the bed material. When the static bed height increased, the minimum fluidization velocity increased, as shown by the location where ΔP/w (bed pressure drop/ bed weight) becomes constant.

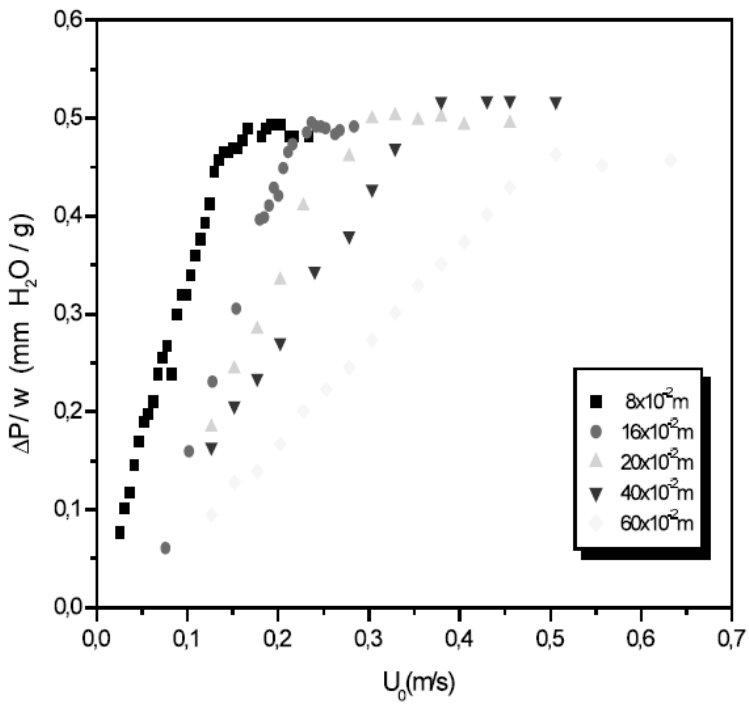

Figure 2.4: Minimum fluidization velocity as a function of bed heights of glass beads (Ramos et al., 2002).

Gunn and Hilal (1997) studied gas-solid fluidized beds using glass beads with beds that had 89 and 290 mm ID. The glass bead diameters were 100 and 500 µm, and they used four different bed heights (20, 30, 40, 50 cm). The results for minimum fluidization velocity showed that for all the material and experimental conditions used in this study, there was no significant change in the minimum fluidization velocity when the bed height was increased. Therefore, U_{mf} was independent of bed height.

Cranfield and Geldart (1974) studied the fluidization characteristics of large particles (1000-2000 μm) of alkalized alumina in a fluidized bed with a cross section area of 61×61 cm at different bed heights (5, 10, 15, 20, 25, and 30 cm). They showed that for 3D beds, the minimum fluidization velocity remained constant no matter the bed height used in the experiments.

2.1.6 Biomass Fluidization

Biomass is defined as organic material of recent biological origin (Brown, 2003) and can be obtained from many different sources including animal waste (manure), agricultural residues (cornstover, bagasse), or municipal waste, as well as from dedicated energy crops like corn or switchgrass. Energy from biomass accounts for about 14% percent of the worldwide energy consumption; a significant portion is consumed in developing countries (35%), while only a minor portion is consumed in industrialized countries (3%) (Demirbas, 2007).

As a renewable resource, biomass has several characteristics like being a renewable organic source, being found in abundance around the world, and having the ability to fix carbon dioxide using photosynthesis. Therefore, these unique characteristics make biomass a very attractive alternative to traditional carbon-based sources like coal for combustion in electricity generation. Biomass can also be used as a replacement to petroleum-based fuels, or in the production of chemicals and plastics. Table 2.3 from Mohan et al. (2006) summarizes the different conditions and variety of products that can be obtained with various thermochemical processes.

Table 2.3: Different thermochemical processes and products (Mohan et al., 2006).

Technology	Residence Time	Heating Rate	Temperature (C)	Predominate Products
carbonization	days	very low	400	charcoal
conventional	5-30 min	low	600	oil, gas, char
gasification	0.5-5 min	moderate	>700	gas
fast	0.5-5 s	very high	650	oil
flash-liquid	<1 s	high	<650	oil
flash-gas	<1 s	high	<650	chemicals, gas
ultra	<0.5 s	very high	1000	chemicals, gas
vacuum	2-30s	high	<500	oil
hydro-pyrolysis	<10s	high	<500	oil

There are several biomass conversion technologies for the products mentioned in Table 2.3. Specific to fuels, biomass can be converted using biological, physical, or thermal (thermochemical) conversion processes. Biomass thermochemical conversion processes are under development worldwide and include combustion, gasification, and fast pyrolysis. Many of these processes are based on effective fluidization and utilize fluidized beds as part of the equipment (Zhong et al., 2008). These three major thermochemical conversion processes will be briefly explained.

In combustion, biomass is exposed to a series of chemical reactions in which carbon oxidizes into carbon dioxide, hydrogen oxidizes into water, and energy is produced in the form of heat (Demirbas, 2007). The most important facts in combustion are: (i) chemical reactions are exothermic, (ii) most combustion reactions are gas-phase due to the high temperatures, (iii) combustion can only take place if there is enough heat to raise the temperature of the unburned gases, and (iv) combustion is more efficient if there is just enough oxygen to burn the fuel that is present (Demirbas, 2007). Dos Santos et al. (2008) recommend the use of a bubbling fluidized bed (BFB) for combustion of biomass due to several attractive characteristics, such as high combustion efficiency, pollutant emissions

control, and a high heat transfer rate between the solid bed material and the injected biomass. Also, combustion in fluidized beds improve combustion efficiency by 96-98% and improve the heat transfer rate by 60-80 times over that of conventional combustors (Abdullah et al., 2003).

Pyrolysis is the thermal decomposition of carbonaceous material without the presence of oxygen. Depending on the conditions like temperature, heating rate, and residence time, pyrolysis can produce a diversity of products. Fast pyrolysis has become more popular among the thermochemical conversion processes because it can operate at atmospheric pressure and because of the moderate temperatures needed to produce a liquid fuel known as bio-oil. Fast pyrolysis consists of three important aspects, described by Bridgwater and Peacocke. (2000): (i) high heat transfer rates requiring fine biomass particles, (ii) controlled temperatures around 500°C, and (iii) rapid cooling of the gases to produce liquid fuel. The yields of bio-oil using fast pyrolysis exceed 70% wt. Bio-oil can be used directly as fuel for several stationary applications like turbines, engines, and boilers, as well as in the chemical industry. Bubbling fluidized beds can be used as fast pyrolysis reactors. However, there are some fast pyrolysis conditions that differ from those of combustion. In fast pyrolysis, the particle is typically between 2-3 mm, the biomass flow rates are higher to achieve the shorter residence times, and due to these high flow rates, the thermal efficiency is reduced to approximately 60-70%.

Finally, gasification converts biomass into gaseous fuel at high temperatures (700-900ºC) with air, oxygen, or steam (Hanping et al., 2008). The gaseous fuel produced is a mixture of various components including carbon monoxide (CO), hydrogen (H_2), methane (CH_4), nitrogen (N_2), carbon dioxide (CO_2), and smaller quantities of higher hydrocarbons. Gasification consists of four steps: (i) heating and drying, (ii) pyrolysis, (iii) gas-solid reactions, and (iv) gas phase reactions. In the heating and drying process,

biomass is heated to eliminate the moisture content present in it. In the pyrolysis stage, several volatile gases are released and some tar is formed. In the final two steps, the final gaseous products are formed as well as some residual tar. Efficiency in typical gasifiers is about 70-90%. Just like in combustion and pyrolysis, fluidized beds are used as gasifiers due to their fuel flexibility and scalability. However, gasification in fluidized beds typically has high power requirements, high particulate loadings, and moderate tar production.

In summary, fluidized beds are widely used in biomass thermochemical conversion processes because they have high heat transfer rates, uniform and controllable temperatures, favorable gas-solid contact, and the ability to handle a wide variety of particulate materials (Zhong et al., 2008). Therefore, it is imperative to gain a better understanding of how biomass properties like density and particle size affects the fluidization characteristics (minimum fluidization velocity and pressure drop) when a fluidized bed system is used for biomass gasification, combustion, or pyrolysis.

2.1.6.1 Material property effects on fluidization

Fluidizing biomass particles is challenging due to their irregular shape, size, and density. Therefore, the influence of these particular characteristics on the fluidized bed hydrodynamics is important to understanding what is going on when biomass is fluidized. The minimum fluidization velocity is one of the most important parameters when characterizing fluidized bed hydrodynamics and quantifies the drag force needed to attain solid suspension in the gas phase; it also constitutes a reference for evaluating fluidization intensity when the bed is operated at higher gas velocities (Zhong et al., 2008).

Zhong et al. (2008) studied the effects of particle size, density, and shape on the minimum fluidization velocity using wood chips, mung beans, millet, corn stalk, and cotton stalk. In this study, they used a rectangular shaped fluidized bed with a cross

section of 0.4 × 0.4 m and air was the fluidizing gas. They determined that for long, thin types of biomass, the minimum fluidization velocity increased with increasing length-to-diameter (L/d_{pt}) ratio. Figure 2.5 shows the results obtained for corn stalk and cotton stalk. Their experiments showed that after the length-to-diameter (L/d_{pt}) ratio exceeded the value of 20, the biomass was not fluidized, indicating that the biomass size and shape affected its fluidization.

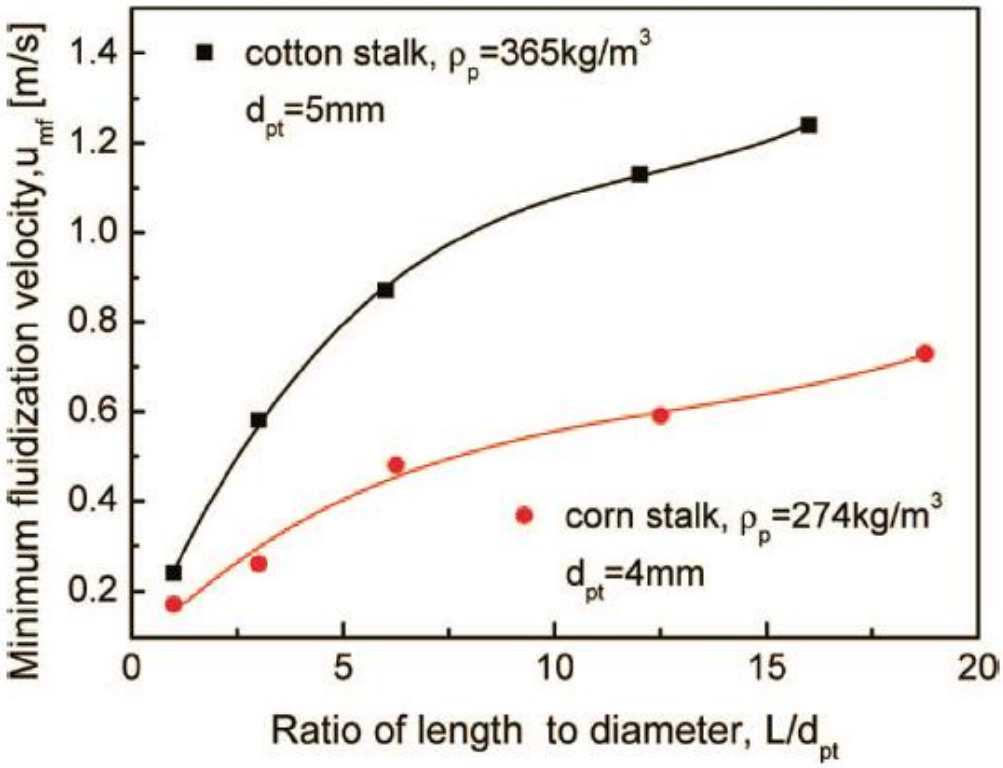

Figure 2.5: Minimum fluidization velocity for cotton stalk and corn stalk as a function of biomass length-to-diameter ratio (Zhong et al., 2008).

Abdullah et al. (2003) also studied the effects of biomass properties, like bulk density and voidage, as well as particle size and diameter, on particle fluidization using rice husk, sawdust, peanut shell, coconut shell, and palm fiber. Table 2.4 summarizes the materials used in this study. The experiments were carried out in a 60 mm internal diameter cylindrical fluidized bed. They determined that bulk density and voidage have an effect in

the quality of the particle fluidization. As the bulk density increased, a better fluidization of the material was achieved. On the other hand, increased voidage produced adverse effects on fluidization because large voids were noticeable as the gas flowed through the bed.

Table 2.4: Materials used by Abdullah et al. (2003).

Material	Diameter (μm)	Bulk density (kg/m^3)	Solid density (kg/m^3)	Bulk Voidage (ε)
Sawdust	786.5	241	570.3	0.58
Rice Husk	1500	129	630.1	0.8
Peanut shell	613.4	250	566.8	0.56
Coconut shell	987.4	430	547.9	0.22
Palm fiber	600	73	407.4	0.82

2.1.6.2 Methods to improve biomass fluidization

As stated above, biomass is difficult to fluidize due to its size and shape characteristics. There are some methods that can improve biomass fluidization by combining biomass with an inert material, like sand or glass beads. In addition to enhancing biomass fluidization, the added sand is also used as a heat transfer medium in gasification, combustion, and pyrolysis processes.

2.1.6.2.1 Binary Mixtures

There are several studies on the fluidization of binary mixtures; most of the mixtures studied involve sand and various types of biomass. Rao and Bheemarasetti (2001) carried out several tests to determine minimum fluidization velocity correlations using two different densities of sand (2.5 and 2.7 g/cm^3), and rice husk, sawdust, and groundnut shell particles as biomass. They maintained a constant mixture effective density, but varied the material particle size. Their fluidized bed was 5 cm in diameter and 100 cm tall. Minimum fluidization velocity (U_{mf}) was determined using both types of sand and various mass fractions of biomass (2, 5, 10, and 15%). This study determined that U_{mf}

increased when the biomass mass fraction increased; it also increased when the sand density or size increased. The results presented by Rao and Bheemarasetti (2001) verified previous studies and the correlations developed in this study satisfactorily predicted U_{mf}.

Zhong et al. (2008) examined the effects of mixtures of biomass and fluidization media (silica sand, continental flood basalt (CFB) cinder, and aluminum oxide) on the minimum fluidization velocity. The biomass included spherical-like biomass like mung beans or wood chips as well as long thin biomass like shredded cotton and corn stalks. For the spherical-like biomass, as long as the biomass mass fraction in the mixture increased, the minimum fluidization velocity increased. Moreover, they also examined the effects of fluidization media diameter and density on the minimum fluidization velocity. Figure 2.6 shows results obtained from wood chip mixtures with silica sand of various diameters. Figure 2.7 shows the results for varying the fluidization media density. Both figures show that increasing the diameter or density of the fluidization media results in an increase of the mixture minimum fluidization velocity. They concluded that for spherical-like biomass particles that had similar characteristics to the fluidization media, an increase in the media diameter or density caused an increase in the mixture effective particle diameter or effective particle density, resulting in an increase in U_{mf}.

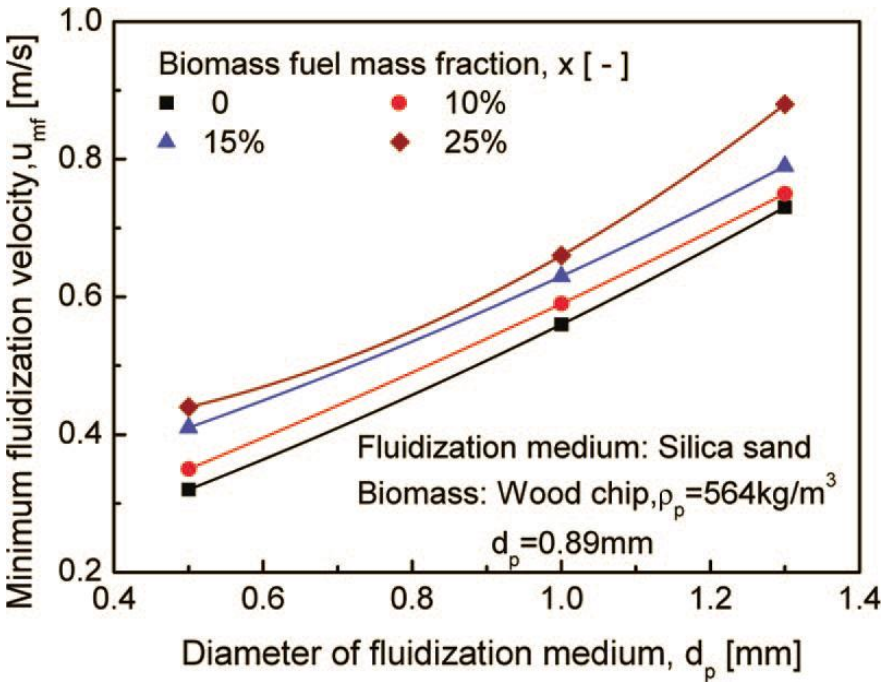

Figure 2.6: Effect of the fluidization media diameter on U_{mf} of the mixture (Zhong et al., 2008)**.**

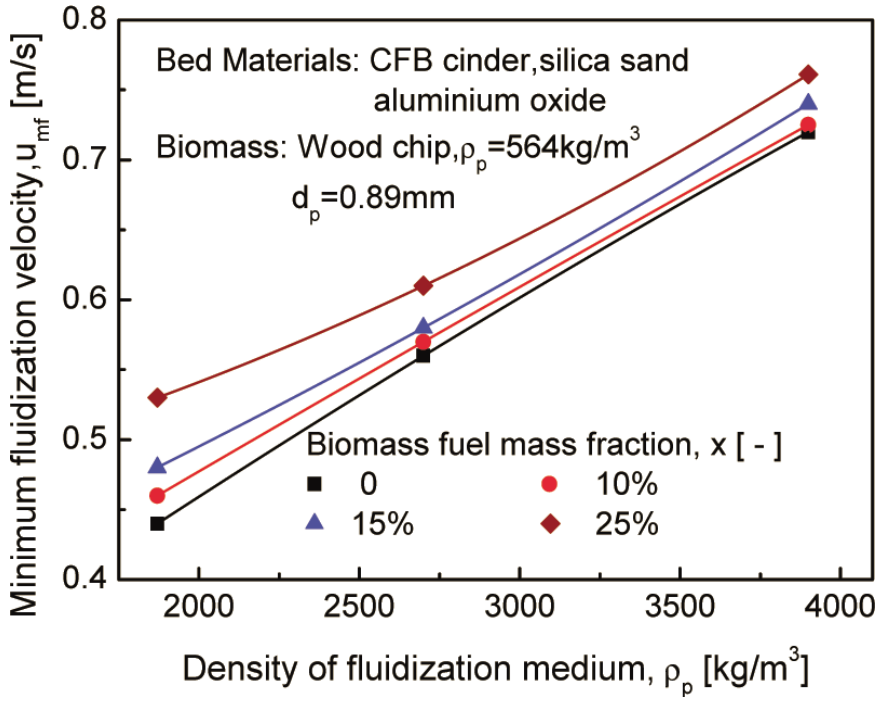

Figure 2.7: Effect of the fluidization media density on U_{mf} of the mixture (Zhong et al., 2008).

When the mixtures contained long thin biomass particles, Zhong et al. (2008) showed the same results as with spherical-like biomass particles, which implied that as the biomass mass fraction increased, the minimum fluidization velocity increased. Mixtures of long thin biomass particles with inert material also improved fluidization when compared to long thin biomass particles alone. The reason for this improvement was the addition of the fluidization media enhanced fluidization and even biomass with large length-to-diameter ratios were fluidized under these conditions.

2.1.6.2.2 Acoustic Fluidized Beds

Acoustic fields can also be used to enhance biomass fluidization. This is an attractive option because no internal changes are made to the bed and there is no limitation to the particle type that can be fluidized. Si and Guo (2008) studied how an acoustic fluidized bed improves the fluidization of two different biomass particles, sawdust and wheat stalks, alone or mixed with quartz sand. They compared the fluidization behavior of the biomass without and with the acoustic field to determine if there was any improvement due to the acoustic field. Moreover, they determined the effects that the sound pressure level (SPL) had on the minimum fluidization velocity. Initially, Si and Guo (2008) found that the biomass by itself fluidized poorly with and without the presence of the acoustic field. Then, they added quartz sand to aid fluidization and maintained the biomass mass fraction at 60%. They observed that below a SPL of 90 dB, plugging and channeling occurred in the fluidized bed. Increasing the SPL diminished the effects of channeling and improved the quality of fluidization. By varying the sound frequency between 50 to 400 Hz, they determined that the minimum fluidization velocity decreased with increasing frequency until it reached a minimum value and then increased with increasing frequency. Examples of their results are shown in Figure 2.8.

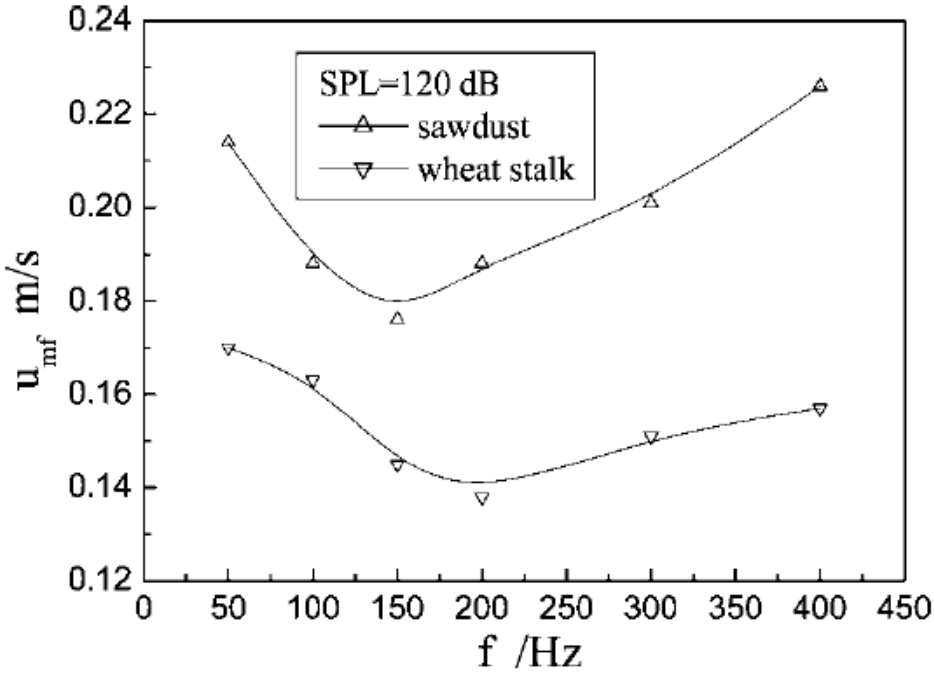

Figure 2.8: Effect of sound frequency on U_{mf} of a quartz sand-biomass mixture (Si and Guo, 2008)

Si and Guo (2008) also fixed the sound frequency at 150 Hz and varied the sound pressure level between 90 and 120 dB. Using these conditions, they determined the effects on the minimum fluidization velocity. As shown in Figure 2.9, when the sound pressure level was above 100 dB, the fluidization quality improved, and they observed that the biomass mixture fluidized smoothly without any obvious slugging or channeling.

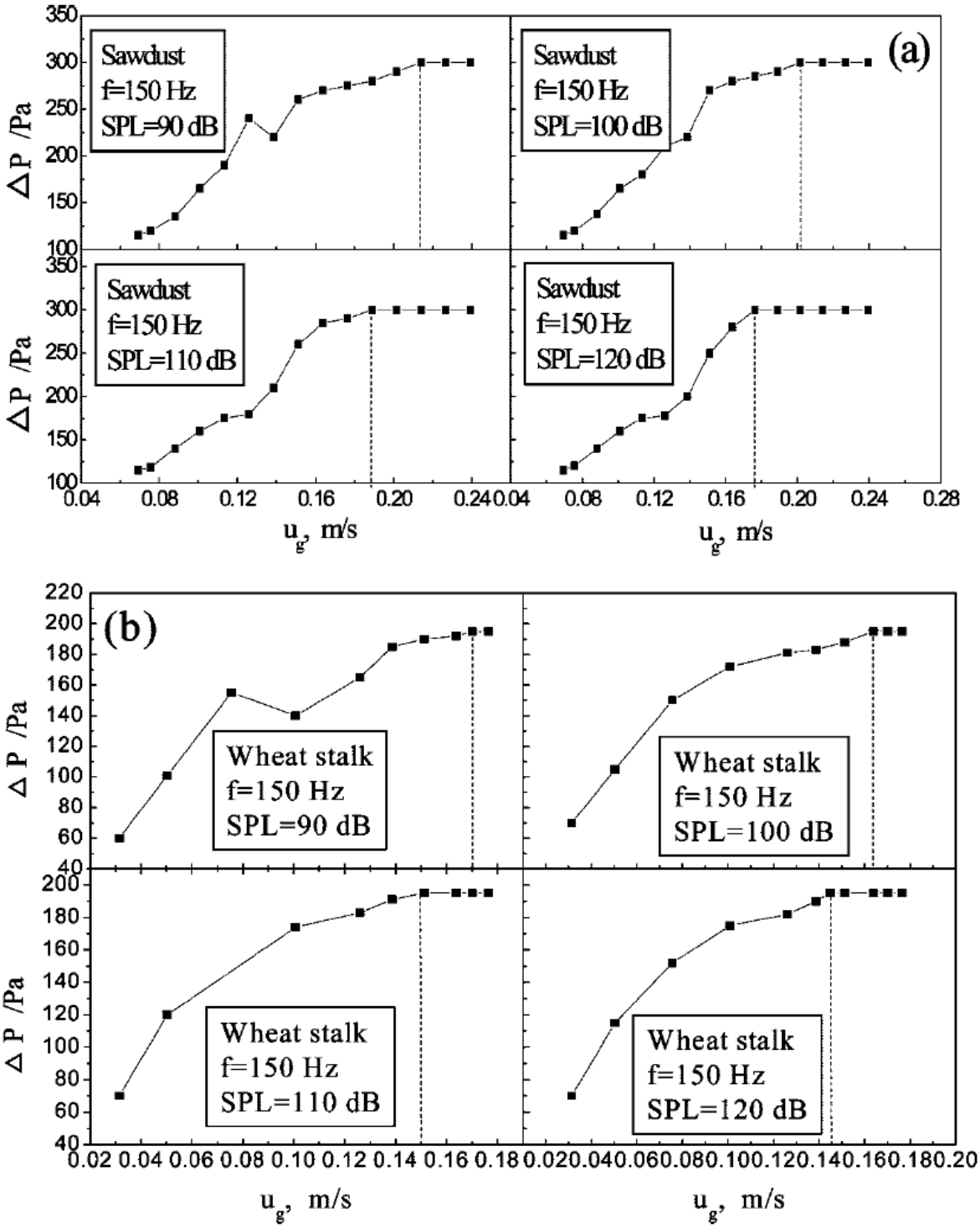

Figure 2.9: Minimum fluidization velocity at different sound pressure levels: quartz sand and a) sawdust or b) wheat stalk (Si and Guo, 2008).

2.2 Fluidized Bed Hydrodynamics: Measurement Techniques

This section overviews several techniques used to visualize and characterize hydrodynamics of opaque multiphase flow systems, emphasizing noninvasive X-ray techniques used in this study such as X-ray computed tomography. The first subsection describes invasive techniques commonly used to visualize and characterize flow systems. The following subsection overviews some noninvasive techniques, with a deeper explanation of X-ray techniques including X-ray radiography, X-ray stereography, and X-ray computed tomography.

Invasive techniques as well as noninvasive techniques are used to obtain information regarding fluidized bed hydrodynamics. However, depending on the scope of the analysis, there are different techniques that work better than others. Therefore, it is important to classify these techniques according to the purpose of the analysis. Boyer et al (2002) classified the measurement procedures distinguishing between time averaged and transient measurements and between local and global measurements.

2.2.1 Invasive Techniques

Invasive techniques are useful in industrial operating conditions, where noninvasive techniques become extremely challenging if at all possible. Figure 2.10 summarizes some of the invasive techniques used in gas liquid and gas-solid-liquid flow systems, the expected outcomes for each technique, the limitations, and the spatial and time resolution for each of the procedures. Needle probe techniques are used for high gas holdup systems. Depending on the type of measurements, there are single tip probes, used to identify gas fraction and bubble frequency, and double tip probes used to measure bubble velocity, local interfacial area, and bubble chord length. There are two types of probes, optical fiber and resistive conductive probes, with optical fiber probes being used

frequently. For example, Mena et al. (2008) used a monofiber optical probe to measure the gas phase characteristics (residence time and velocity) in a three phase flow system. Results showed that the probe was capable of obtaining reliable measurements for some hydrodynamic characteristics of the multiphase flow, like bubble coalescence, and transition regimes. However, there were some limitations; for example, for gas holdup measurements, the precision was low compared to other techniques and required a larger experimental setup effort.

Techniques	Applications	Expected results	Limitations	Spatial resolution	Time resolution
Needle probe	Mainly gas–liquid, but gas–liquid–solid also	• Gas holdup • Bubble velocity • Bubble chord distribution • Size distribution → • Bubble shape → • Interfacial area	• Low solid hold-up • Not adapted to wall vicinity • Adapted fluid (conductive liquid for impedance probes) • Model required • Multiple tip probes: reconstruction needed	++	++
Heat transfer probe	Mainly gas–liquid, but gas–liquid–solid also	• Gas holdup • Liquid average velocity • Liquid RMS velocity	• Low solid holdup • Liquid phase homogeneous in temperature • Adapted signal analysis required • Not adapted to small velocities	++	++
Ultrasound probe • Attenuation technique	G–L and G–L–S	Gas holdup or interfacial area	Low gas holdup (< 20%)	+	+
• Doppler technique	→	Bubble diameter or bubble velocity	• Spherical bubbles • Small distance measurements	+/−	+
Pitot tube	G–L and G–L–S	• Flow direction or • Pressure drop • Liquid velocity	Moderate gas holdup	−/+	−/+

Figure 2.10: Invasive techniques classification (Boyer et al., 2002)

Heat transfer probes may be used to describe the liquid phase within two-phase flows that have a moderate gas holdup. Hot film anemometry measures gas fraction and liquid-phase characteristics, like mean velocity and RMS fluctuating velocity. The principle

used in these probes is based on the heat transfer between an electrically heated probe and the liquid medium surrounding it.

Ultrasound probes use the principle of ultrasound wave propagation, which can be divided into two categories: wave propagation by attenuation, used to measure gas holdup and time averaged local interfacial area, and wave propagation by the Doppler Effect, which is used to find bubble characteristics. Finally, Pitot tubes use pressure measurements to characterize local velocity measurements of the multiphase flow system.

Invasive techniques present several limitations. Optical and resistive probes cannot be used in all organic liquids because there are small differences in the refraction index with the gas phase, and also the low conductivity is sometimes very small for impedance probes (Boyer et al., 2002). For ultrasound probes, the limitation arises under high gas holdup conditions, causing a loss of effectiveness in the measurements. Therefore, invasive techniques are not commonly used, particularly in fluidized beds, causing noninvasive techniques to be popular among the techniques used to characterize multiphase flow systems.

2.2.2 Noninvasive Techniques

Noninvasive techniques are valuable because they provide insight into the flow behavior and general hydrodynamic characteristics of multiphase flow and opaque systems (Yates et al., 2002). There are several noninvasive techniques used to measure gas/liquid holdup, pressure drop, flow regime, bubble size and distribution, and gas and liquid velocity. Contrary to the invasive techniques, noninvasive techniques are able to measure several of the characteristics listed above. According to Chaouki et al. (1997), noninvasive techniques can be classified into tomography and radiography techniques and velocimetry techniques. Tomographic and radiographic techniques are divided into two categories: nuclear based imaging techniques like gamma-ray computed tomography

(GRT), X-ray computed tomography (XCT), positron emission tomography (PET), X-ray diffraction tomography (XDT), X-ray and neutron transmission radiography, nuclear magnetic resonance imaging (MRI or NMRI), and non-nuclear based techniques like electrical capacitance tomography (ECT), optical tomography, and ultrasonic tomography. On the other hand, positron emission particle tracking (PEPT), radioactive particle tracking (CARPT or RPT), cinematography, laser Doppler anemometry (LDA), and particle image velocimetry (PIV or PTV) are forms of velocimetry techniques.

Even though there are several techniques for visualization and measurement of multiphase flow systems, not all the techniques are applicable to fluidized beds. Gamma-ray tomography (GRT) uses a gamma-ray source and detector to quantify the gamma-ray attenuation through an object. The attenuation provides a measure of the local mass density distribution along the path traversed by the gamma beam (Chaouki et al., 1997). Patel et al. (2008) used GRT to determine the gas maldistribution of a gas-solid fluidized bed drier and how the gas maldistribution was affected by various parameters, such as particle size, particle density, and superficial gas velocity. Results showed that GRT was a reliable technique that provided a good estimation of the gas maldistribution with a good spatial resolution (Patel et al., 2008).

ECT is another tomography technique used in fluidized beds. The ECT principle uses electrical measurements like capacitance, resistance, or inductance, for imaging the distribution of these parameters within a medium. This technique is safer and faster than nuclear based techniques, it also provides more flexibility to accommodate large or small vessels. However, the spatial resolution provided is lower than the nuclear based techniques (Chaouki et al., 1997). Du et al. (2003) used the ECT technique to study the dynamic behavior of a turbulent gas-solid fluidized bed. From the ECT images, they quantified the dynamic characteristics of the bubble/void phase and the emulsion phase of

the system. Results showed that ECT imaging provided robust and reliable measurements and showed similar results compared with other techniques like optical probes.

2.2.3 Noninvasive X-ray techniques

X-rays have been used to study gas-solid fluidized beds as well as two and three phase fluidized systems for more than 50 years (Yates et al., 2002). They are commonly employed in noninvasive techniques because they are safer than other nuclear based techniques which cannot be turned on and off at will, have high resolution, and can be controlled by varying the voltage or current to improve penetration or contrast (Franka, 2008). X-rays are produced by accelerated electrons emitted from a heated cathode; the electrons hit an anode producing a deceleration of the electrons and an emission of electromagnetic radiation. The interaction between X-rays and the materials through which they pass cause a decrease in the X-rays intensity (Grassler and Wirth, 2000). Among the noninvasive X-rays techniques, X-ray computed tomography, X-ray radiography, and X-ray stereography are the most common procedures used in laboratory scale. The following sections describe each technique in detail.

2.2.3.1 X-Ray Radiography

X-ray radiography records the attenuation of the X-ray beam using, for example an image intensifier camera; if the X-ray is a cone beam, the camera records a two dimensional projection of the three dimensional object, located between the X-ray source and the detector. Figure 2.11 shows a schematic of this technique. The speed at which images can be acquired, the flexibility in manipulating and storing the images, good temporal and spatial resolution are some of X-ray radiography advantages (Heindel et al., 2008). Heindel et al. (2008) applied X-ray radiography to visualize two different multiphase flow systems in a spouted column. The first system used was water with 50% by weight polyethylene glycol, and the second system was 500 μm glass beads. Applying

a false colored scale, X-ray images showed the different attenuation of the beams at the moment that bubbles pass through the column, because air attenuates X-rays less than water or glass beads.

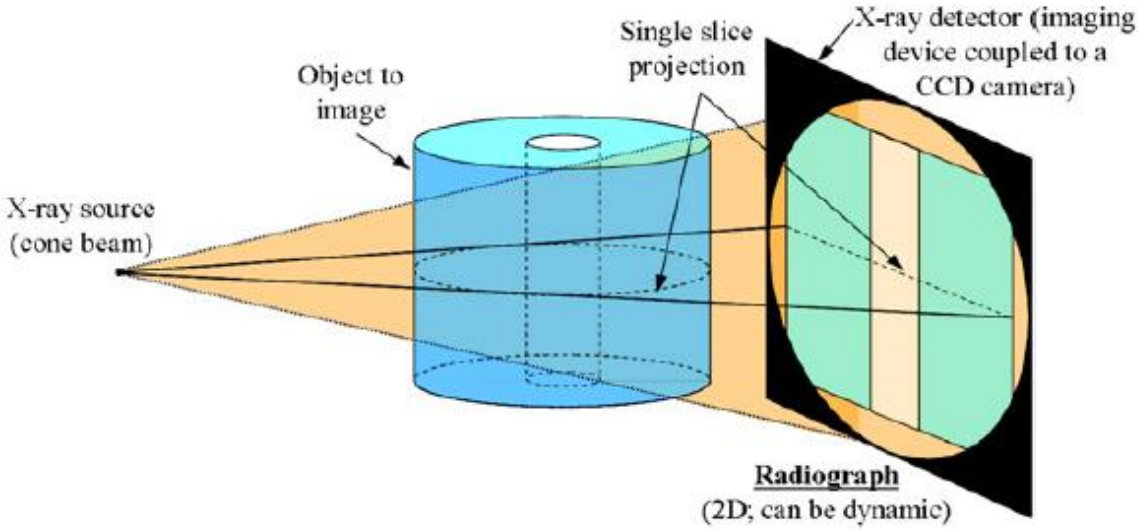

Figure 2.11: X-ray radiography schematic (Heindel et al., 2008).

Visualizing and characterizing hydrodynamics of fluidized beds have been studied using X-ray radiography. Franka et al. (2007) used radiographic images of glass beads, ground corncob, ground walnut shell, and melamine to visualize the fluidization behavior of each material inside a 9.5 cm diameter fluidized bed. Radiographic images were taken at a rate of 20 frames per second for 30 seconds. Results showed that visualization of bubbles in glass beads was difficult due to the high density of the material. As the material density decreased, X-ray penetration increased and the internal structure of the material became more distinguishable.

2.2.3.2 X- Ray Stereography

X-ray stereographic methods use information from two 2D projections to calculate the 3D location of features in an object. This can be accomplished by analyzing two images

of an object which are taken at different positions either due to a rotation or translation of the sample (Heindel et al., 2008). Figure 2.12 shows a schematic of how X-ray stereography images are acquired. X-ray stereography can be classified both as a tomographic/radiographic method and a velocimetry technique. X-ray particle tracking velocimetry (XPTV) uses stereographic images to calculate the fluid velocity by monitoring the movement of tracer particles. In XPTV, the fluid is seeded with X-ray absorbing particles with similar density to the fluid. Since two projections are imaged simultaneously, three dimensional velocity profiles can be generated (Franka, 2008).

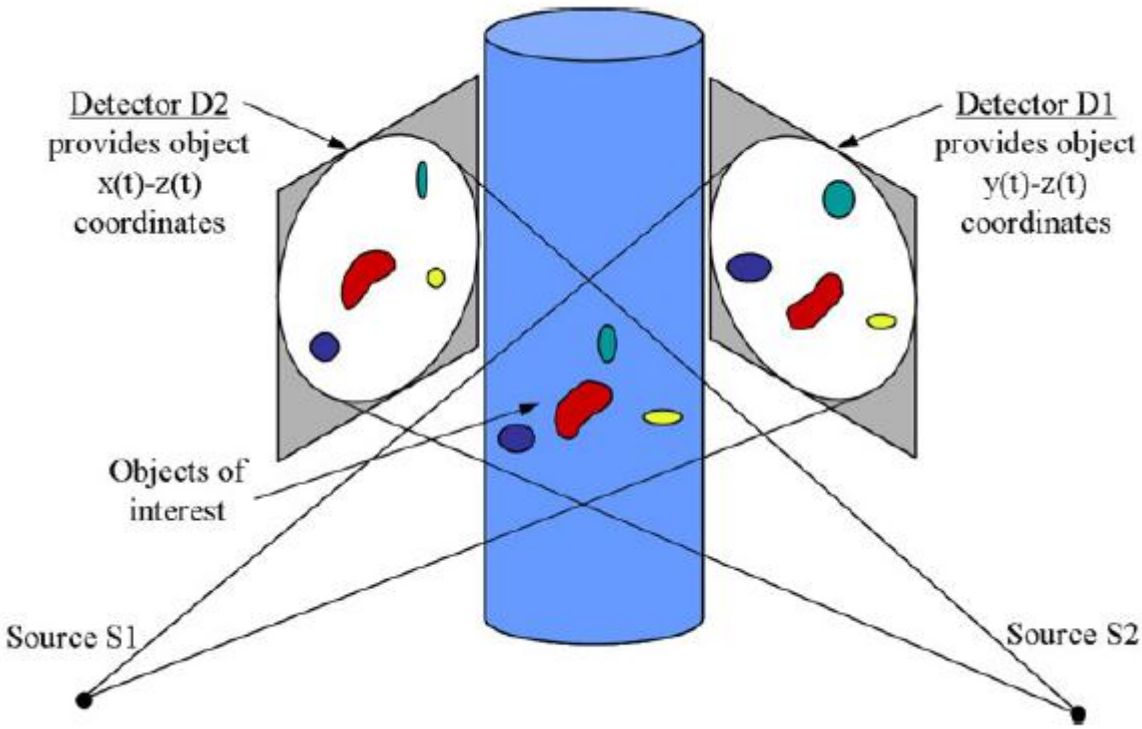

Figure 2.12: X-ray stereography schematic (Heindel et al., 2008).

Seeger et al (2003) used X-ray stereography with XPTV to measure the local solid velocity and the local solid gas holdup of a three phase flow system in a cylindrical fluidized bed of 104 mm inner diameter. The solid material used in the experiment was polymethylmethacrylate. Conversely, the tracking particles were made of polyurethane

with a cylindrical insert of a tin alloy, which absorbs the X-rays allowing the visualization of them inside the opaque system. Results showed that using X-ray stereography and XPTV was suitable for 3D measurements of velocity profiles as well as local solid gas holdups. Some of the advantages presented by this method were: it did not present limitations with large voids or solid holdups, the solid velocity was calculate through several points in the volume simultaneously and three dimensionally, it was quick, and both solid gas holdup and velocity were measured at the same time (Seeger et al., 2003).

2.2.3.3 X-Ray Computed Tomography

X-ray computed tomography (XCT) can generate a 3D image of the object of interest. X-rays pass through the object and the intensity values are recorded at several projections by an imaging device. After the images are collected, computer algorithms reconstruct the images to produce a 3D representation of the object. Figure 2.13 shows how XCT images are taken. However, due to the number of projections that must be acquired in order to obtain a whole reconstruction of the object, this technique does not have a good temporal resolution. Conversely, having multiple scans from different projections give a high spatial resolution to this technique, a characteristic that can be used to measure the local time-average gas holdup in a very efficient way.

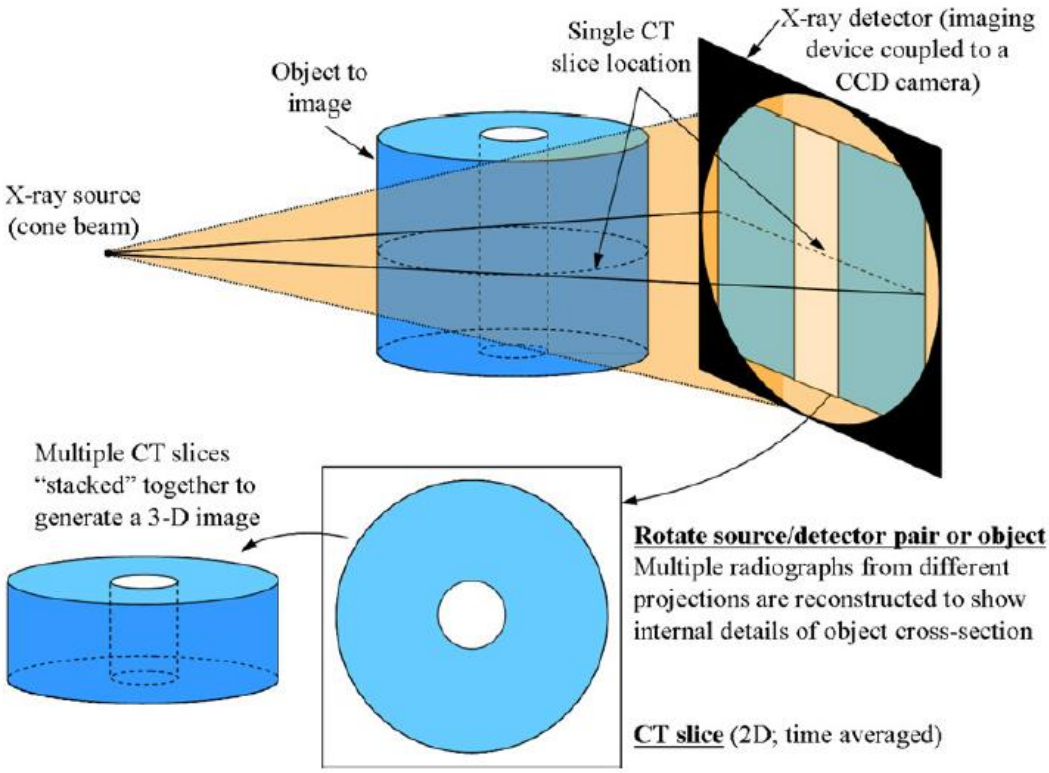

Figure 2.13: X-ray computed tomography schematic (Heindel et al., 2008).

XCT is widely used in measuring multiphase flow characteristics. Franka et al. (2007) used XCT in four different materials (glass beads, melamine, ground walnut shell and ground corncob) to visualize and compare the fluidization structure between the materials. Results showed that in terms of fluidization uniformity, glass beads fluidize symmetrically about the center of the bed and maintain a constant uniformity as the gas velocity increased while less dense melamine, ground walnut shell, and ground corncob showed regions where jetting, spouting, and channeling effects appeared and decreased the bed uniformity. However, as gas velocity increased the uniformity of the non-glass materials increased too, obtaining a better gas distribution inside the material. Kantzas et al. (1997) used X-ray computed tomography to analyze channelling in a gas-solid system composed of polyethylene resin at various gas flow rates and bed heights. With the help of CT scans, they determined the voidage distribution along the bed, identifying the

regions with high gas holdup as areas of gas channelling. Channelling was dependent on the gas velocity and the bed height. Their results showed that as the gas superficial velocity increased or the bed height decreased, channelling inside the resin increased.

Moreover, XCT images and data allow the calculation of time average local gas holdup or solid holdup. Grassler and Wirth (2000) used XCT to determine the solids concentration in a 0.19 m of diameter circulating fluidized bed with 50-70 µm glass beads as the bed material. Tests were carried in two different systems. In the first, solid concentrations were calculated with an up flow system. Results for this system showed that radial solid concentration exhibited a parabolic shape with a maximum concentration close to the wall of the reactor and a minimum concentration in the center of the bed. For the second, the solid concentration was calculated with a down flow system. For this case, the solid concentration distribution was much more complex and depended upon the gas-solids distributor operating conditions. Results showed various solid concentration distributions from a homogeneous distribution with a parabolic profile to concentrated strands in the center of the bed. Finally, the study also showed that the solids concentration was accurately calculated within 5% error for concentrations up to 20 vol% with a minimum resolution of 0.2 mm (Grassler and Wirth, 2000).

Franka and Heindel (2009) studied the effects of side air injection, superficial gas velocity, and bed material on the local time-average gas holdup of a 10.2 cm fluidized bed, using X-ray computed tomography. Using different materials (glass beads, ground corncob, and ground walnut shell), superficial gas velocities (U_g), and side air injection flow rates (Q_{side}) they determined the variations on the fluidization hydrodynamics of the bed. They found that with side air injection, the side air flow rose near the wall but then expanded into the bed as height and Q_{side} increased. As U_g increased the effects caused by the side air injection were less pronounced, the overall gas holdup in the system

increased. Fluidization in other materials had similar behaviors with some notable differences. Side air injection was less influential on the less dense material and gas holdup was lowest for the denser material. Finally, they demonstrate the usefulness of X-ray computed tomography in visualizing the internal features of fluidized beds (Franka and Heindel, 2009)

2.3 Summary

This chapter reviewed two important topics related to the following work. In section 2.1, fluidization was examined. The section described fluidized beds and the different fluidization regimes present in a multiphase flow system, and how important hydrodynamic parameters, such as gas holdup and minimum fluidization velocity, are influenced by bed material and bed height. Unique characteristics of biomass fluidization, thermochemical conversion processes, and methods to improve biomass fluidization were also explained in this section. In section 2.2, different techniques used for the visualization and characterization of multiphase flow systems were described. This section described invasive and noninvasive techniques, with a particular focus on noninvasive X-ray techniques used in this research. Understanding this background is very important for the subsequent work.

Multiphase flow systems are widely used in industrial settings, and are becoming important in bioprocessing. Such systems present hydrodynamic behaviors that, even though there is a lot of information in the literature, are still very complex and not well understood for biomass systems. The goal of this research is to use an X-ray technique (XCT) to understand the hydrodynamics in a fluidized bed, specifically, what is the effect of bed material and bed height on the minimum fluidization velocity and gas holdup. The

results of these experiments will help to better understand the structure of a multiphase flow system in a fluidized bed.

Chapter 3: Experimental Setup

A summary of the basic equipment, techniques, and procedures used in this research is provided in this chapter. In section 3.1, a description of the equipment is provided, including the fluidized bed reactor, air system, and pressure and flow instrumentation. Section 3.2 outlines the material selection and preparation procedures. Section 3.3 summarizes the experimental procedures used to determine the minimum fluidization velocity for the respective materials. Finally, section 3.4 describes the X-ray equipment, X-ray CT imaging procedures, calibration requirements, and how gas holdup is calculated from the CT images.

3.1 Equipment

This section describes the equipment used for this research including the fluidized bed reactor, the air flow system, and the instrumentation used to measure pressure and gas flow rates.

3.1.1 Fluidized Bed Reactor

The reactor used in these experiments is a cold flow fluidized bed reactor. The cylindrical fluidized bed was fabricated from 10.2 cm internal diameter (ID) acrylic tubing with a 0.64 cm wall thickness. As shown in Figure 3.1, the reactor consists of three main chambers: the top chamber or freeboard region, the bed chamber, and the plenum. Fluidization occurs in the bed chamber which is 30.5 cm tall and 10.2 cm ID. Square flanges (16.5×16.5 cm) connect each section.

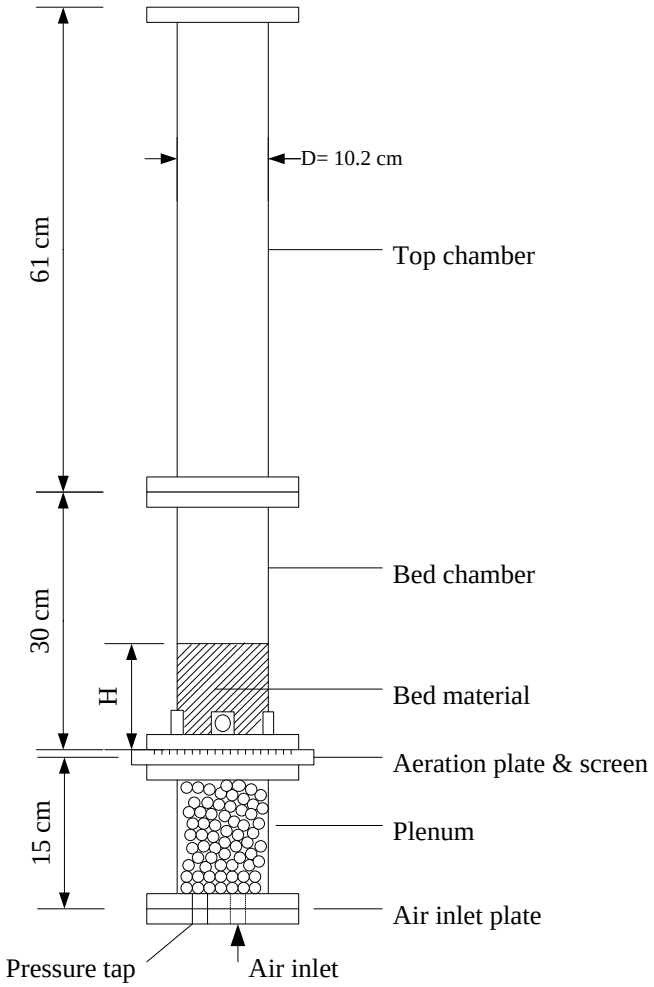

Figure 3.1: Fluidized bed reactor schematic (not to scale). The static bed height is identified by H.

An aeration plate is located immediately below the bed chamber; it is fabricated from a 1.27 cm thick acrylic plate with 62, 1 mm diameter holes spaced approximately 1.27 cm apart in a circular grid for a total open area of 0.62 %. To avoid material blocking the aeration holes, a 45 mesh screen with openings of 0.04 cm is attached to the plate using silicone adhesive.

3.1.2 Air Flow and Pressure Measurement

Compressed air from the laboratory's building air supply is used as the fluidizing gas for this research. The pressure at which the compressed air is delivered inside the laboratory is 620 kPa (90 psi). However, since the flow rates used for fluidization vary

depending of the specific conditions of each experiment, an air flow control board with four independent air lines is used to deliver the required air to the fluidized bed (Figure 3.2). Since the air injection system (used for side air input) is not used in this work, it will not be discussed.

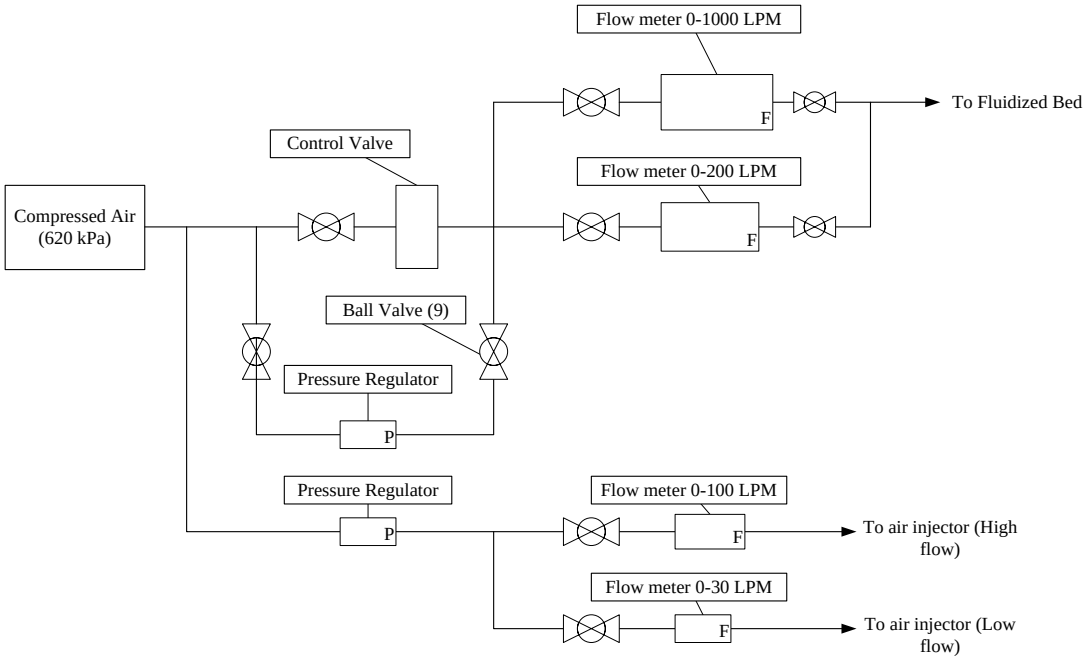

Figure 3.2: Schematic of the air flow system.

The fluidized bed air flow can be regulated by either an automatic control valve or a manual stainless steel pressure regulator and attached filter. The manual pressure regulator is used in this research and has a pressure range of 0-862 kPa (0-125 psi) and maximum inlet pressure of 2.07 MPa (300 psi). The regulated air flows through two different mass flow meters: a 0-1000 Lpm stainless steel Aalborg GFM771 flow meter, which is used for high gas flow applications, and a 0-200 Lpm Aalborg GFM571 flow meter, used in lower gas flow applications. This allows for better measurement resolution. The flow through the respective mass flow meter is controlled through ball valves. The mass flow meters for this study have an error of 2%.

Pressure is measured with a Dwyer 0-34.5 kPa (0-5 psig), 4-20 mA output pressure transducer located in the bottom of the plenum. The signals obtained from the pressure transducer and mass flow meters are connected to a computer controlled data acquisition system. Pressure readings have an estimated error of 1% to 4%.

LabView 8.5 acquisition software records real-time pressure and flow rate measurements over a user-specified period, and then the average pressure and flow rate are calculated and recorded. Average measurements are necessary due to the highly variable pressure signal caused by the bubbling fluidized bed. In this study, data collection occurs at a rate of 1000 Hz for a time interval of 5 seconds. Average pressure and gas flow rate are subsequently written to a data file.

As any other measurement device, the pressure transducer and flow meters are calibrated before starting the experiments. The technique used to calibrate the pressure transducer was to fill up a tube with water, and then measure the hydrostatic pressure at different water level heights. Since the output signal of the transducer is a voltage, the specified pressure is linearly related to the output voltage, which is then used in a calibration function in the data acquisition software. The mass flow meters are calibrated using a calibration drum. The output voltage of the flow meters is measured as a function of the calculated mass flow that passes through the drum during a specified time period. Afterwards, a linear curve fit is applied and used as the calibration function in the data acquisition software.

3.2 Bed Material

The bed material is a significant parameter in this study. The following section describes the criteria used to select the material, how it was prepared, and the calculation of important material properties.

3.2.1 Material Selection and Preparation

For this study, three different materials were selected using the four criteria specified by Franka (2008). These four criteria were: (i) fluidization behavior, (ii) size range, (iii) density, and (iv) aspect ratio. The fluidization behavior refers to how easily the particles can be fluidized. To compare the fluidization characteristics, the chosen particles must fall within the same fluidization category. The particle size between the compared materials follows that of Franka (2008) and corresponds to 500-600 μm. This size range is chosen because of its availability and low cost. When imaging fluidized beds with X-rays, X-ray attenuation will be influenced by material density; low density materials have less attenuation than high density materials. Finally, the aspect ratio desired for the particles should be on the order of 1 to allow comparisons with glass beads, which are common reference materials. Additionally, particles that have a uniform shape provide a better quality of fluidization. Thus, the three materials used in this study are glass beads, ground corncob, and ground walnut shell. As shown in Figure 3.3, all three materials fall within the Geldart Type B

classification.

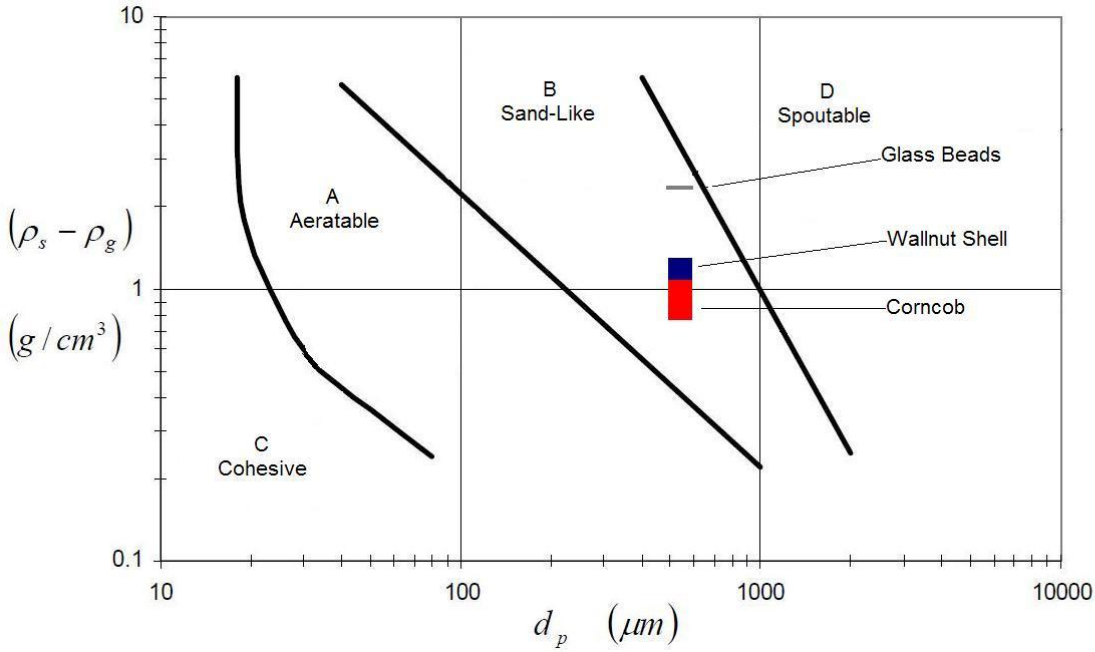

Figure 3.3: Material selection based on Geldart's classification (Geldart, 1973).

To prepare the materials for the fluidization experiments, they are initially sieved to a 500-600 µm size range using a series of sieves of different sizes and a shaker. This process is repeated several times to ensure that the selected particles are located within the desired size range. The procedure is repeated for all three materials, being careful to clean the sieves before changing material to avoid material contamination.

The bed bulk density is determined knowing the material mass and the static bed volume. Bed material is slowly added until the desired static bed height is determined, which corresponded to H/D = 0.5, 1, 1.5, 2, or 3. Before the bed height is measured the bed is fluidized and then allowed to collapse to avoid any packing effects due to the filling process. The material mass is then measured and the given bed bulk density is calculated. Table 3.1 summarizes the characteristics of the various fluidized beds used in this study. Note that the bed bulk density generally decreases slightly as the bed height

increases because the amount of air entrainment increases as the bed is filled. The bulk density error presented in Table 3.1 represents one standard deviation, calculated between the values of bulk density for each H/D ratio, for five measurements.

Table 3.1: Summary of bed characteristics.

	Glass Beads				
Bed Height (cm)	5.1	10.2	15.3	20.4	30.6
H/D	0.5	1	1.5	2	3
Diameter (µm)	500-600	500-600	500-600	500-600	500-600
Bed Weight (g)	590	1180	1775	2440	3640
Bulk Density (kg/m^3)	1410±30	1410±30	1420±30	1465±30	1455±30
Particle Density (kg/m^3)	2600	2600	2600	2600	2600
	Ground Corncob				
Bed Height (cm)	5.1	10.2	15.3	20.4	30.6
H/D	0.5	1	1.5	2	3
Diameter (µm)	500-600	500-600	500-600	500-600	500-600
Bed Weight (g)	155	340	505	690	1030
Bulk Density (kg/m^3)	370±20	410±20	400±20	415±20	410±20
Particle Density (kg/m^3)	800-1200	800-1200	800-1200	800-1200	800-1200
	Ground Wallnut Shell				
Bed Height (cm)	5.1	10.2	15.3	20.4	30.6
H/D	0.5	1	1.5	2	3
Diameter (µm)	500-600	500-600	500-600	500-600	500-600
Bed Weight (g)	235	465	645	900	1365
Bulk Density (kg/m^3)	565±20	560±20	515±20	540±20	545±20
Particle Density (kg/m^3)	1200-1400	1200-1400	1200-1400	1200-1400	1200-1400

3.3 Identifying the Minimum Fluidization Velocity

The minimum fluidization velocity is defined as the minimum superficial gas velocity where particle fluidization is achieved. For this study, the minimum fluidization velocity is used as a reference for different bed heights and bed materials; it is also used as a reference in the X-ray CT imaging work. This section describes the method used to determine the minimum fluidization velocity for each material and for each specific bed height.

To avoid electrostatic effects that may build up during fluidization, the fluidization air is passed through a humidifier before entering the fluidized bed inlet. Several trials in the laboratory have shown that using this simple solution completely eliminated electrostatic effects.

Minimum fluidization velocity is determining using the following pressure measurement procedure. First, the reactor is filled with the desired material to a specified height. Air at $U_g = 40.8$ cm/s is passed through the bed for about an hour to condition the material; this process is repeated each time the material is replaced. After this conditioning period, the pressure and flow rate are acquired using the DAQ system. Data are collected at 1000 Hz over a 5 second interval, averaged over this period, and then output to an Excel file. Next, the air flow rate is decreased by 1 cm/s by closing the pressure regulator. After waiting 60 seconds, a period such that the bed was determined to be in a quasi steady state, the pressure and flow rate were again averaged over a 5 second interval. This process is repeated until the flow rate reaches $U_g = 0$ cm/s; at this point the test is completed. For statistical purposes, each test for the specified material and bed height is repeated 5 times.

After all the bed material data are collected, the same procedure is repeated in an empty reactor. This is done to quantify the pressure drop through the aeration plate and plenum. The empty reactor pressure data are then subtracted from the fluidized bed data at the respective superficial gas velocity. Since the flow rates between the empty reactor and fluidized bed tests do not match exactly, a linear interpolation method is employed to calculate the empty bed pressures corresponding to the fluidized bed flow rates. Finally, the bed pressure drop is plotted as a function of superficial gas velocity and the minimum fluidization velocity is defined as the point in which the pressure drop across the bed remains constant. Figure 3.4 shows a sample plot obtained for glass beads where the

static bed height corresponds to H/D = 1. The minimum fluidization velocity (U_{mf}) is equal to 21.3 cm/s, which is similar to that determined by Franka (2008).

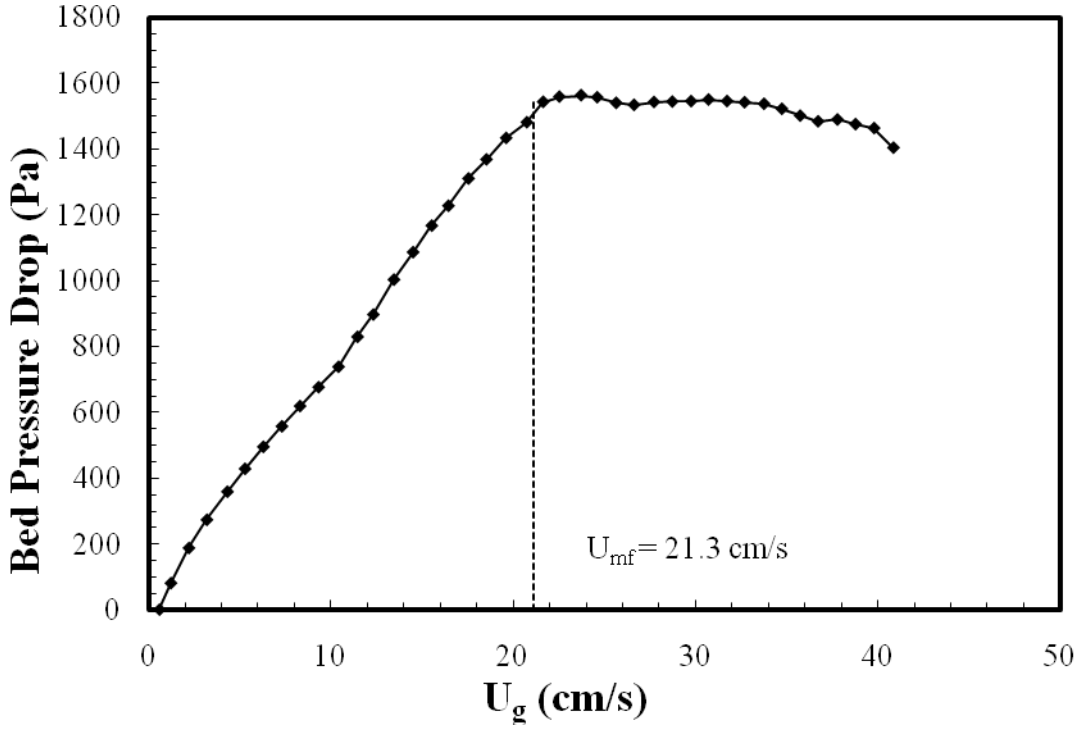

Figure 3.4: Sample minimum fluidization plot for glass beads with H/D = 1.

3.4 X-ray Facility

The X-ray equipment present in the X-ray Flow Visualization (XFloViz) facility at Iowa State University for the study of multiphase flow systems is described in this section. The first subsection describes the different components of the X-ray facility, followed by a description of the X-ray computed tomography imaging procedures as well as calibration techniques. Finally, the last subsection explains how gas holdup data is obtained using the CT images of the object of interest.

3.4.1 X-ray Equipment

The X-ray equipment used in this research is the same as that described by Heindel et al (2008). The equipment consists of two LORAD LPX200 portable X-ray sources. X-rays are emitted from the beryllium window on the tubehead in a 60° horizontal, 40°

vertical conical beam. The beam spot size of each source is 1.5 mm. Current and voltage can be adjusted from 0.1 to 10.0 mA and 10 to 200 kV, respectively, with a maximum total power of 900 W. The X-ray tubes are liquid-cooled with two LORAD pump systems. X-ray energy is limited by a collimator surrounding the source. Copper and aluminum filters may be placed in front of the source to reduce the low energy radiation. Filters are used according to the attenuation characteristics of the object being visualized.

An X-ray detector/CCD camera pair is located opposite each X-ray source. The XFloViz facility has two image intensifier/CCD camera detectors which are used primarily for radiographic and stereographic imaging due to their relatively high temporal resolution and good spatial resolution. A second detector/camera pair is primarily used for CT imaging because of its high spatial resolution. In addition, individual radiographs may be captured. For this system, incident X-ray energy is transformed into visible light by a square 44×44 cm cesium-iodide (CsI) scintillator screen. A 50 mm Nikon lens captures images which are digitized by an Apogee Alta U9 system. This system has 3072×2048 active pixels and is thermoelectrically cooled to allow long exposure times with low noise conditions. One difficulty in using the CsI scintillator screen is in the response of the scintillation crystals at the beginning of an X-ray test. If the detector is used without previously exciting the crystals, the detector's response will change throughout a test, causing inaccurate data. To overcome this problem, the scintillator is excited with X-rays for approximately 20 minutes before data collection. Additionally, the scintillator requires about 5 minutes without incident X-rays to completely return to an unexcited state.

The detectors and sources are mounted on extension arms from a 1.0 m ID rotation ring that can rotate 360º around the fluidized bed. The rotation ring is controlled by a stepper motor to allow for different visualization orientations. The facility also features a

vertical lift which is located under the imaging region to adjust the vertical location of an object. The lift is controlled by a 910 kg winch to provide 2.75 m of vertical travel, giving an overall span of 4 m. The data are acquired using software developed at Iowa State University. The software allows control of both detectors and provides motion control for the rotation ring.

3.4.2 X-ray Computed Tomography

X-ray computed tomography (CT) scans are captured for all three materials at different H/D ratios (0.5, 1, 1.5, 2, 3) and different superficial gas velocities U_g = 1.25, 1.5, 1.75, 2, 3 U_{mf}. CT images allow for quantitative analysis of the time-average local gas holdup, and identified the effects that different bed heights and material densities have on the hydrodynamic behavior in a fluidized bed.

3.4.2.1 Experimental Procedures

The following procedure is used for each acquired CT scan in this study. First, the X-ray source that is located opposite the CT detector is warmed up at the same time the thermoelectric cooler on the camera is simultaneously cooled to 0°C to reduce noise and allow for long CT scans. Software called PS_CT is used to initiate the system. This program captures the CT images, controls the camera settings, controls the rotation ring motion, and displays real-time X-ray images. After completing the warm-up process, the X-ray voltage and current, as well as the camera exposure time and binning options are adjusted based on the bed material in the imaging region. For this study, the power settings are constant for each material, regardless of flow and bed height conditions. Glass beads are acquired at a voltage of 150 keV and a current of 3.5 mA, ground corncob and ground walnut shell images are acquired at 130 keV and 3.2 mA. For this research, the exposure time is set to 1 second and the binning is set to 4×4. After the power settings are adjusted, two images are taken without any object located in the

imaging region. A dark image is captured without incident X-ray energy, and a flat image, which is captured using incident X-ray energy at the power settings determined for each material, which corresponds to near image saturation. These two images are used for a linear normalization calibration discussed in the following section.

Next, the fluidized bed is placed in the imaging region and the scintillation crystals in the detector are excited with X-rays for 20 minutes. The fluidized bed is positioned in the same location for the three materials. However, as the H/D ratio increases, it is necessary to move the bed stand down so that all bed material is located within the imaging region and CTs can be acquired. CT scan settings are then adjusted; including the number of vertical slices (horizontal cross-sections), slice interval, and slice start location. Once the settings are adjusted, the system is ready to start a CT scan. Each CT scan in this research is completed in approximately 45 minutes. The CT data are stored in a series of sinogram (.sin) files, each with information for 10 vertical cross-sections of data. Glass bead sinograms are corrected for beam hardening (to be explained in the following subsection) using another computer program. After, the sinogram files are saved, the next step is to find the center of rotation (COR). This parameter determines the alignment of the detectors and is necessary for the reconstruction of the volume files. This parameter is iteratively found by reconstructing a single horizontal cross-section of the volumetric image using several COR values; the value yielding the clearest image is chosen as the COR for the volume file. COR values are determined for both the bottom and top slice of the volumetric image to account for rotational alignment (Franka, 2008). For this study, the location of the detectors remained constant, therefore the COR is the same for all the experiments and in this case is 379. This number represents the center of the image at the radial axis, for both the top and bottom slices; the same number is used to interpolate for the rest of the slices at the reconstruction process.

After the sinogram files are generated and the COR determined, the files are transferred to a cluster at CNDE (Center for Nondestructive Evaluation) for reconstruction. Volume files are reconstructed and analyzed using X-ray Image Processor (XRIP) software specifically developed for the XFloViz facility. XRIP allows selecting the region of interest (ROI) in the image and generated 2-D images of different planes. For this study, three viewing axes are selected, images in the x-y plane at different heights, x-z plane in the center of the bed, and y-x plane passing through the center of the bed. Figure 3.5 shows the different CT imaging slices used in this study. A false color scale is applied to each image to have better appreciation for the flow structure.

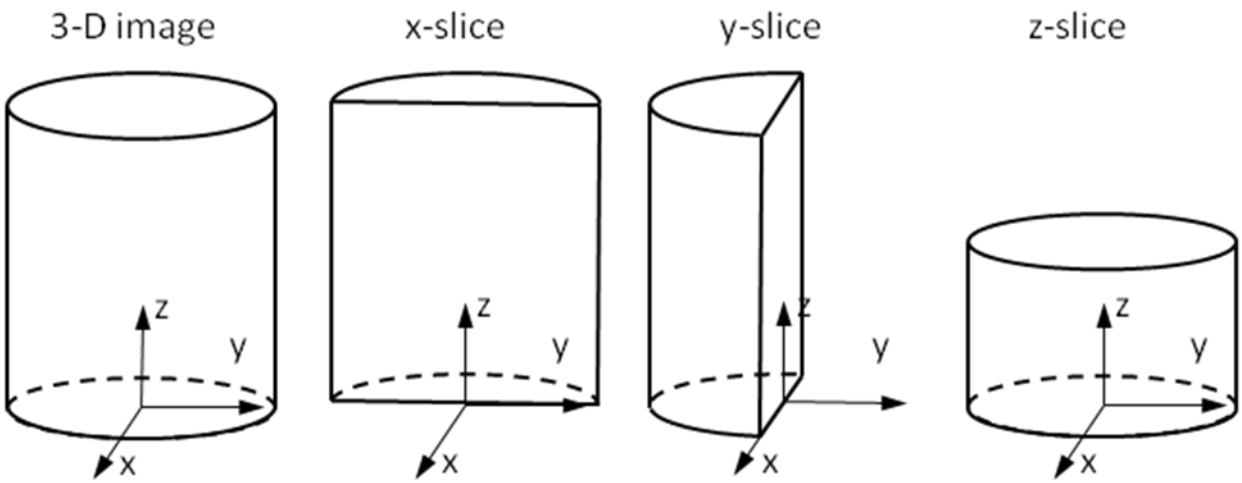

Figure 3.5: CT imaging slices (Franka, 2008)

3.4.2.2 Calibrations

Several techniques are applied to the data to reduce the effects of the artifacts caused by the CT imaging system. Ketcham and Carlson (2001) discussed several artifacts produced by CT imaging systems; some of the most frequent artifacts presented are beam hardening, ring artifacts, and partial volume effects. For this study, calibrations to correct pixel normalization and beam hardening effects are applied, as well as a calibration to

correct a reference difference in the volume files, due to the movement of the stand where the fluidized bed is situated.

3.4.2.2.1 Pixel Normalization

When reconstructing CT images it is important to account for pixel response uniformity, which ideally each pixel in the detector should react identically to the same X-ray intensity. However, in real conditions this ideal situation does not happen and a nonuniform pixel response in the detector is common (Heindel et al., 2008). Therefore, these nonuniformities are corrected to avoid their presence in the resulting CT images which typically produce ring artifacts. In this study, linear pixel normalization is applied to reduce the effects of the pixel nonuniformities. This method uses two images, a dark and a flat image, to get an average pixel response of each pixel in the entire imaging region. Then, assuming a linear response, a normalization factor for each pixel is determined comparing the pixel intensity with the average response. These factors are stored in the PS_CT software to be applied to subsequent scans.

3.4.2.2.2 Beam Hardening

Beam hardening is a common artifact present during the reconstruction of CT volume files, and is caused by the difference in which lower energy X-rays are attenuated in comparison with higher energy X-rays. This difference produces dark regions around the center and lighter regions around the edges of the CT images. Beam hardening effects appears in most materials; however, denser materials like glass beads exhibit more beam hardening than lower density materials like ground corncob, or ground walnut shell (Franka, 2008).

For this study, beam hardening corrections are applied just to glass bead sinogram files where beam hardening is noticeable, while in ground corncob and ground walnut shell no corrections for beam hardening are applied. The methods used to correct beam

hardening effects are explained in detail by Franka (2008). This study used filters to suppress low energy X-rays; for the three materials the filters used are copper and aluminum with a thickness of 0.6 mm and 1.5 mm, respectively. The correction factor curve fit used by Franka (2008) is applied to the raw sinogram files using the SAS Beam Hardening program developed by CNDE. The corrected files are then used in the reconstruction of the volume files.

3.4.2.2.3 Volume File Correction

As height-to diameter ratio (H/D) increased, it is necessary to move the stand down in order to have the region of interest located within the imaging region of the detector and be able to acquired the CT images.

Several trials at the laboratory showed that when the stand is moved to a different position inside the X-ray facility, a discontinuity in the results may be observed due to background CT intensity variations. To correct this variation, CT scans were taken without any object between the X-ray source and the detector at the two different stand positions. Once the sinogram files were reconstructed into a volume file, the average of the intensity values were calculated using XRIP software. Then, the difference between the values at the two different positions was calculated.

With this correction factor, the volume files containing the information of the different materials at the different flow and H/D conditions, as well as the volume files containing the bulk material and the air information were arithmetically manipulated using XRIP software to include this correction factor into their CT intensity values. These corrected volume files were used to determine the gas holdup for the three materials.

3.4.3 Determining Gas Holdup from CT Data

Time-average local gas holdup information is calculated using the data obtained from the CT reconstruction volume files. Gas holdup as mentioned in Chapter 2 is the amount

of gas present in the solid material, and is useful to characterize the hydrodynamic behavior of the multiphase flow system. Quantifying the local time-average gas holdup, ε_g, using the XRIP program requires the CT intensity of the empty reactor (I_g), a CT intensity of the reactor filled with a fixed bed of the bulk material (I_b), and a CT intensity of the reactor under specified fluidization conditions (I_f). To ensure the same response for each condition from the detector system, each CT is taken with the same X-ray source power settings for the respective conditions.

The local time-average gas holdup is then determined from the two reference CT images and the flow CT image (Franka, 2008):

$$\varepsilon_g = \frac{I_f - I_b + \left(I_g - I_f\right)\left(\varepsilon_{g,b}\right)}{I_g - I_b} \tag{3.1}$$

where the bulk void fraction, $\varepsilon_{g,b}$, is defined as:

$$\varepsilon_{g,b} = 1 - \frac{\rho_b}{\rho_p} \tag{3.2}$$

where ρ_b and ρ_p are the measured bulk and particle density, respectively.

The method used to calculate the gas holdup using XRIP is the following: the air and the bulk files pass through a smoothing process. Smoothing takes a volumetric pixel (voxel) value and averages it with the 27 surrounding voxels; this procedure reduces the noise caused by each local voxel. After the smoothing process is finished, XRIP calculates the gas holdup using the derivation explained above. The resulting file is passed through another smoothing process to further reduce the effects of noise. Finally, the resulting file is analyzed to determine the effects that material density and bed height have on the gas holdup.

3.5 Summary

This chapter described the equipment and the experimental procedure used for this research project. The first section described the cold-flow fluidized bed reactor components, the air flow system, and the instrumentation used in this study. The next section overviewed the procedure used to select and prepared the material for the experiments. Three different materials, glass beads, ground corncob, and ground walnut shell, located in the Geldart B classification, allowed for comparisons between materials. The process followed to determine the minimum fluidization velocity at different flow rates and different bed heights was also explained in this section.

The XFloViz facility was used to perform the noninvasive analysis of the flow structure behavior in the fluidized bed. The description of the X-ray equipment, as well as the procedure used to take X-ray CT scans was explained in section 3.4. Moreover, several calibration procedures used to eliminate image artifacts and noise from the resulting images was briefly described.

Finally, time-average local gas holdup was calculated using the software XRIP developed in our laboratory. The method used to calculate gas holdup uses a smoothing process of the gas and bulk volume files, then calculates the gas holdup with the intensity values of the gas, bulk and flow files, and finally passes the resulting 3D file through another smoothing process to minimized noise. The results obtained for the minimum fluidization velocity and for the time-average local gas holdup for the three materials operating at the different experimental conditions are presented in the following chapter.

Chapter 4: Results and Discussion

This chapter presents and discusses the results obtained from this research, focusing on explaining the hydrodynamic behaviors of the fluidized bed with the different tested conditions. The first subsection overviews the bed height and material density effects on the minimum fluidization velocity experiments. The second subsection summarizes the results obtained on the local time-average gas holdup experiments, first describing the effects of bed height on local time-average gas holdup, and then analyzing the material density effects on the local time-average gas holdup.

4.1 Minimum Fluidization Velocity

Minimum fluidization velocity results for glass beads, ground walnut shell, and ground corncob at five different height-to-diameter ratios (H/D) are presented in this section. Each material was tested 5 times at each H/D ratio for statistical purposes.

Furthermore, as shown in Figure 4.1, bed pressure drop increased when the H/D ratio increased. This effect is related to the bulk density and mass of the material. Hence, the bed pressure drop for glass beads is larger than for ground corncob and ground walnut shell.

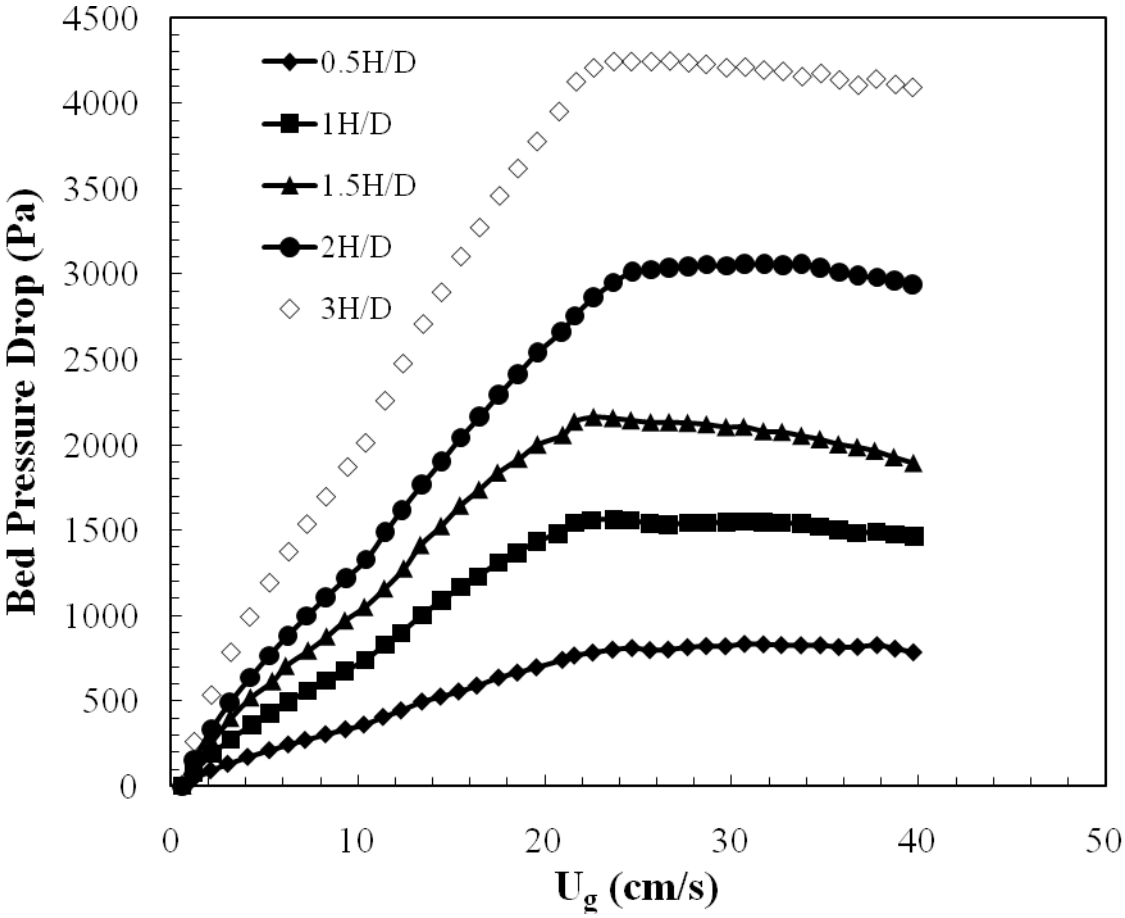

Figure 4.1: Bed pressure drop as a function of superficial gas velocity for glass beads.

Minimum fluidization velocity, on the other hand, did not show considerably changes when the H/D ratio increased. Figure 4.2 shows that the minimum fluidization velocity for the three materials is approximately constant. Note the error bars represent 1 standard deviation from the average of the five tests. Hence, it can be concluded that there is not a correlation between bed height and minimum fluidization velocity for this cylindrical fluidized bed. Table 4.1 provides a summary of the numerical values presented in Figure 4.2.

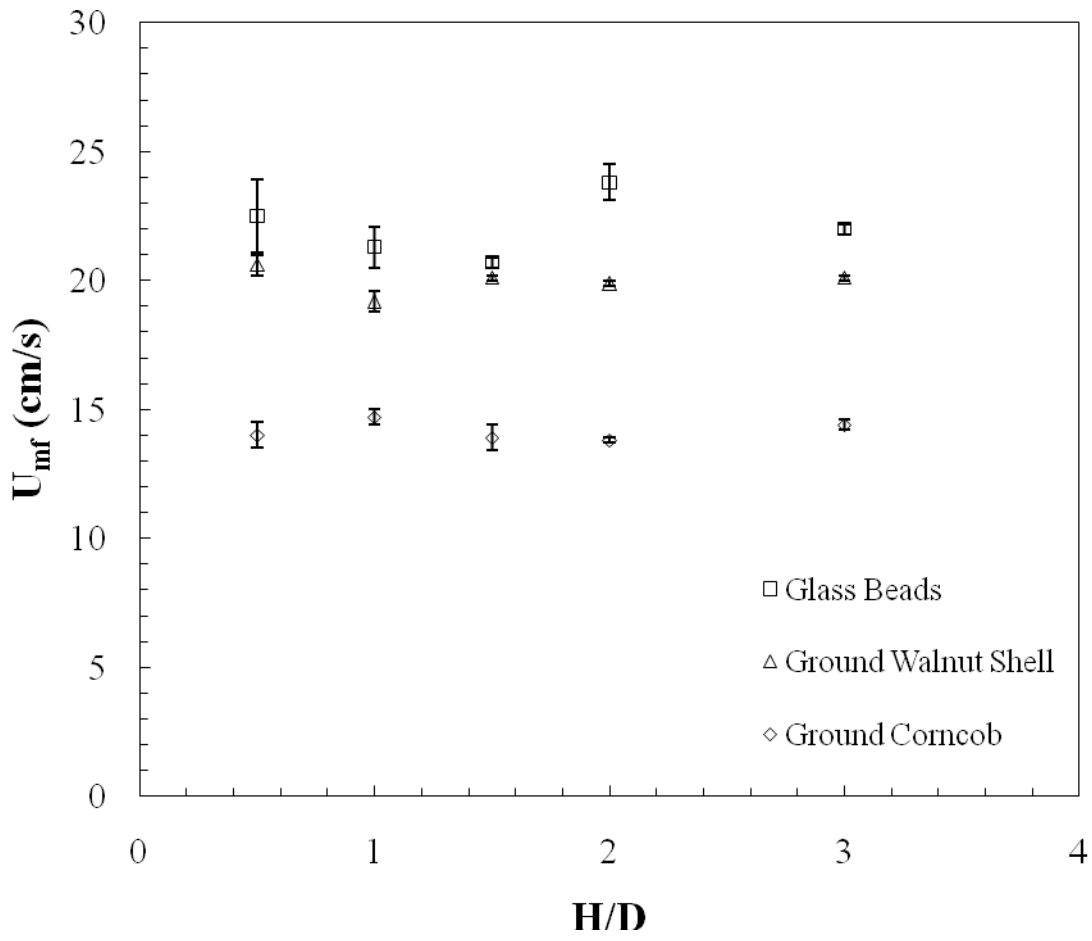

Figure 4.2: Minimum fluidization velocity as a function of height-to-diameter ratio (H/D).

Table 4.1: Minimum fluidization velocity results.

	Glass Beads	**Ground Corncob**	**Ground Walnut Shell**
H/D	**U_{mf} (cm/s)**	**U_{mf} (cm/s)**	**U_{mf} (cm/s)**
0.5	22.5 ± 1.4	14 ± 0.5	20.6 ± 0.4
1	21.3 ± 0.8	14.7 ± 0.3	19.2 ± 0.4
1.5	20.7 ± 0.2	13.9 ± 0.5	20.1 ± 0.1
2	23.8 ± 0.7	13.8 ± 0.1	19.9 ± 0.1
3	22 ± 0.2	14.4 ± 0.2	20.1 ± 0.1

A force balance between the gravity and pressure force was obtained for each material to emphasize the minimum fluidization velocity. As it is shown in Figures 4.3 - 4.5, the knee of the graphs indentifies U_{mf} and is approximately independent of bed height for the three materials, and is located on the y-axis near 1. However, the values of the bed

pressure force over the bed weight that surround the knee of the graph are not perfectly 1 due to non-spherical particle effects as well as wall effects. In these figures, the U_{mf} values is the average of all tests for the respective material.

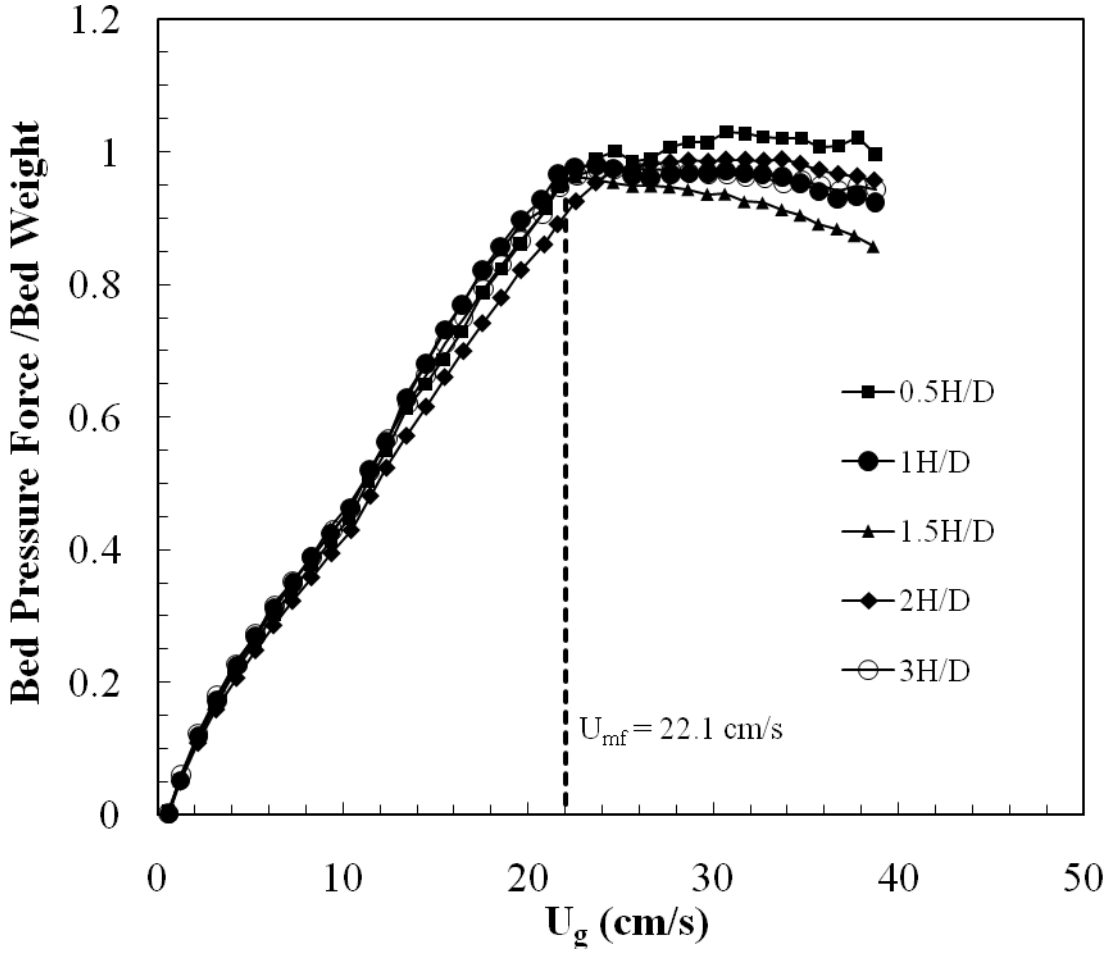

Figure 4.3: Bed pressure force/bed weight as a function of superficial gas velocity for glass beads.

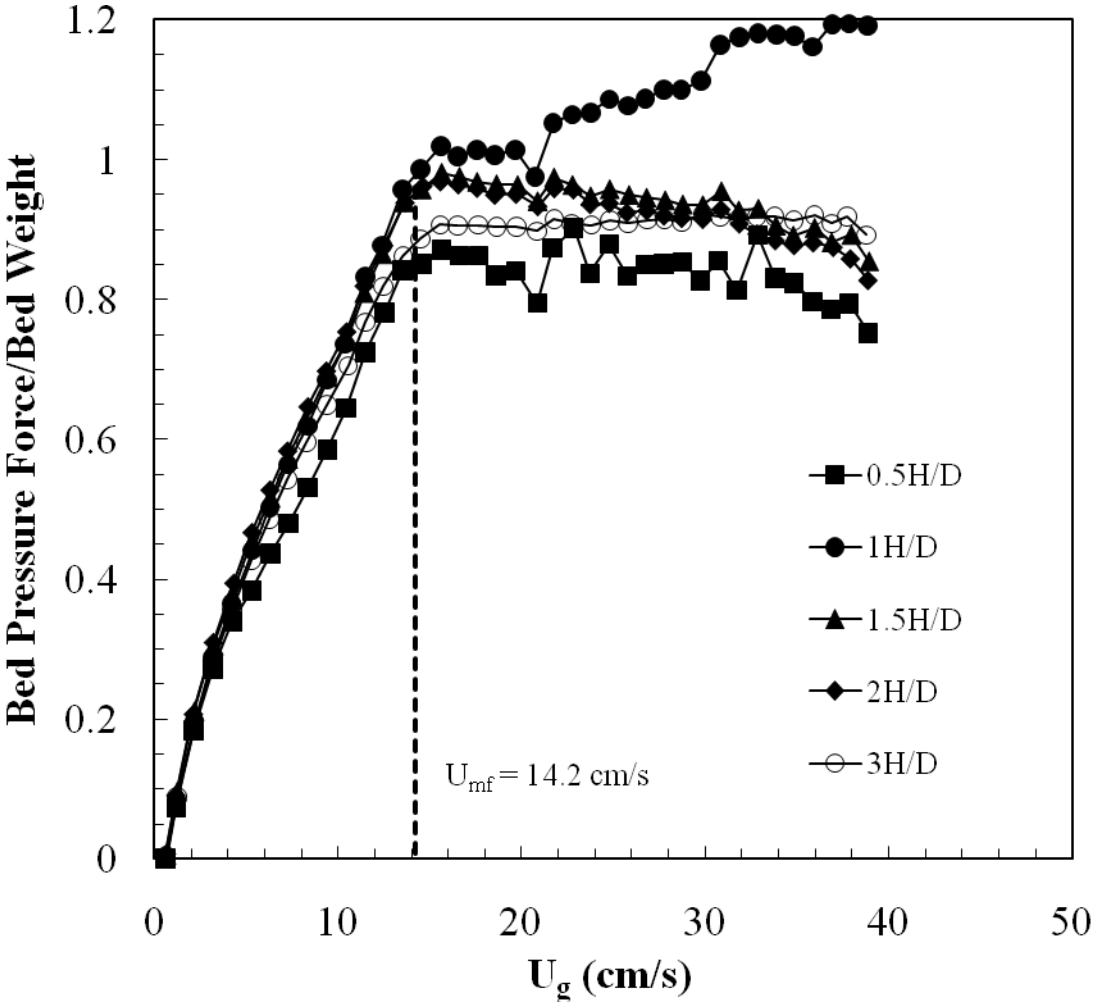

Figure 4.4: Bed pressure force/bed weight as a function of superficial gas velocity for ground corncob.

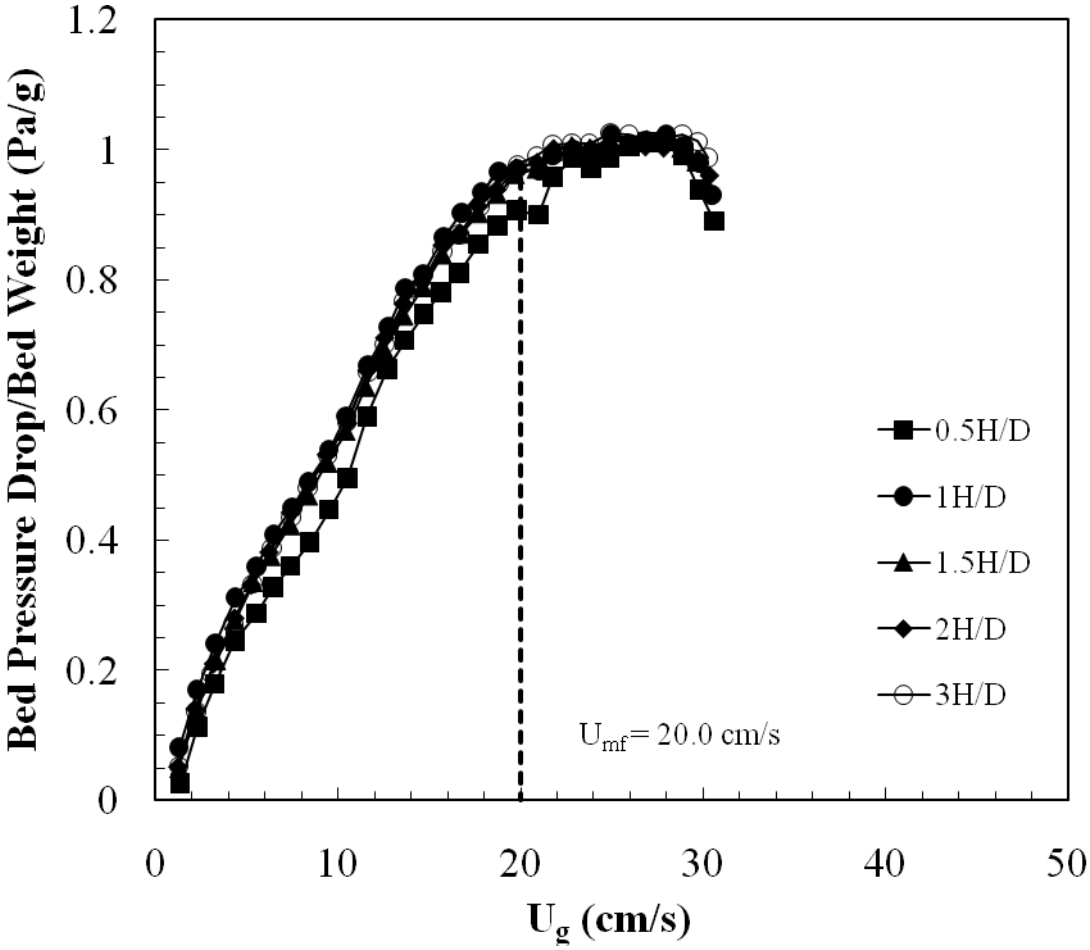

Figure 4.5: Bed pressure force/bed weight as a function of superficial gas velocity for ground walnut shell.

At higher superficial gas velocities, the ratio between bed pressure drop and bed weight shows a slight decrease, which is attributed to the frictional forces on the walls of the fluidized bed. However, it is interesting that for one test of ground corncob with H/D = 1 (Figure 4.4), the behavior is inverse to that of the other materials. This behavior can be attributed to the low density of the material, and at higher superficial gas velocities, some of the material is elutriated, causing less material to be present inside the bed chamber reducing the bed weight. Subsequent experiments were completed with a screen over the top chamber to minimize this effect.

The minimum fluidization velocity is influenced by changes in density, as shown in Figure 4.6. In this figure, denser material (glass beads) exhibit a larger pressure drop than less dense materials (ground walnut shell, and ground corncob). Since the volume of each material is constant, high density materials have more mass than low density materials. Therefore, in order to fluidize the material, a higher superficial gas velocity is required to overcome the bed weight. Consequently, a larger pressure drop is produced with high density materials, increasing U_{mf}.

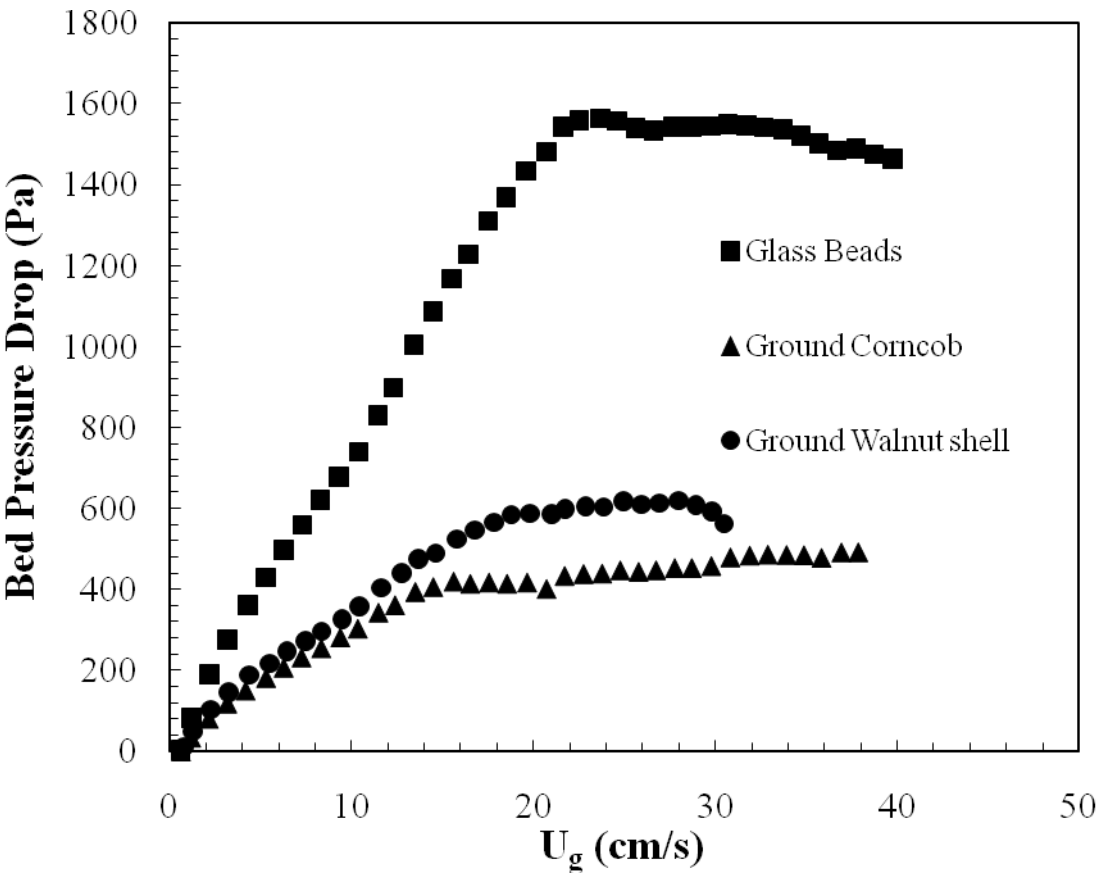

Figure 4.6: Bed pressure drop as a function of gas velocity for glass beads, ground corncob, and ground walnut shell for H/D = 1.

Comparing the fluidization force to the bed height clearly shows material density effects on U_{mf}. A denser material requires more bed pressure force to equalize the gravity force of the bed in order to achieve fluidization. Figure 4.7 shows the effect of material density on the fluidization force balance. The knee, indicating the minimum fluidization

velocity, occurs approximately at a force balance equal to 1. This figure clearly shows U_{mf} increases with increasing material density.

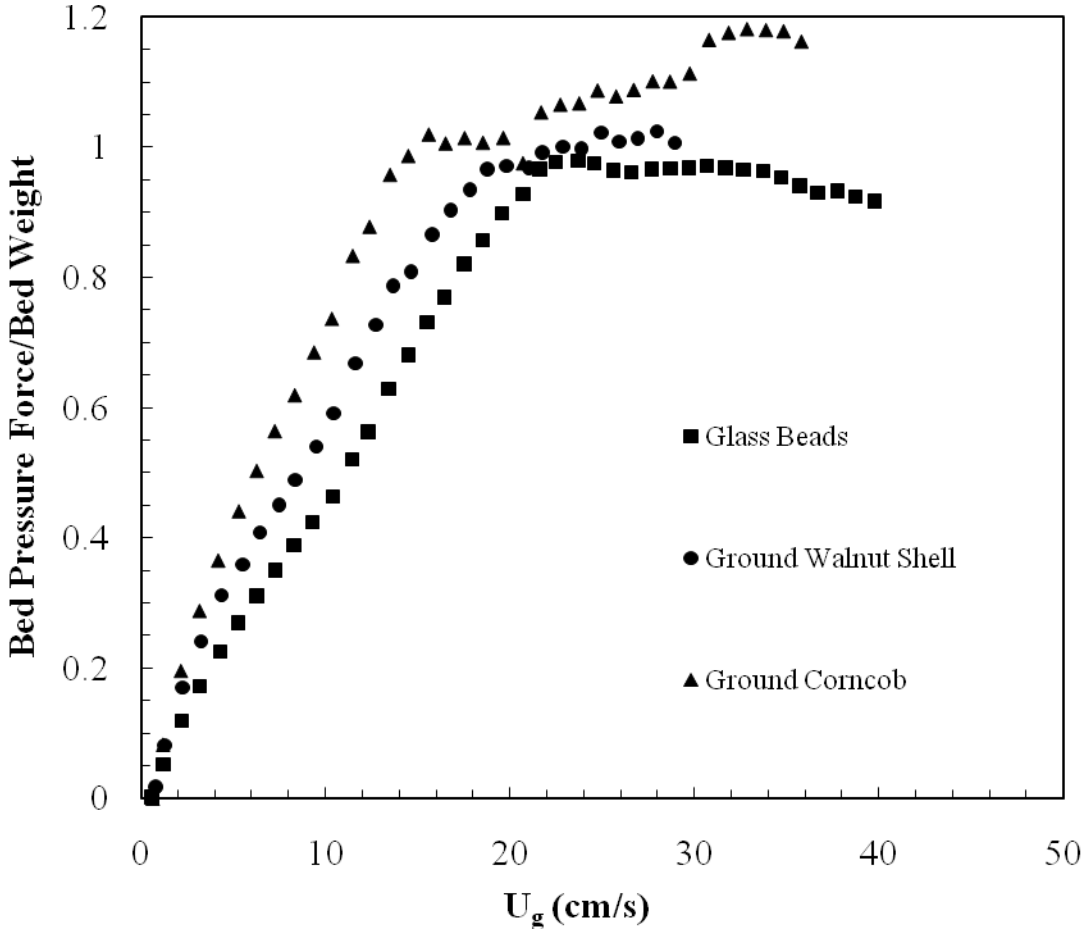

Figure 4.7: Effect of material density on fluidization force balance for H/D = 1.

4.2 Gas Holdup

Local time-average gas holdup results obtained using X-ray computed tomography for glass beads, ground corn cob, and ground walnut shell at different height-to-diameter ratios (H/D), with different fluidization conditions, are presented in this section. Table 4.2 outlines the experimental conditions for each material. The first subsection addresses the effects caused by the change in the H/D in the gas holdup, while the following subsection identifies the effects caused by the different material density.

Table 4.2: Experimental conditions

Glass Beads	
U_{mf} (cm/s)	**22.1**
$U_g = 1.25\ U_{mf}$	27.6
$U_g = 1.5\ U_{mf}$	33.2
$U_g = 1.75\ U_{mf}$	38.7
$U_g = 2\ U_{mf}$	44.2
$U_g = 3\ U_{mf}$	66.3
H/D = 0.5, 1, 1.5, 2	
Ground Corncob	
U_{mf} (cm/s)	**14.2**
$U_g = 1.25\ U_{mf}$	17.8
$U_g = 1.5\ U_{mf}$	21.3
$U_g = 1.75\ U_{mf}$	24.9
$U_g = 2\ U_{mf}$	28.4
$U_g = 3\ U_{mf}$	42.6
H/D = 0.5, 1, 1.5	
Ground Walnut Shell	
U_{mf} (cm/s)	**20**
$U_g = 1.25\ U_{mf}$	25
$U_g = 1.5\ U_{mf}$	30
$U_g = 1.75\ U_{mf}$	35
$U_g = 2\ U_{mf}$	40
$U_g = 3\ U_{mf}$	60
H/D = 0.5, 1, 1.5	

To allow for qualitative gas holdup comparisons, a series of 2D y- and z- slices images are presented. These images contribute to the understand of the behavior and symmetry of the fluidization as the flow and height conditions change. Moreover, to show more quantitative results, time-average local gas holdup data are plotted as a function of spatial location inside the fluidized bed.

4.2.1 Height-to-Diameter Ratio Effects on Local Gas Holdup

The 3D time-average gas holdup obtained from Eq. (3.1) can be viewed anywhere within the fluidized bed. Images of y-slice and z-slice gas holdup at specific superficial gas velocities for glass beads at different H/D ratios are presented in Figures 4.8 - 4.12, y-

slice images are taken in the center of the bed, while z-slice images are taken at five different axial heights (h = 2.5 cm, 5.1 cm, 10.2 cm, 15.3 cm, and 20.4 cm) to show how fluidization structure and gas holdup change with increasing superficial gas velocity and increasing H/D ratio. When $U_g = 1.25U_{mf}$ (Figure 4.8), the gas holdup map is similar for all H/D values. Observing the different slices at H/D= 0.5, the gas holdup range is between 0.4 and 0.6, with the highest local gas holdup located near the reactor walls.

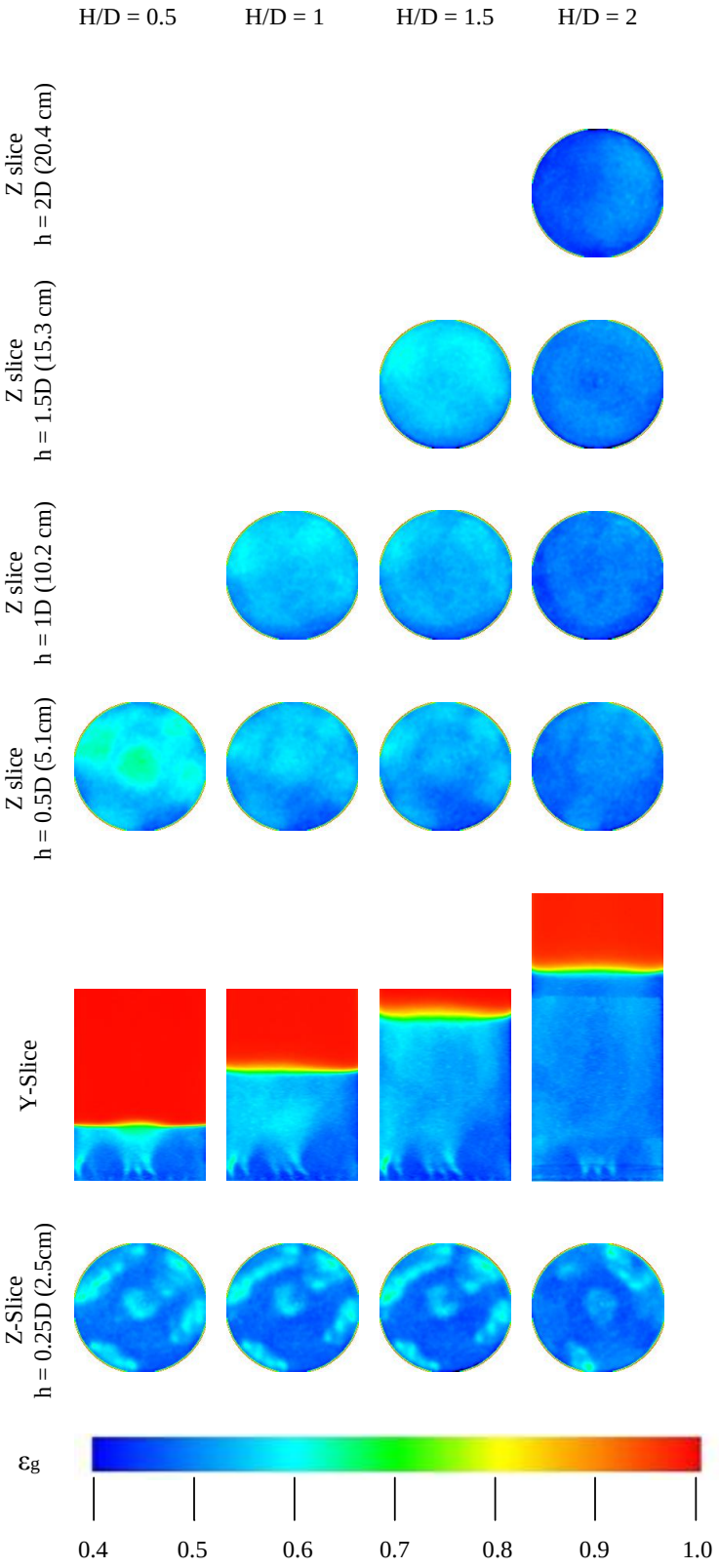

Figure 4.8: Glass beads gas holdup y- and z- slices for $U_g = 1.25U_{mf}$ at different H/ D ratios.

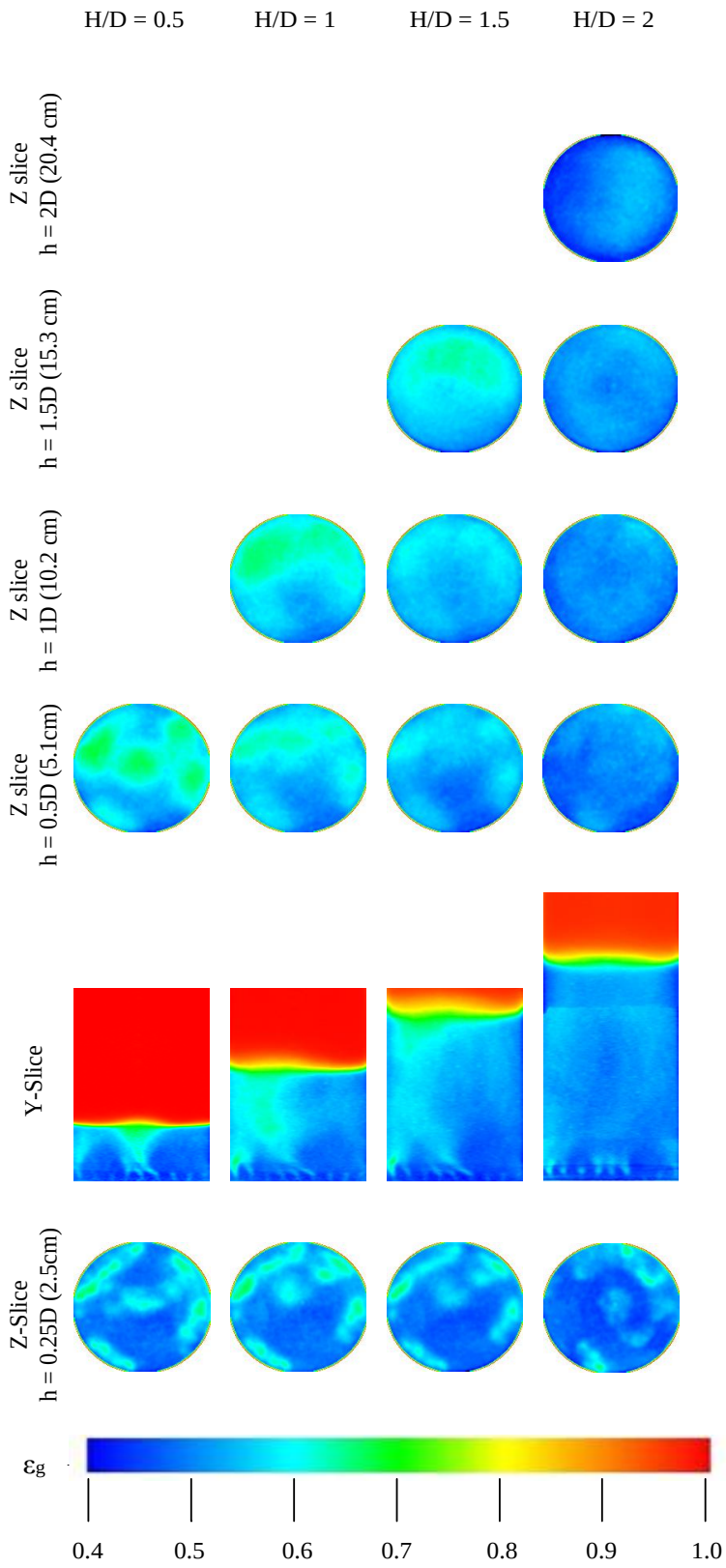

Figure 4.9: Glass beads gas holdup y- and z- slices for $U_g = 1.5U_{mf}$ at different H/ D ratios.

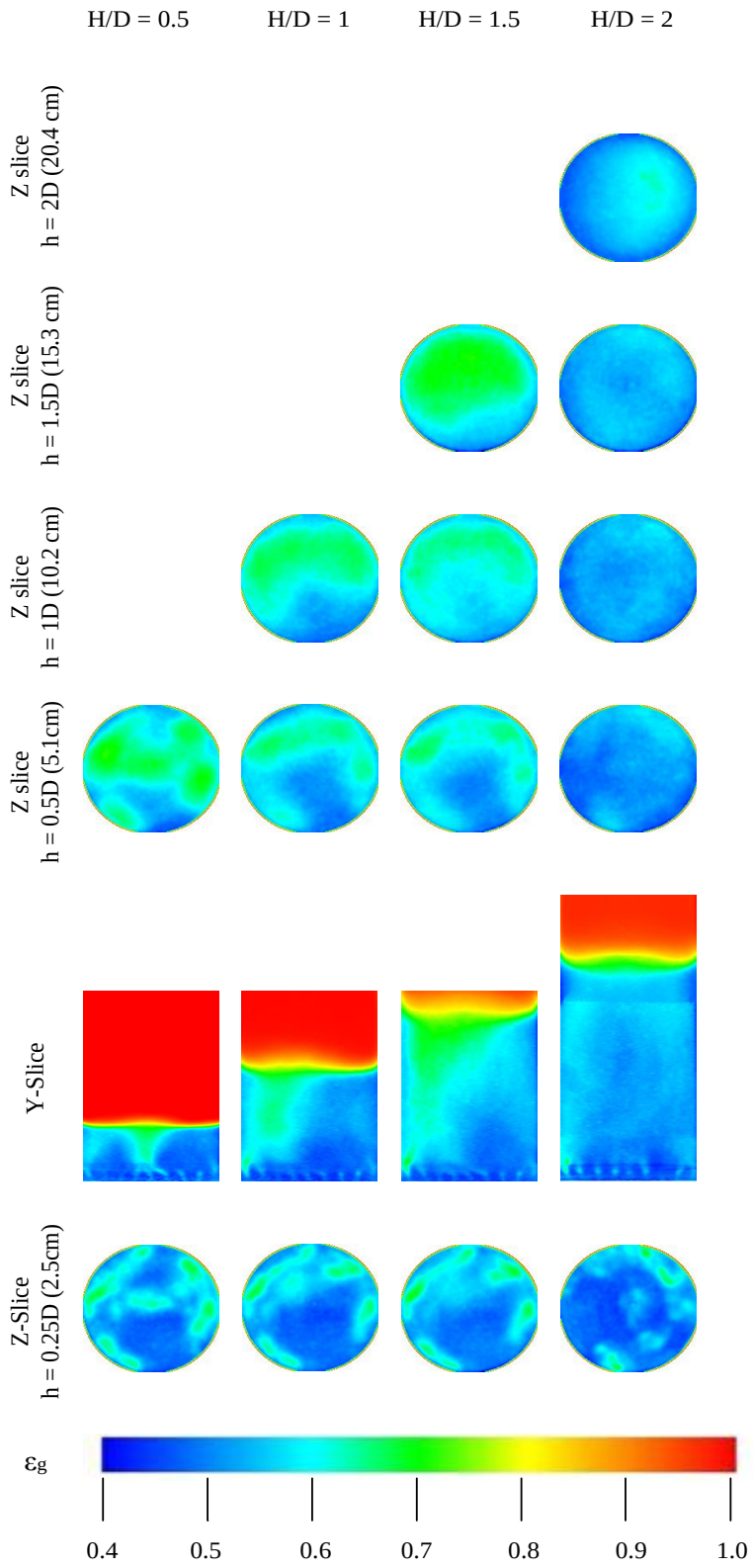

Figure 4.10: Glass beads gas holdup y- and z- slices for $U_g = 1.75U_{mf}$ at different H/ D ratios.

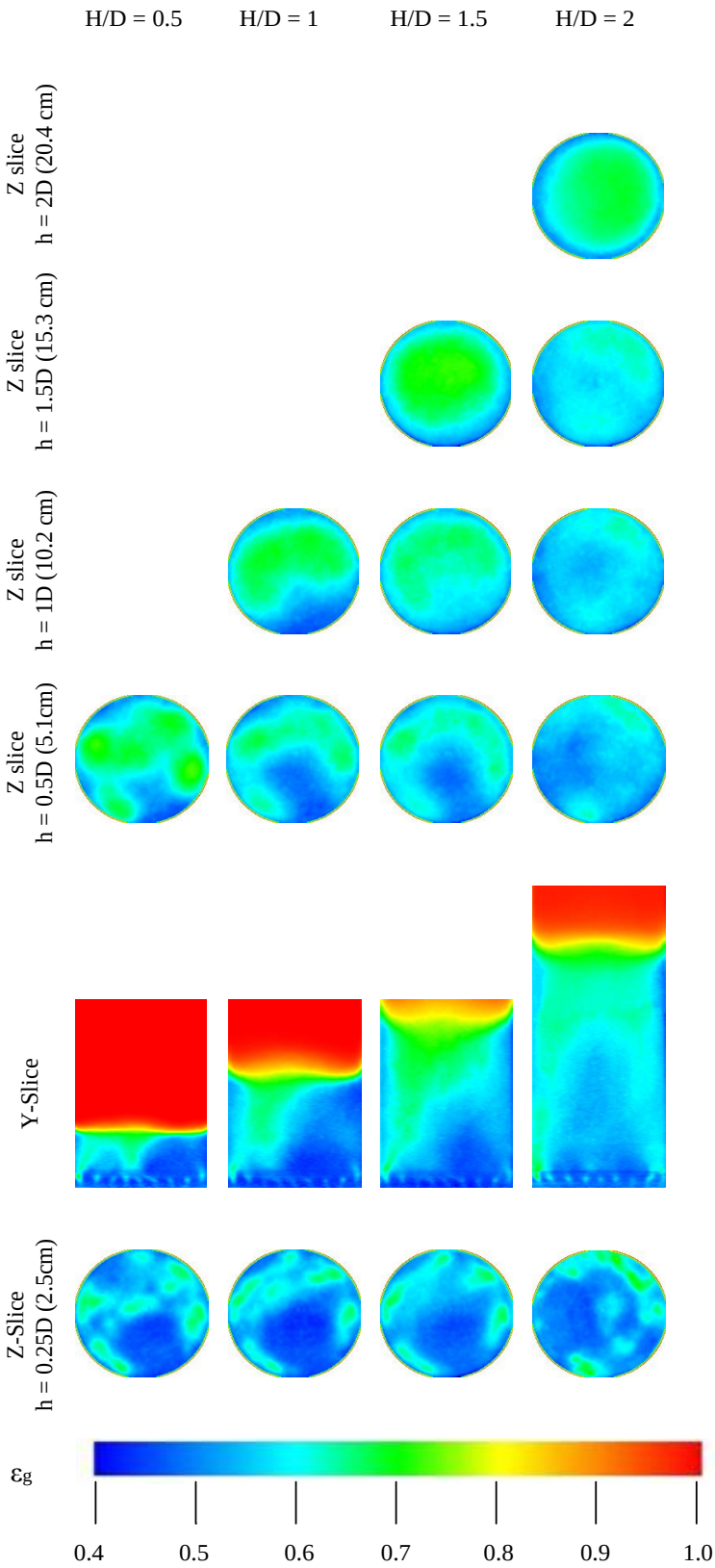

Figure 4.11: Glass beads gas holdup y- and z- slices for $U_g = 2U_{mf}$ at different H/ D ratios.

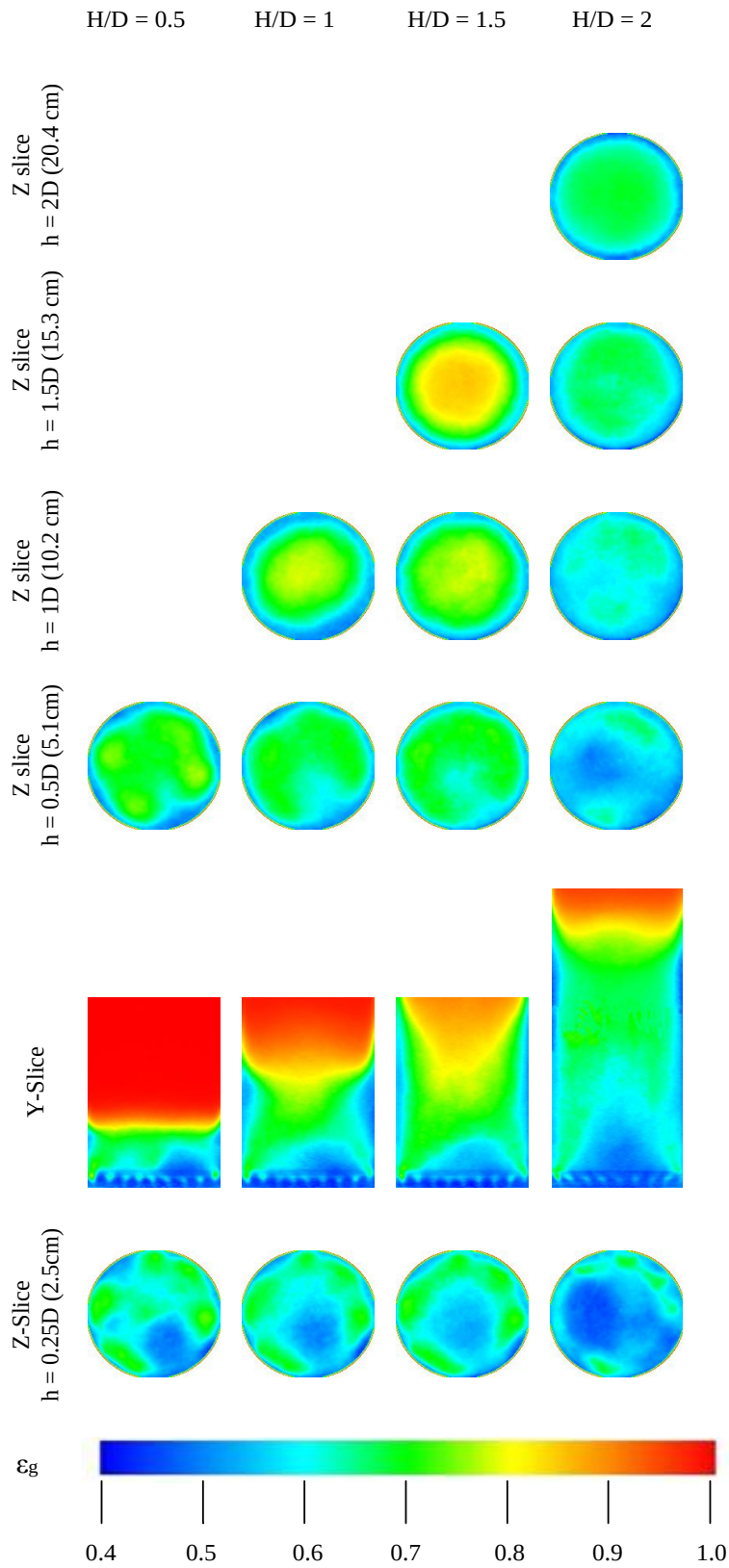

Figure 4.12: Glass beads gas holdup y- and z- slices for $U_g = 3U_{mf}$ at different H/ D ratios.

Jetting from individual aeration holes is observed in the y-slice images in the above figures. It is observed that increasing U_g increases the number of active aeration holes. Additionally, increasing U_g decreases the jet length because mixing in the fluidized bed increases and the individual jets lose their identity.

Gas holdup increases as superficial gas velocity increases; this is primarily attributed to a higher volume of air passing through the bed. For $U_g = 1.25U_{mf}$, a high local gas concentration is located in the bottom-center of the bed as well as in the edges of the bed as it can be seen in the y-slice and in the z-slice located at h=0.25D (2.5 cm) (Figure 4.8), this behavior indicates that the air is flowing mostly through the center of the bed, this structure is observed at all the H/D ratios tested. Above this region, the local gas holdup is generally uniform. For the case of $1.5U_{mf}$ and $1.75U_{mf}$, the air is no longer concentrated in the center of the bed as observed in Figures 4.9 and 4.10, but mostly is flowing around the bed walls. However, this behavior is observed just for H/D ratios of 1 and 1.5. In the case of H/D = 0.5, the trend follows the one described for $U_g = 1.25U_{mf}$. As the superficial gas velocity increases to $U_g = 2U_{mf}$ and $U_g = 3U_{mf,}$ particularly for H/D greater than 0.5, regions of low gas holdup are shown in Figure 4.11 and 4.12 near the bottom center of the bed. Above this low gas holdup region, a high gas holdup is observed because as the bubbles rise, they coalesce and migrate toward the bed center, increasing the gas holdup in this region. The large bubbles erupt from the bed near the center, throwing glass beads against the wall, which fall back into the bed. These hydrodynamics create high gas holdup regions near the top center of the bed while lower gas holdup regions (higher solids concentration) are found along the bed walls. Increasing the H/D ratio allows for additional bubble coalesce creating slugs inside the bed, which rise in the bed center, enhancing the gas holdup differences near the top of the bed.

Moreover, flow structure for ground corncob is presented in Figures 4.13 and 4.14 at two fluidization conditions ($U_g = 1.25U_{mf}$ and $3U_{mf}$) for different H/D ratios. Ground corncob at lower superficial gas velocities (Figure 4.13) presents a uniform fluidization structure throughout the bed. However, at higher superficial gas velocities (Figure 4.14), the fluidization uniformity of the material change, high gas holdup paths are visualized flowing through the center of the bed surrounded by low gas holdup regions near the walls of the bed; once again this effect is attributed to the natural motion of the particles when they are ejected out of the bed by the rising bubbles and then falling back into the bed around the walls of the fluidized bed. Looking at the different z-slices in Figures 4.13 and 4.14, the small red line that appears surrounding the slices are gas holdup values that are located just outside the region of interest, therefore they do not represented any trend or fluidization structure, those were captured when the images where processed.

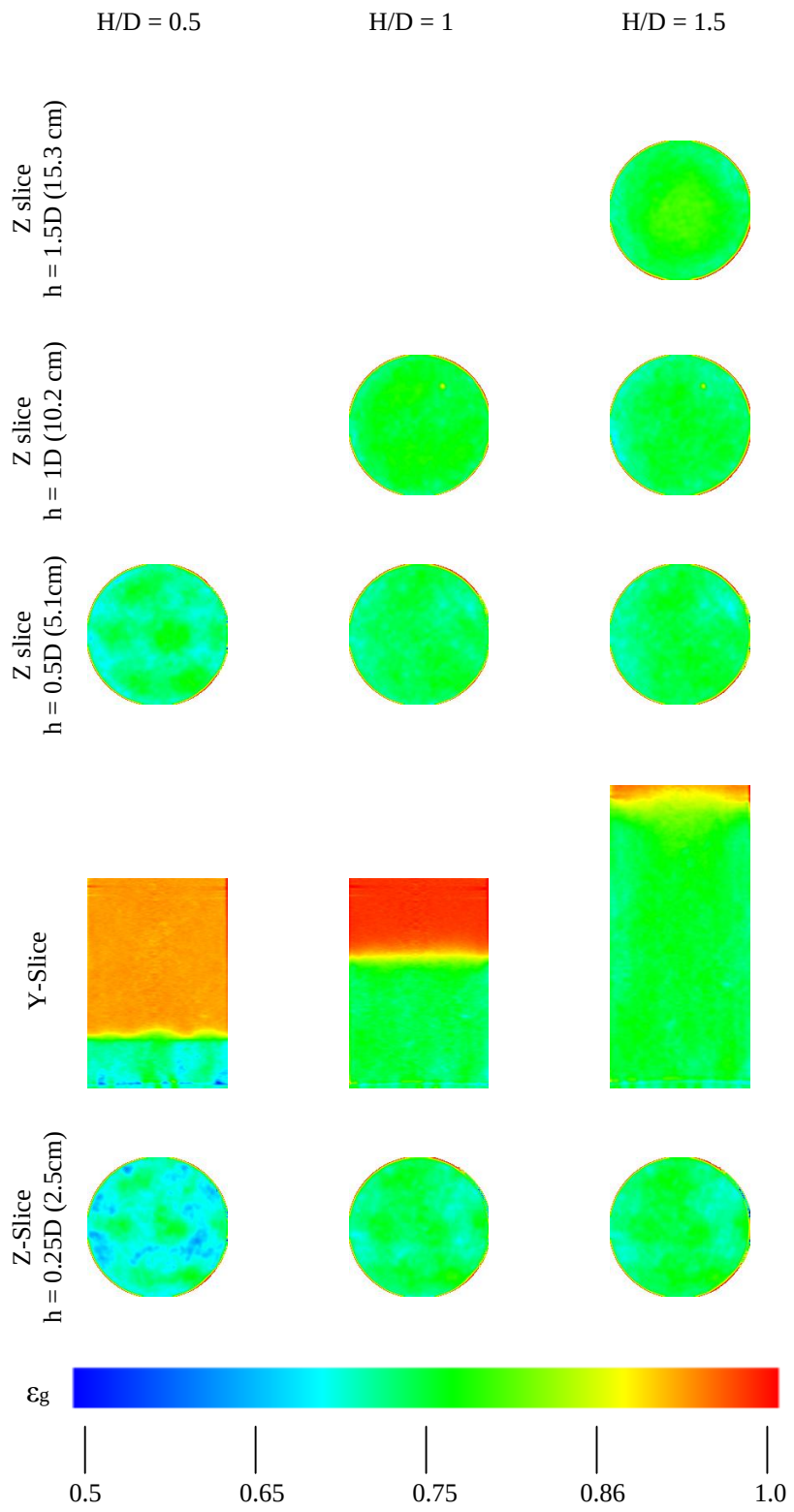

Figure 4.13: Ground corncob holdup y- and z- slices for $U_g = 1.25U_{mf}$ at different H/ D ratios.

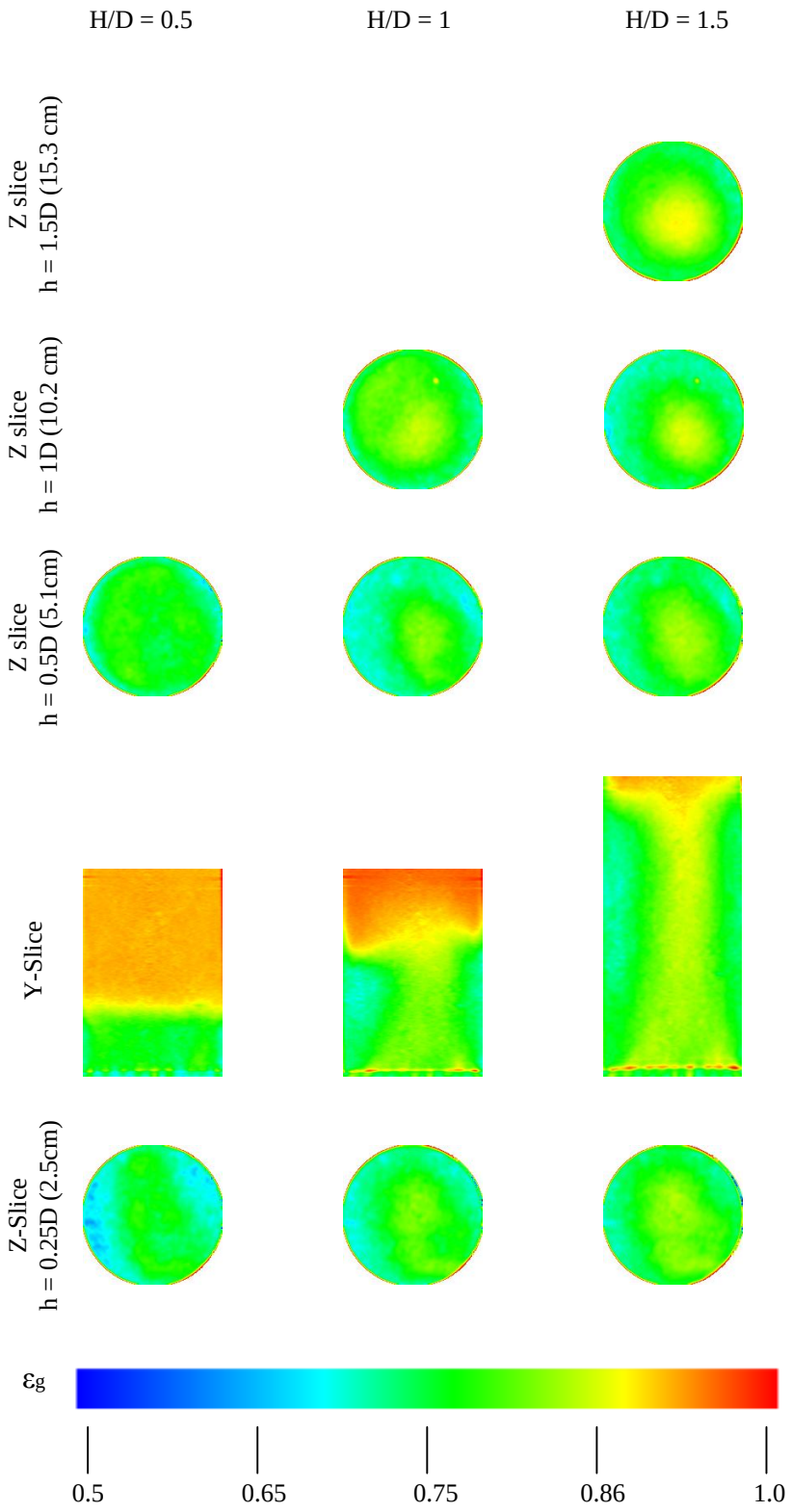

Figure 4.14: Ground corncob holdup y- and z- slices for $U_g = 3U_{mf}$ at different H/ D ratios.

On the other hand, ground walnut shell (Figures 4.15 and 4.16) presented similar characteristics of the flow structure observed in glass beads. However, for ground walnut shell as H/D increases, based on the color scale, gas holdup in the fluidized bed does not appear to have a considerable change. Increasing the superficial gas velocity produces an increase in gas holdup, a trend that was observed in the three materials and in every H/D ratio tested. Also, as shown in Figures 4.13 and 4.14, z-slices for ground walnut shell (Figures 4.15 and 4.16) exhibit the same red line surrounding the slices, which is related to the same effect discussed in the previous paragraph for ground corncob.

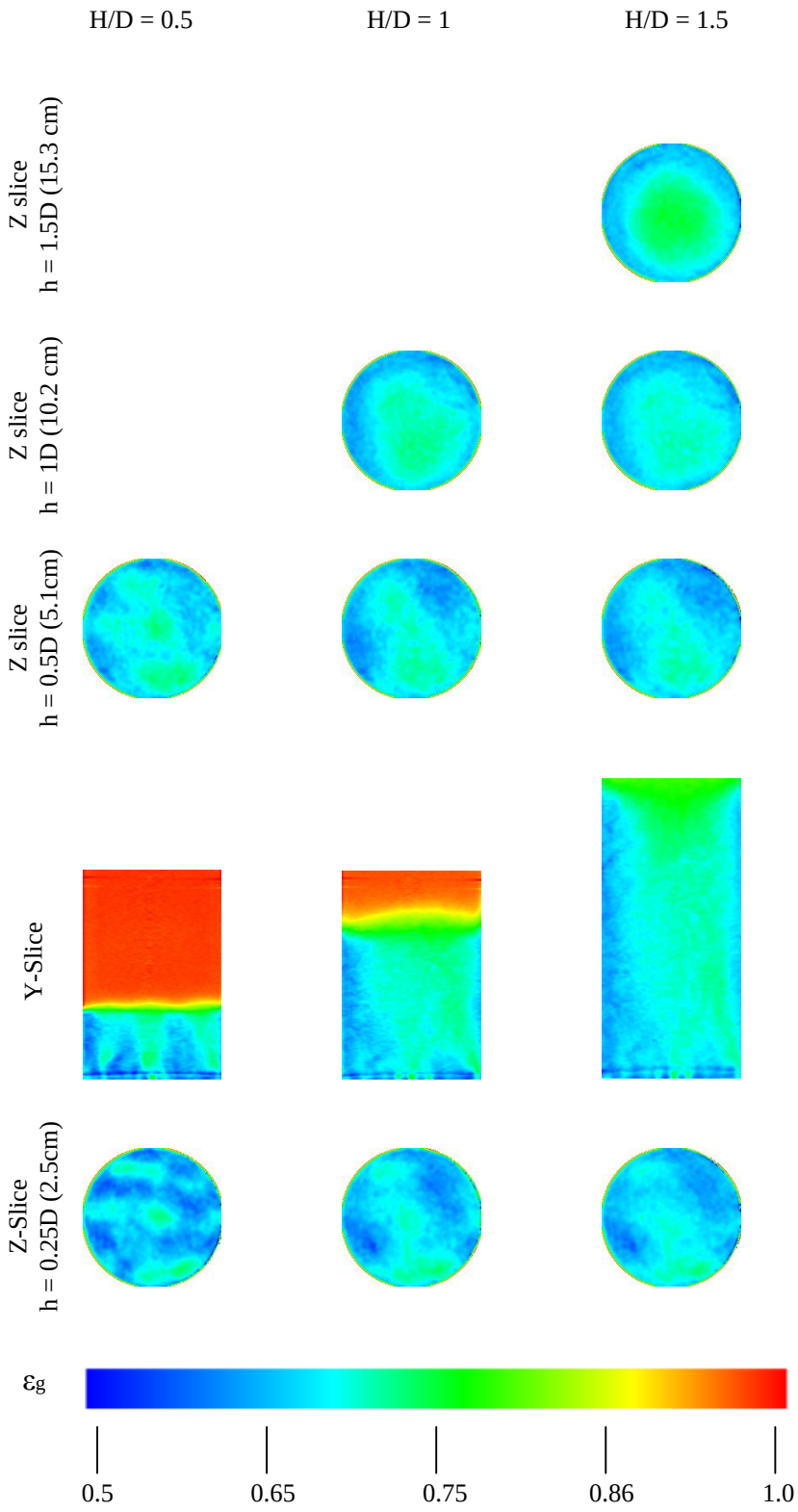

Figure 4.15: Ground walnut shell holdup y- and z- slices for $U_g = 1.25U_{mf}$ at different H/ D ratios.

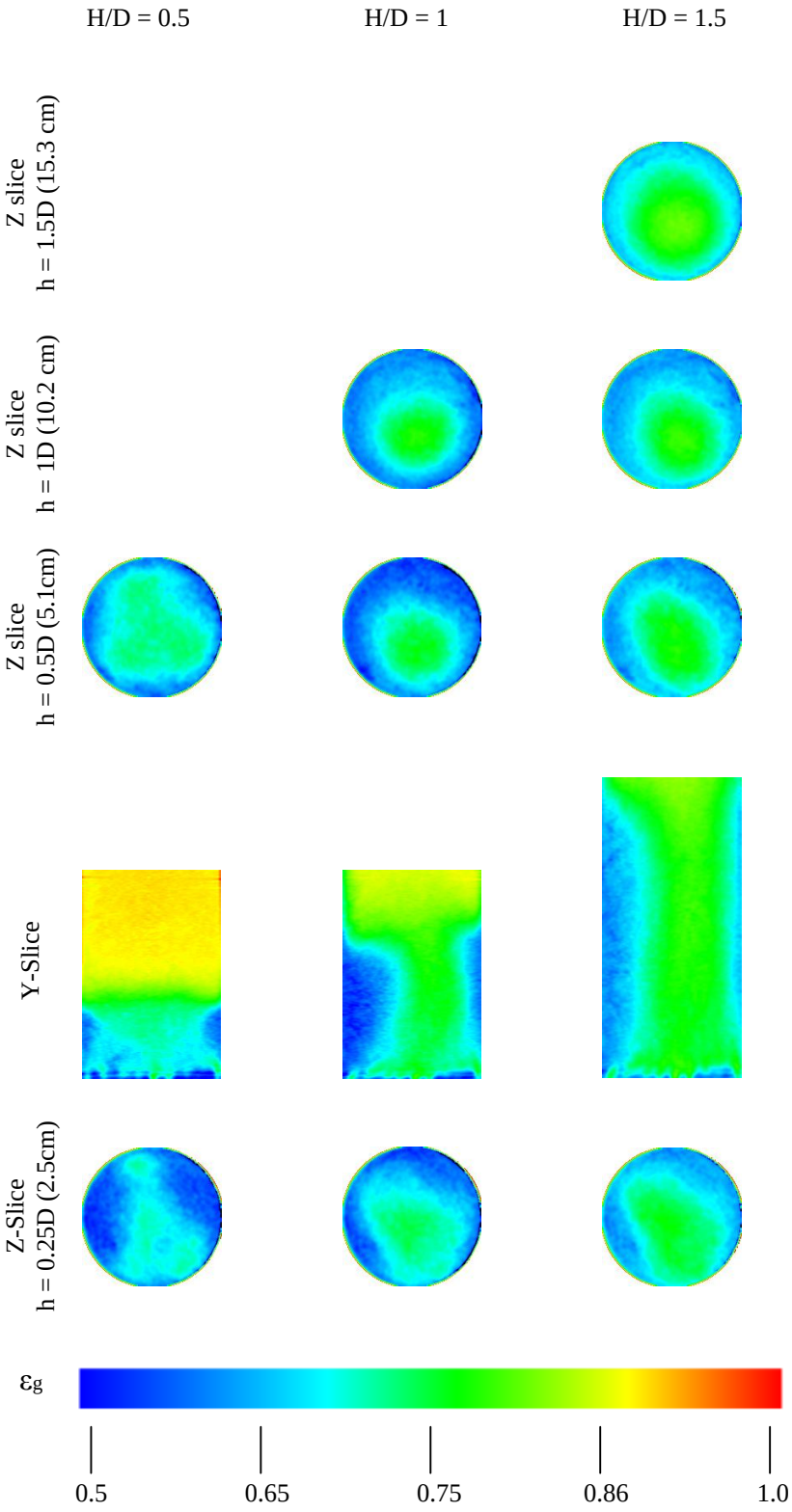

Figure 4.16: Ground walnut shell holdup y- and z- slices for $U_g = 3U_{mf}$ at different H/D ratios.

The y- and z-slices images shown in Figures 4.8 - 4.16 reveal qualitative information about the bed hydrodynamics. The actual gas holdup values within the bed are used to obtain quantitative information. The local gas holdup values can be averaged across a horizontal slice to show how gas holdup varies with bed height. Figures 4.17 and 4.18 show the glass beads horizontal-average and time-average gas holdup for H/D = 1 and H/D = 1.5, respectively, as a function of different superficial gas velocities. There is an increase in the overall gas holdup with an increase in superficial gas velocity. This effect is attributed to the higher volume of air that is passing through the bed material. This trend is observed for all the H/D ratios tested in this study. It is important to mention that plots of horizontal average gas holdup show variations in the lower region of the fluidized bed (h/D < 0.2), which are attributed primarily to the presence of noise and CT imaging artifacts inherent to the system.

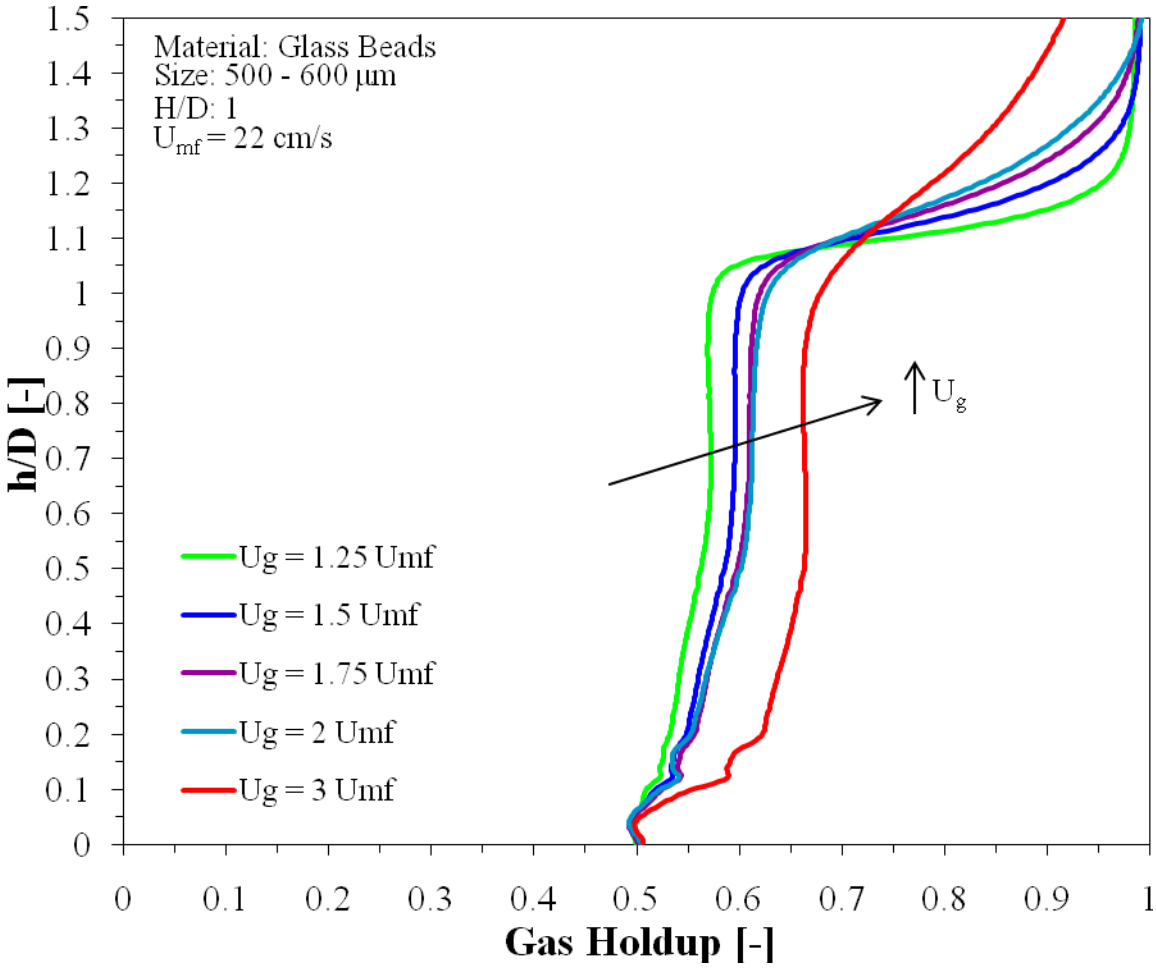

Figure 4.17: Effect of superficial gas velocity on horizontal-average and time-average gas holdup for different U_g values at H/D = 1.

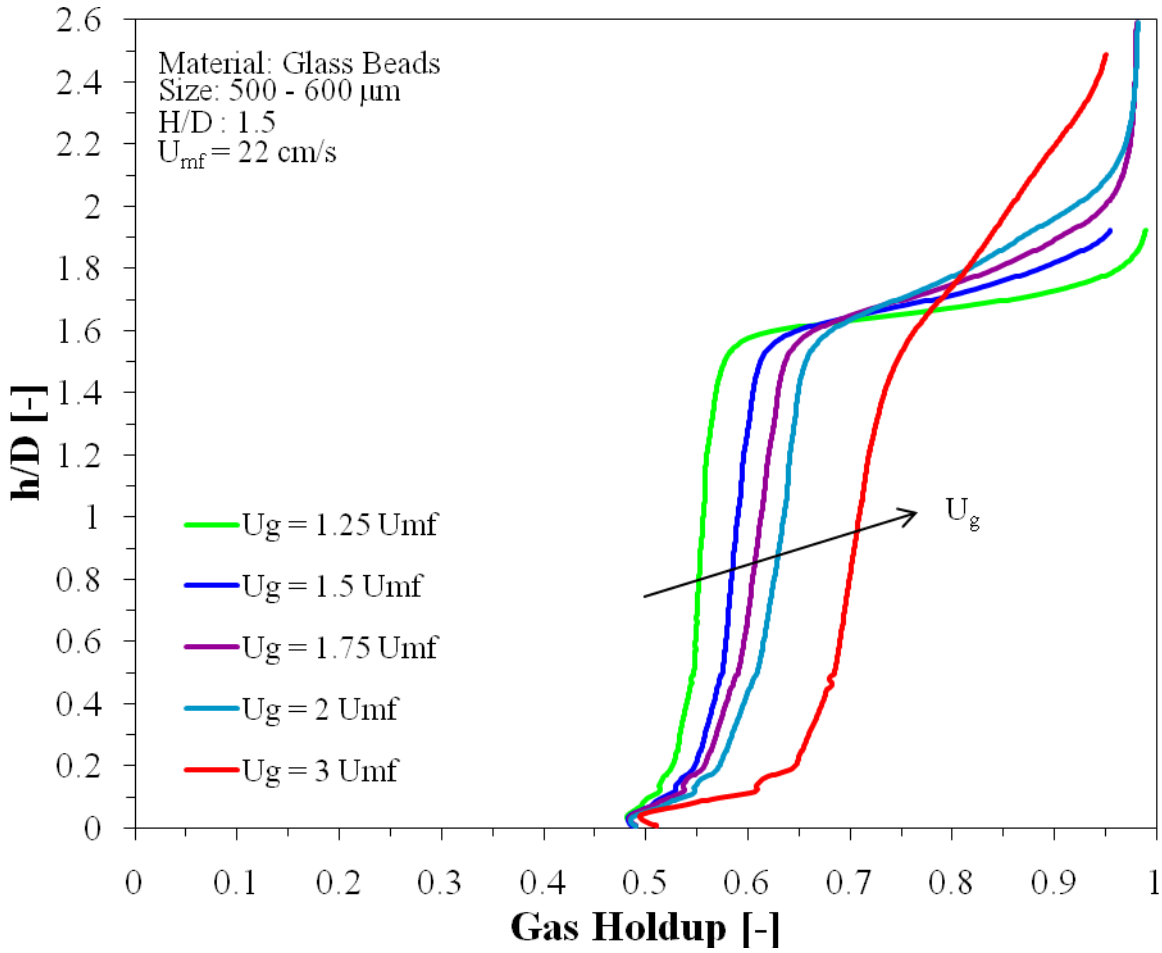

Figure 4.18: Effect of superficial gas velocity on horizontal-average and time-average gas holdup for different U_g values at H/D = 1.5.

Figures 4.17 and 4.18 show that there is a slight increase in the average gas holdup as axial height increases, but overall the horizontal-average gas holdup is approximately constant throughout the fluidized bed. As U_g increases, bed expansion is more noticeable in the plots, especially in the section above the initial bed height. This is caused by the higher superficial gas velocities pushing more material to the bed surface and then expelling it along the walls, making the surface of the bed less distinguishable. This also causes a thin layer of glass beads to form along the wall outside the imaging region and then fall back down into the bed, preventing the average gas holdup from asymptoting to 1 as h/D gets larger.

Moreover, as H/D increases, there is a decrease in the horizontal-average gas holdup because more material is present in the fluidized bed, reducing bed expansion. This effect is shown in Figure 4.19, where the horizontal-average gas holdup is plotted as a function of the axial height for a superficial gas velocity of $1.25U_{mf}$, and different H/D ratios.

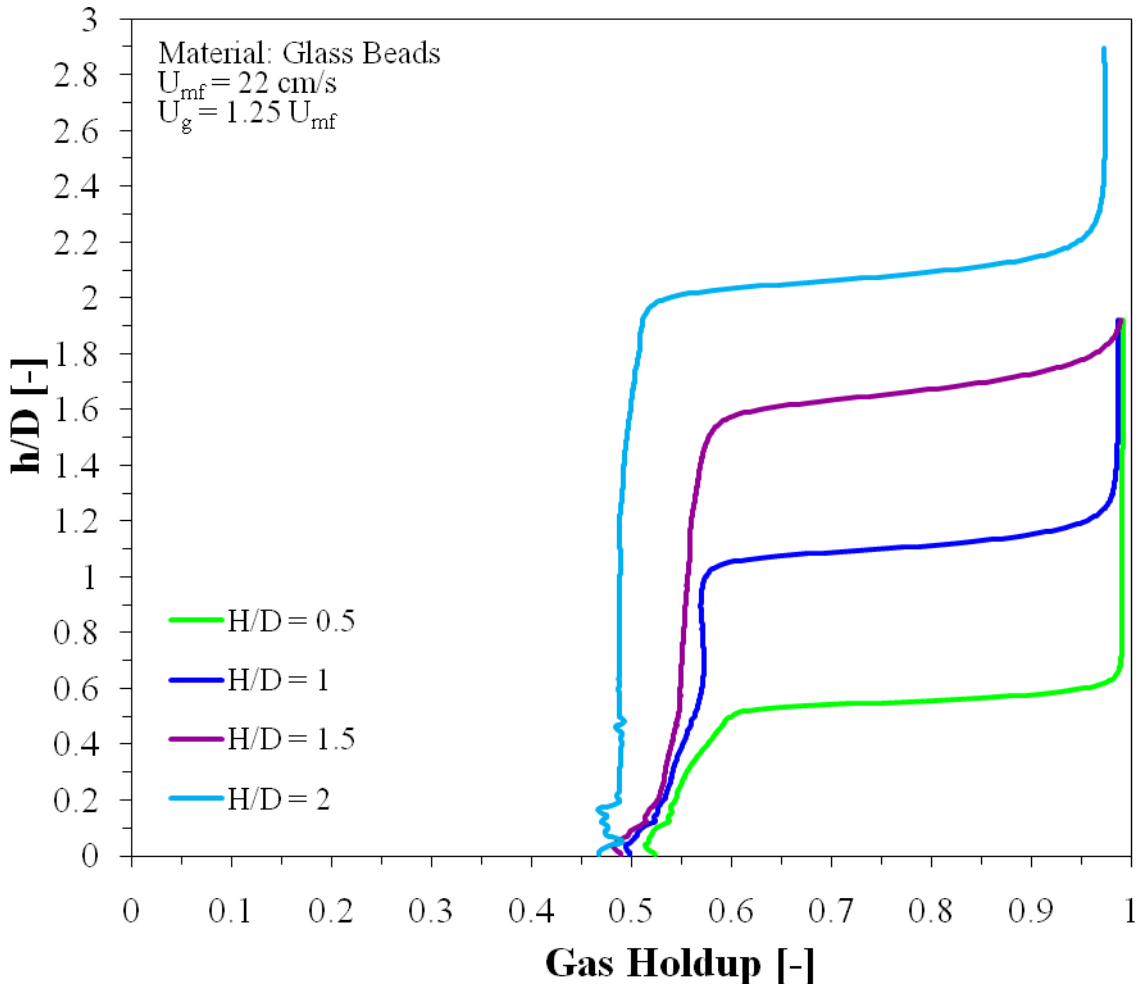

Figure 4.19: Gas holdup as a function of height for glass beads for different H/D ratios and $U_g = 1.25U_{mf}$.

As superficial gas velocity increases, the effect of H/D ratio in the horizontal-average gas holdup follow the same trend observed at lower gas superficial gas velocities, there is a decrease in the gas holdup as H/D increases. This is particularly apparent for H/D = 2.

However, as shown in Figure 4.20 for $U_g = 3U_{mf}$, deviations exist, particularly for H/D = 1.5, when this trend is not strictly observed.

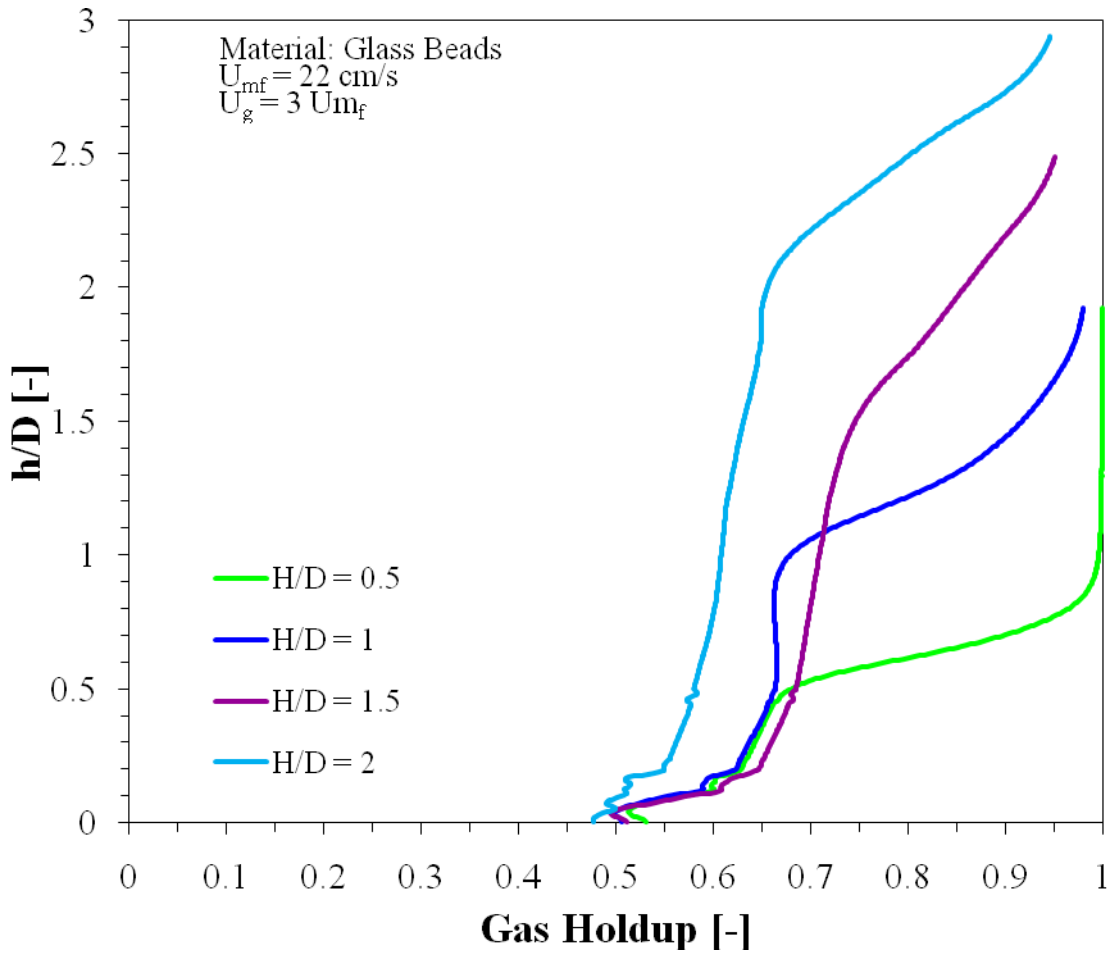

Figure 4.20: Gas holdup as a function of height for glass beads for different H/D ratios and $U_g = 3U_{mf}$.

The change in H/D ratio does not produce the same effect observed in Figure 4.19, when the material changes to ground corncob and ground walnut shell. As the H/D ratio increases in a fluidized bed filled with ground corncob, the horizontal-average gas holdup shows a slight increase as it shown in Figure 4.21. On the other hand, for ground walnut shell H/D ratio changes do not affect the overall average gas holdup at low superficial gas velocities (Figure 4.22), but as superficial gas velocity increases there is an increase in the overall average gas holdup values as the H/D ratio increases (Figure 4.23). These plots

show that effects caused by H/D ratio in the fluidization and gas holdup results are strongly dependent on the material properties; this dependency is the focus of the next subsection.

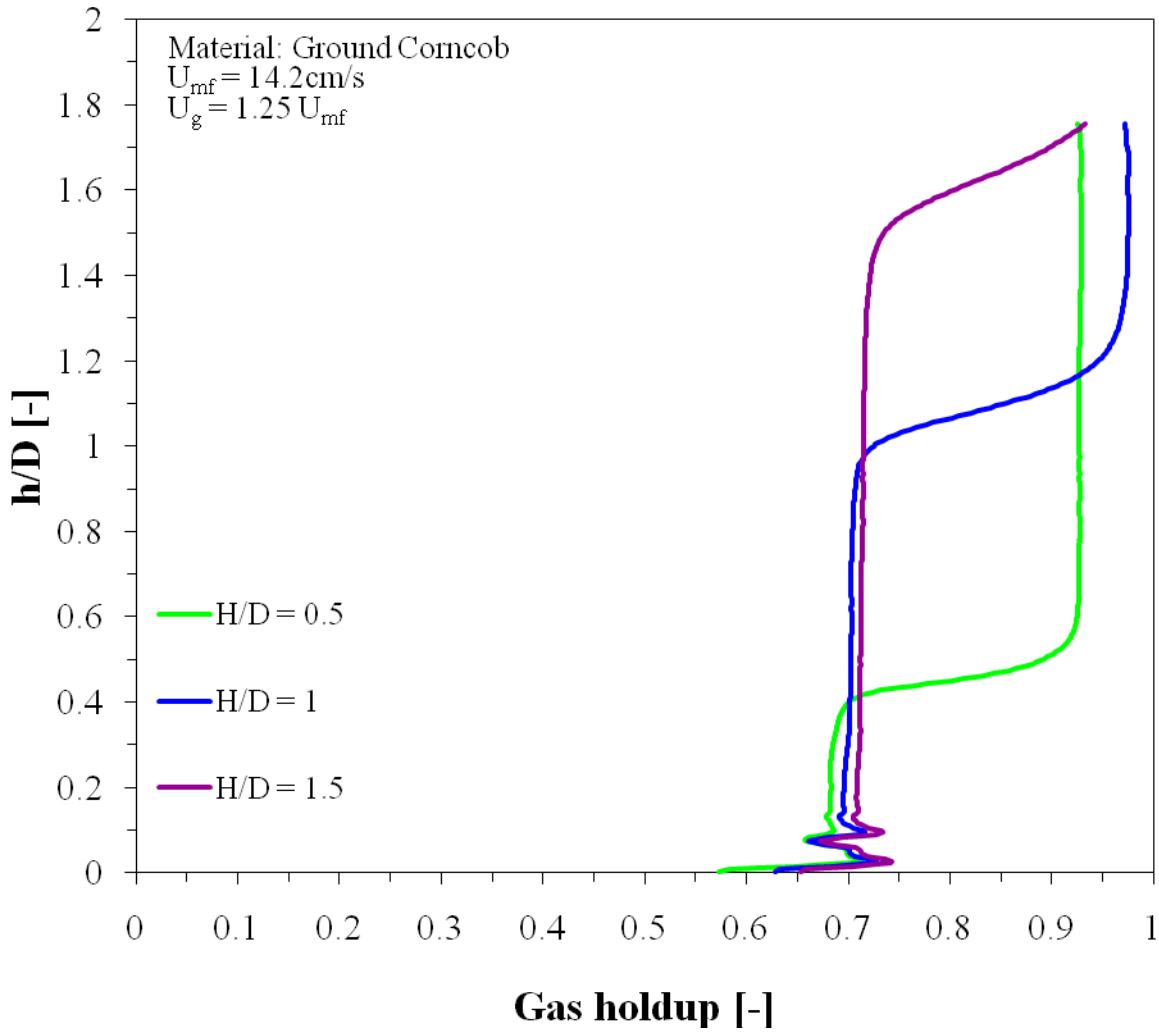

Figure 4.21: Gas holdup as a function of height for ground corncob for different H/D ratios and $U_g = 1.25U_{mf}$.

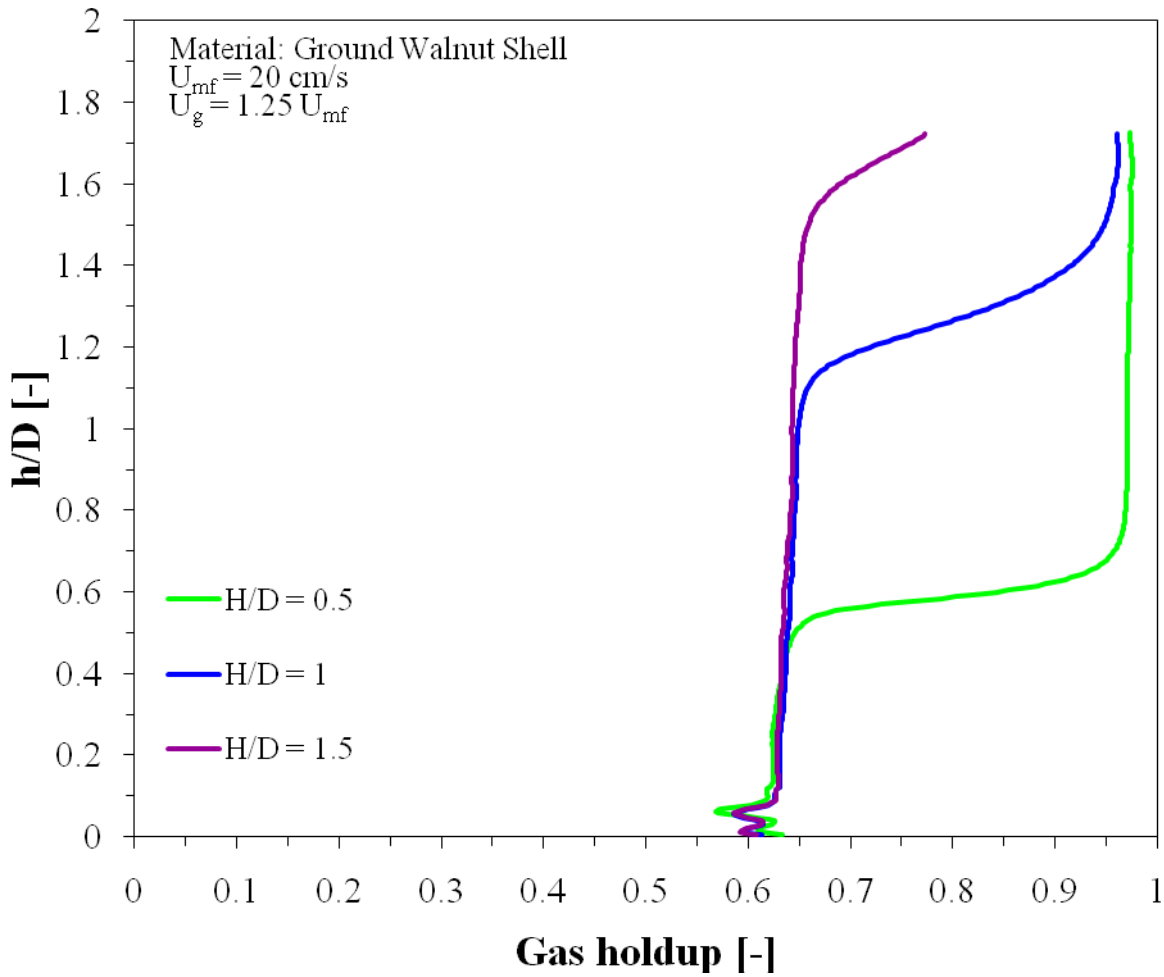

Figure 4.22: Gas holdup as a function of height for ground walnut shell for different H/D ratios and $U_g = 1.25U_{mf}$.

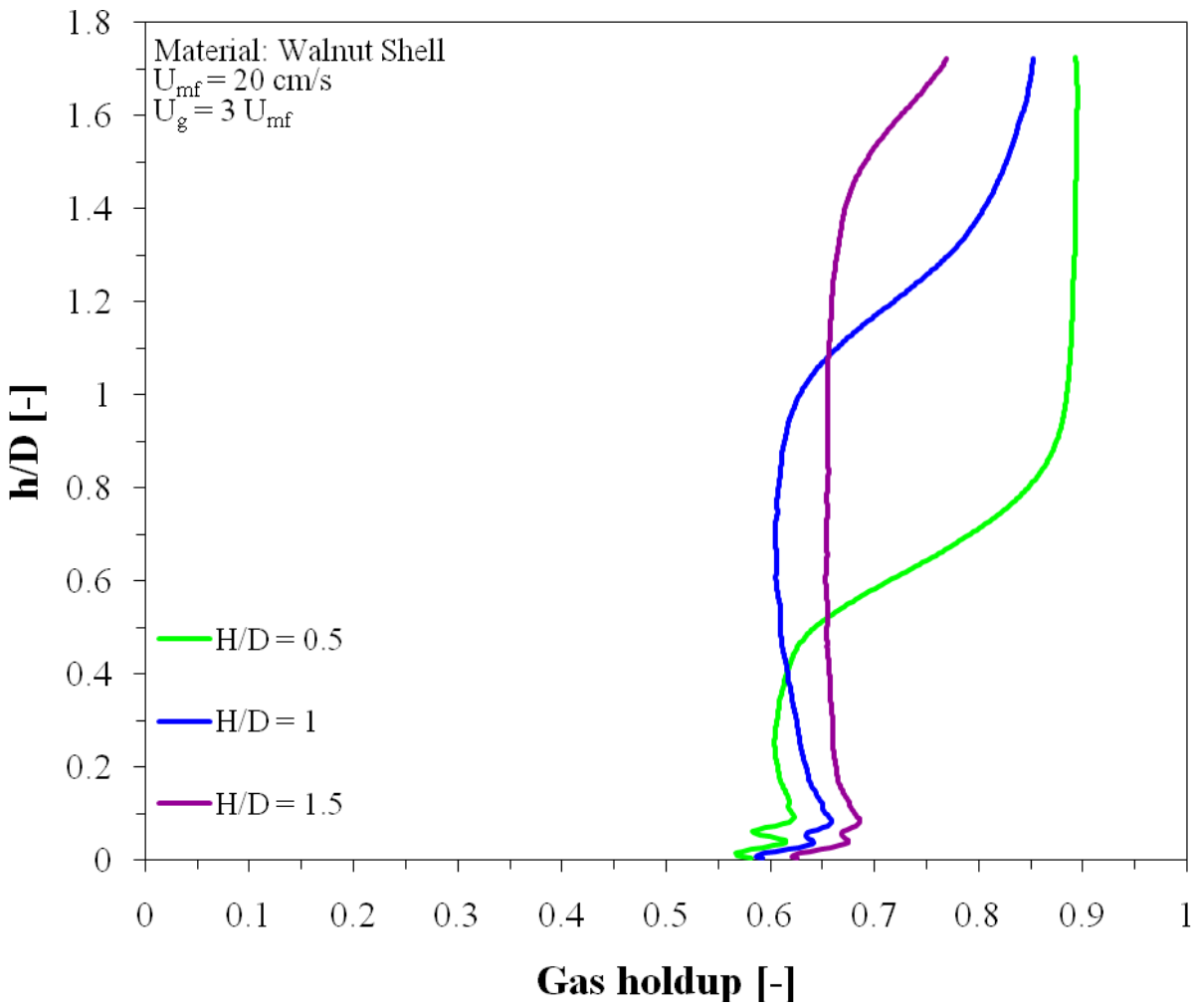

Figure 4.23: Gas holdup as a function of height for ground walnut shell for different H/D ratios and $U_g = 3U_{mf}$.

It is important to notice that in Figure 4.21, for the curve of H/D = 0.5, and in Figure 4.23 for the H/D = 0.5 and H/D = 1 curves, the upper part of the curves are expected to asymptote to 1. Failure to do so is caused primarily by fluctuations in the CT intensity, and reasons for this are still being investigated. Also, the curve of H/D = 0.5 in Figure 4.21 implies that the initial bed height may be lower than the specified value of H/D = 0.5. This phenomenon is attributed primarily to a small error in the bed filling process. However, this material difference does not introduce considerable errors or changes in the results.

Local time-average gas holdup is plotted as a function of location along two mutually perpendicular lines that pass through the center of the bed for the four H/D ratios tested with $U_g = 1.25U_{mf}$. Figure 4.24 shows the local gas holdup data along the y-slice at an axial height h = 0.25D (2.5cm), while Figure 4.25 shows the data along the x-slice. The local rise and fall in gas holdup is attributed to the presence of jets from the aeration plate. Overall, the trends for the different H/D ratios are similar.

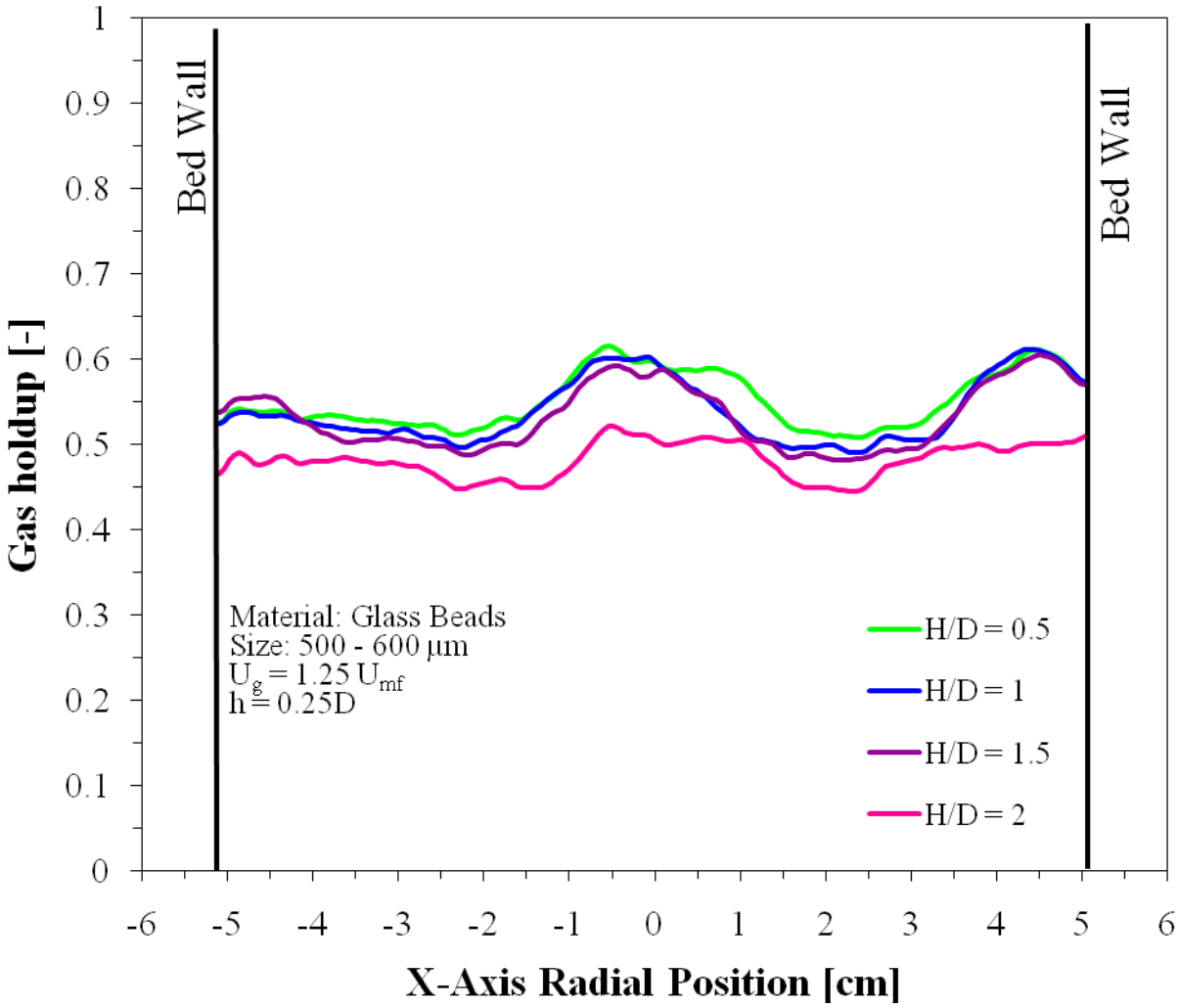

Figure 4.24: Y-slice local gas holdup as a function of location at h = 0.25D for glass beads.

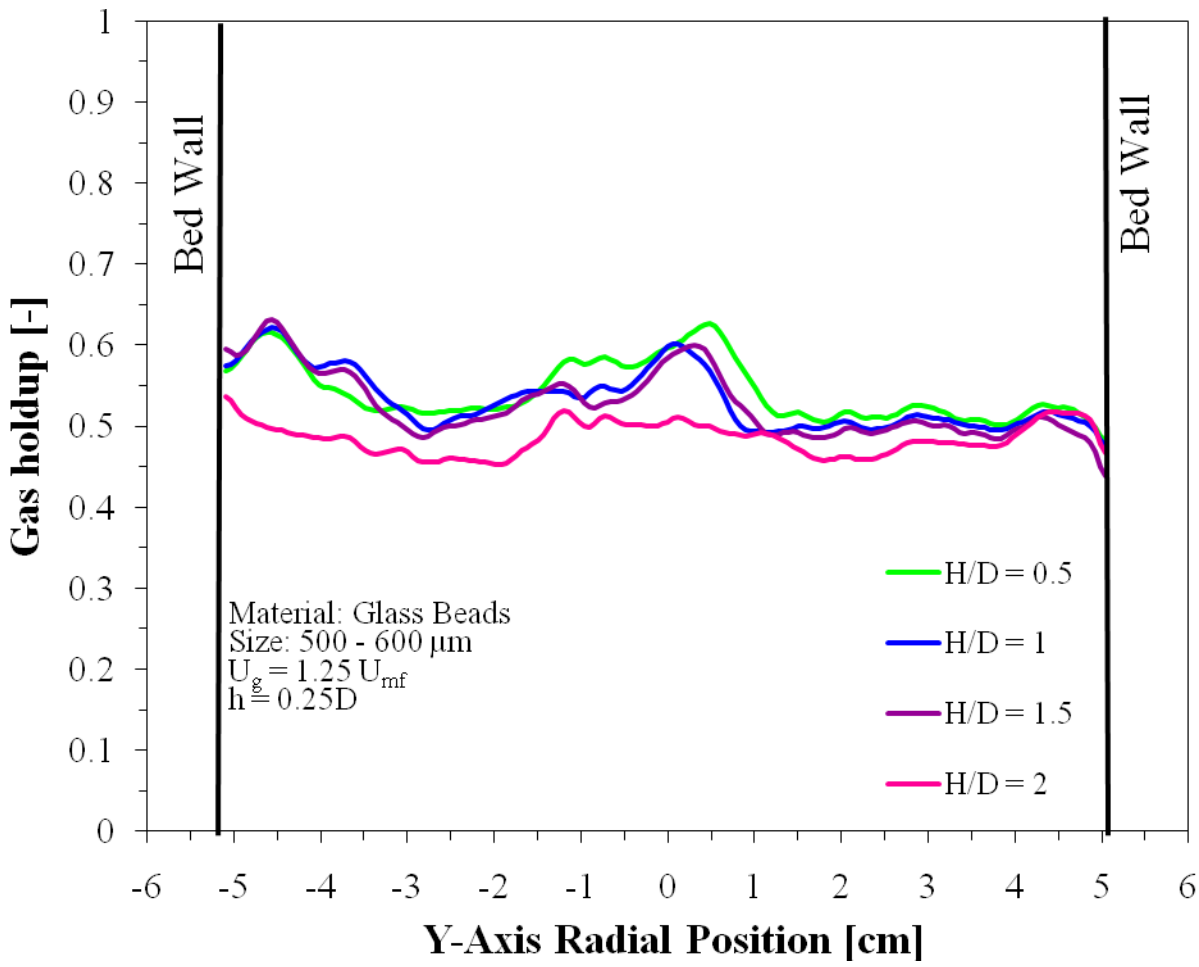

Figure 4.25: X-slice local gas holdup as a function of location at h = 0.25D for glass beads.

Figures 4.26 and 4.27 show the local time-average gas holdup for $U_g = 1.25U_{mf}$ at h = 0.5D (5.1 cm) along the same two planes. Increasing the height from the aeration plate diminishes the variations in local gas holdup. There is a slight decrease in gas holdup as the H/D ratio increases due to the increase in bed mass above this location hindering bed expansion. This decrease was also observed in Figure 4.19. For example, at H/D = 0.5, the bed can freely expand at h = 0.5D, whereas with H/D = 1, expansion is suppressed. This trend is observed as the axial height increases further into the bed.

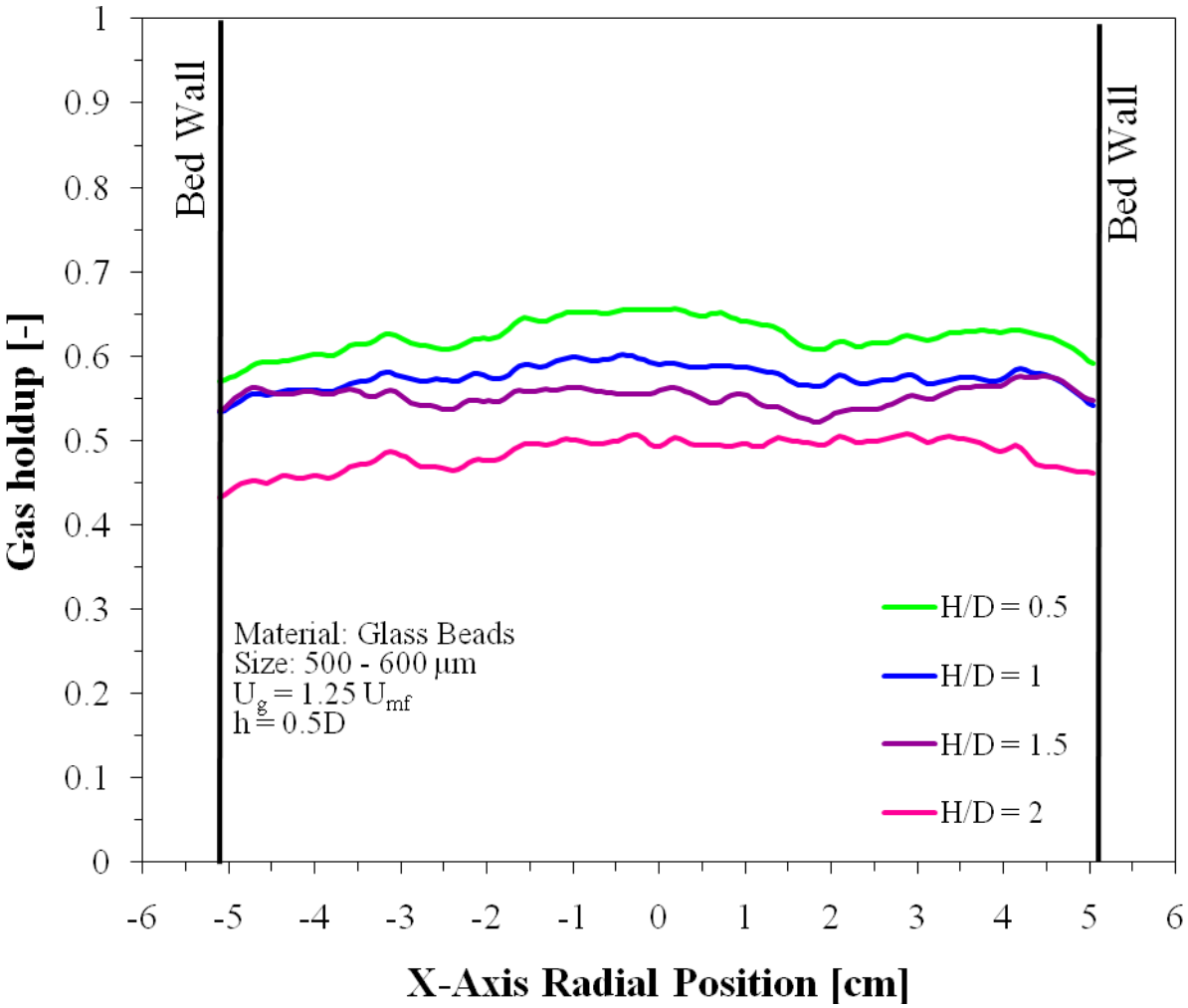

Figure 4.26: Y-slice local gas holdup as a function of location at h = 0.5D for glass beads.

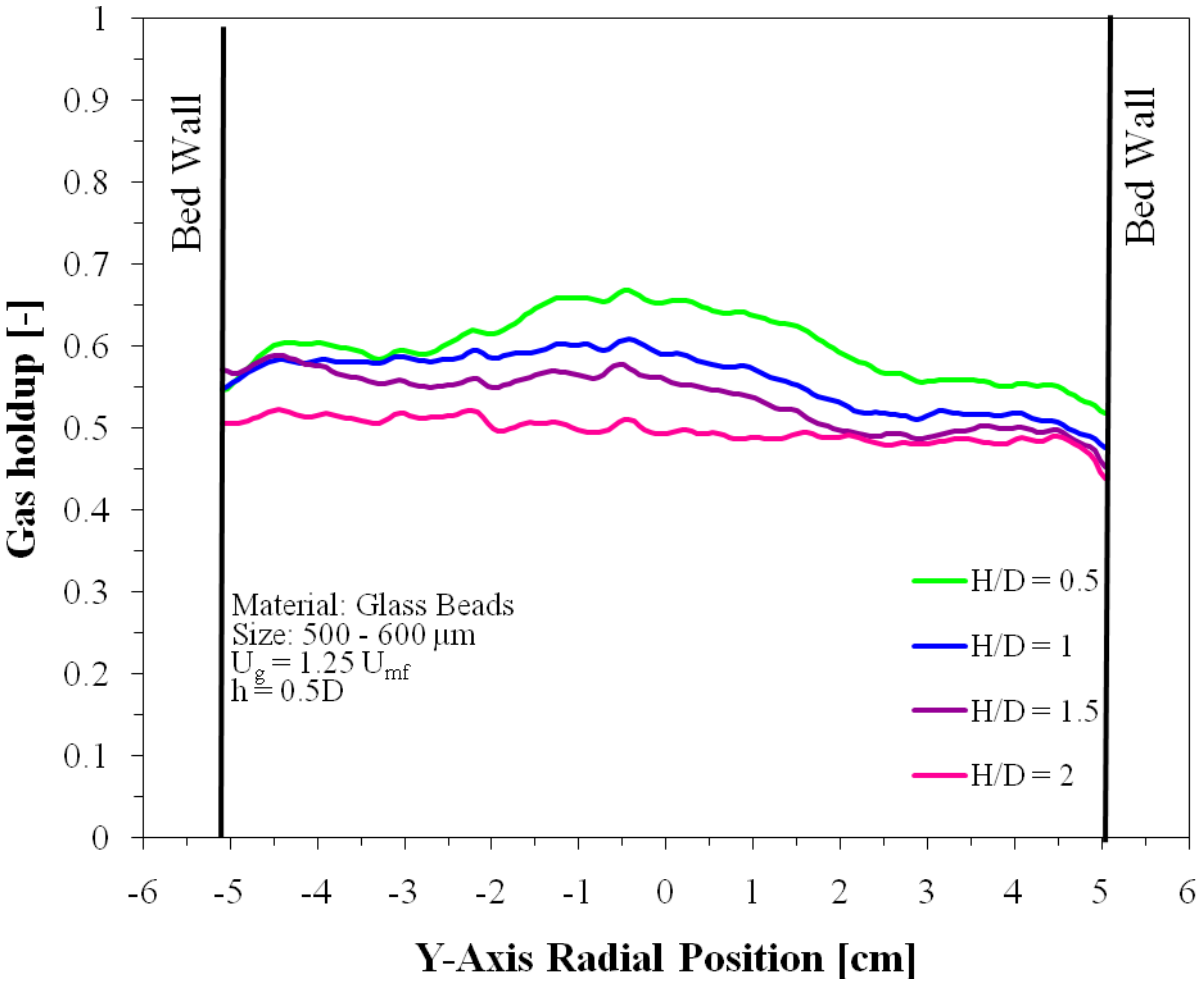

Figure 4.27: X-slice local gas holdup as a function of location at h = 0.5D for glass beads.

The local time-average gas holdup as a function of spatial location for ground corncob (Figures 4.28 and 4.29) and ground walnut shell (Figure 4.30 and 4.31) is plotted to analyze the average gas holdup trends observed for these materials. Figures for ground corncob and ground walnut shell show a slight decrease between H/D = 0.5 and the rest of the H/D ratios, this is attributed to the fact that at h = 0.5D, the bed with a H/D = 0.5 can freely expand whereas in the H/D = 1 and H/D = 1.5, the expansion is suppressed at this axial height, showing the same behavior as glass beads. Furthermore, according to the trend present in Figure 4.20 for corncob, as axial height increases and H/D ratio increases, there is an slight increase in the overall average gas holdup as shown in Figure

4.29, which is taken at an axial height of h = 0.75D. Whereas, for ground walnut shell in Figure 4.31 the H/D ratio does not affect the values of the local time-average gas holdup at lower U_g, which was also observed in Figure 4.21.

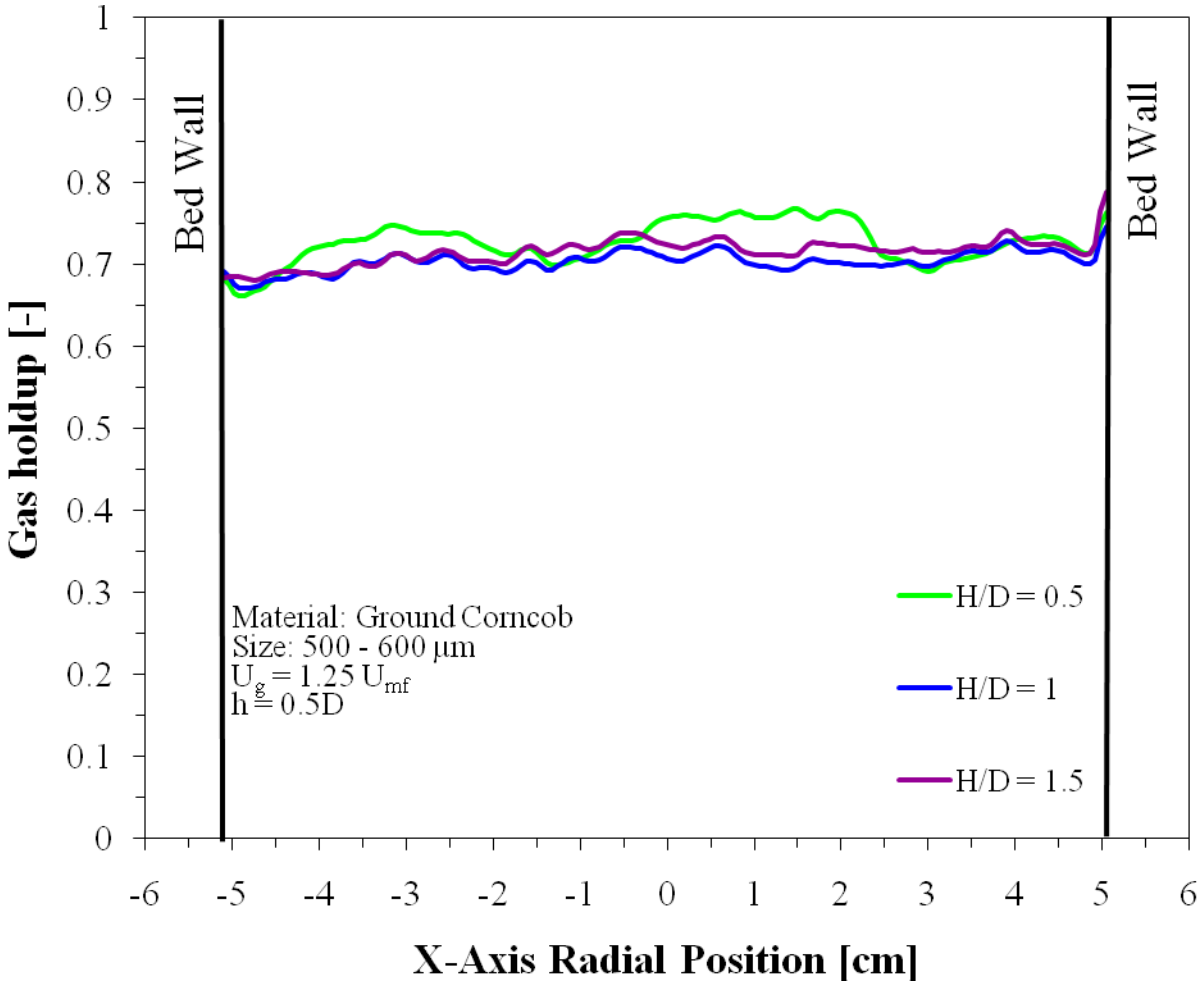

Figure 4.28: Y-slice local gas holdup as a function of location at h = 0.5D for ground corncob.

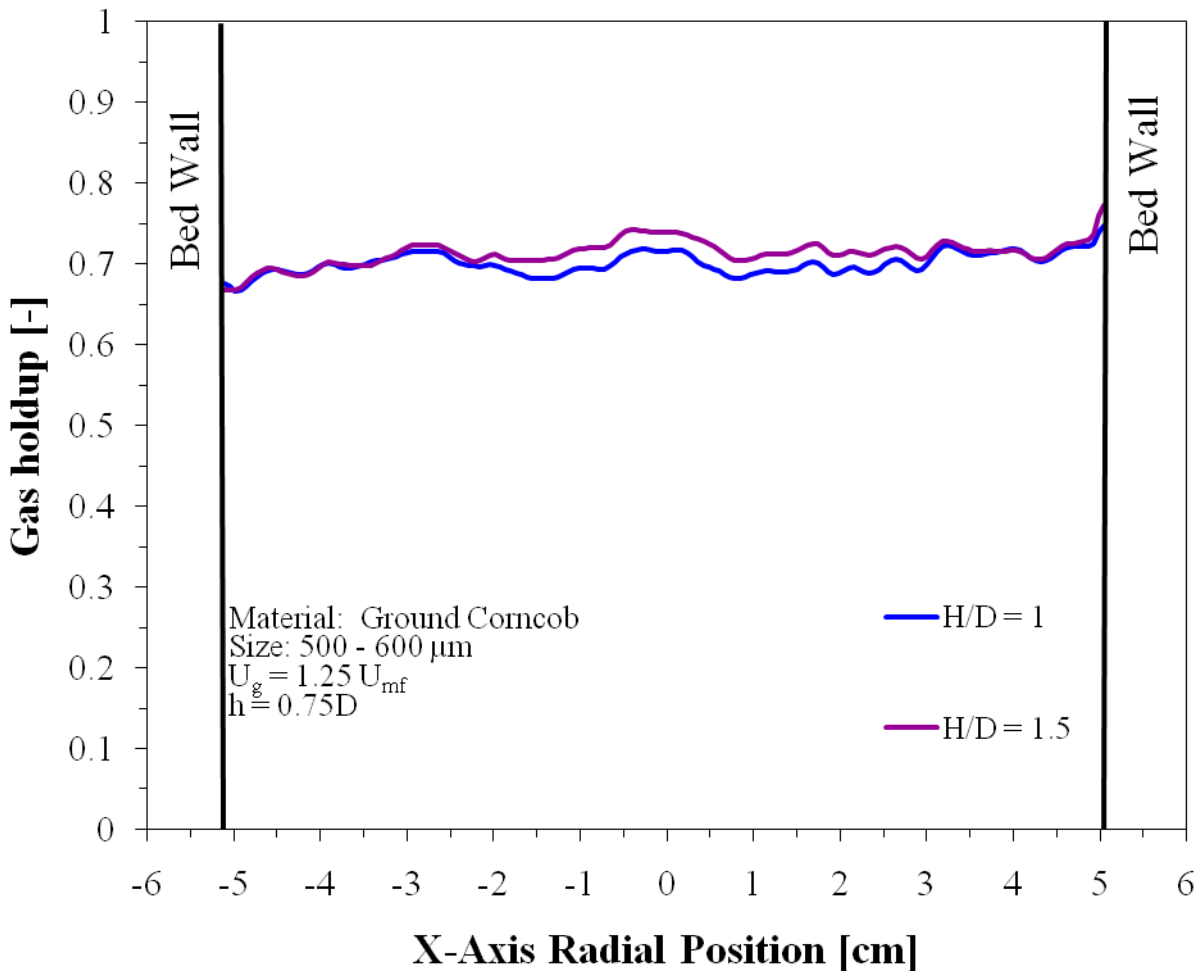

Figure 4.29: Y-slice local gas holdup as a function of location at h = 0.75D for ground corncob.

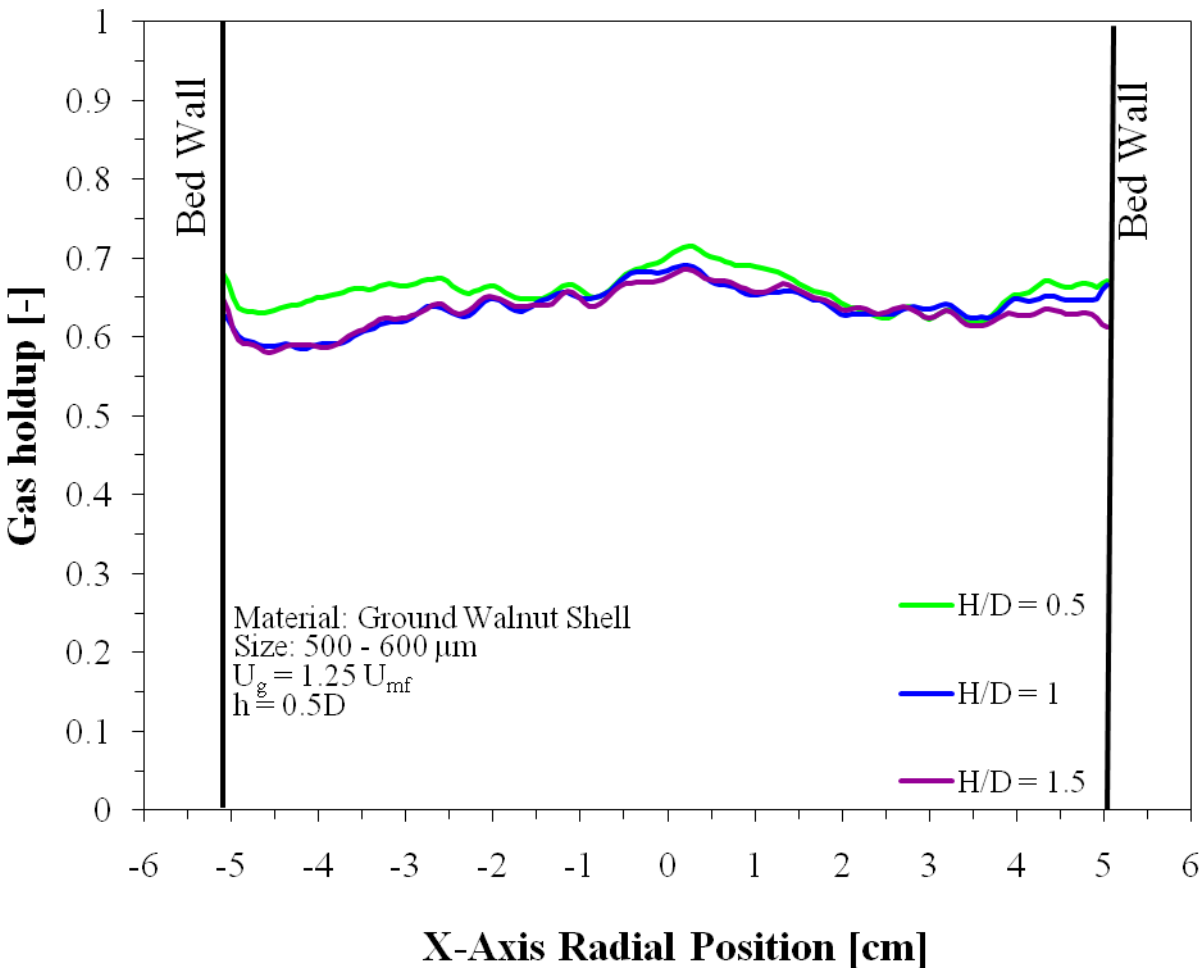

Figure 4.30: Y-slice local gas holdup as a function of location at h = 0.5D for ground walnut shell.

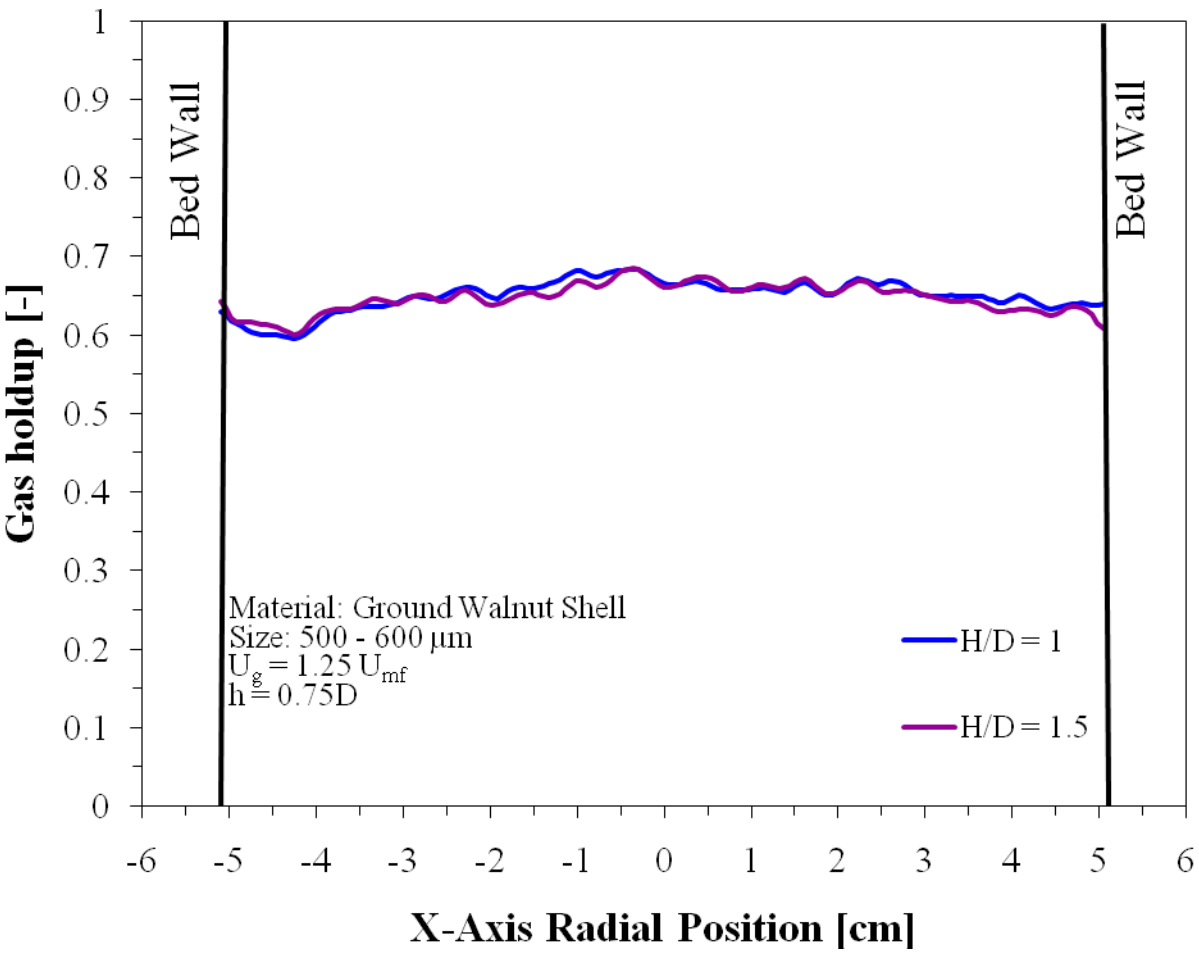

Figure 4.31: Y-slice local gas holdup as a function of location at h = 0.75D for ground walnut shell.

4.2.2 Bed Material Density Effects on Local Gas Holdup

Local time-average gas holdup is a function of material density. Several y-slices were taken at two different superficial gas velocities ($U_g = 1.25U_{mf}$ and $3U_{mf}$) and three different H/D ratios (H/D = 0.5, 1, 1.5) to visualize the effects that material density have on the fluidization structure, on the time-average gas holdup, and to compare these effects between materials (Figures 4.32 and 4.33). It is important to notice that the color scale used in the figures is common for all materials, even though the initial bulk density for the three materials differs considerably.

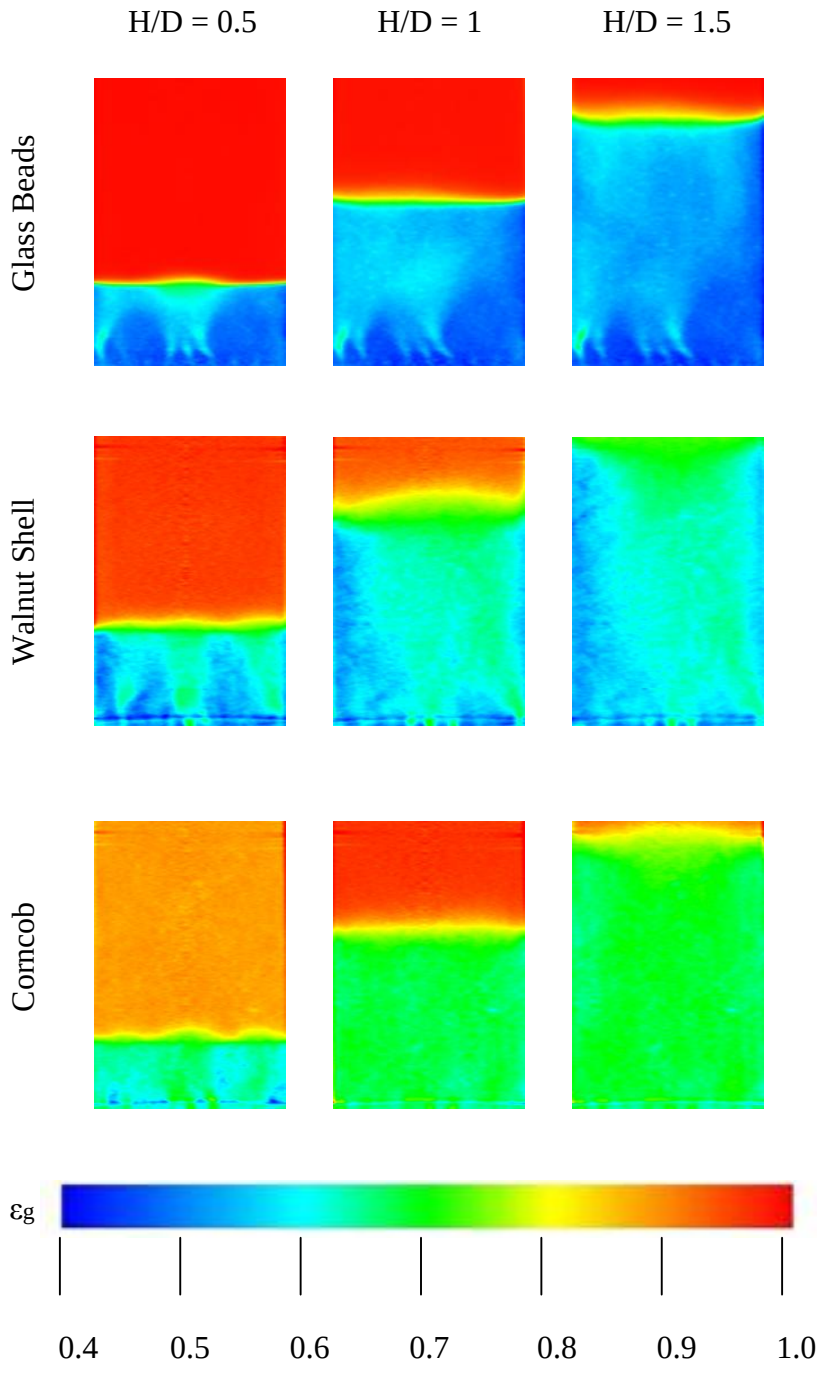

Figure 4.32: Gas holdup y-slice for all materials at $U_g = 1.25U_{mf}$ for different H/D ratio.

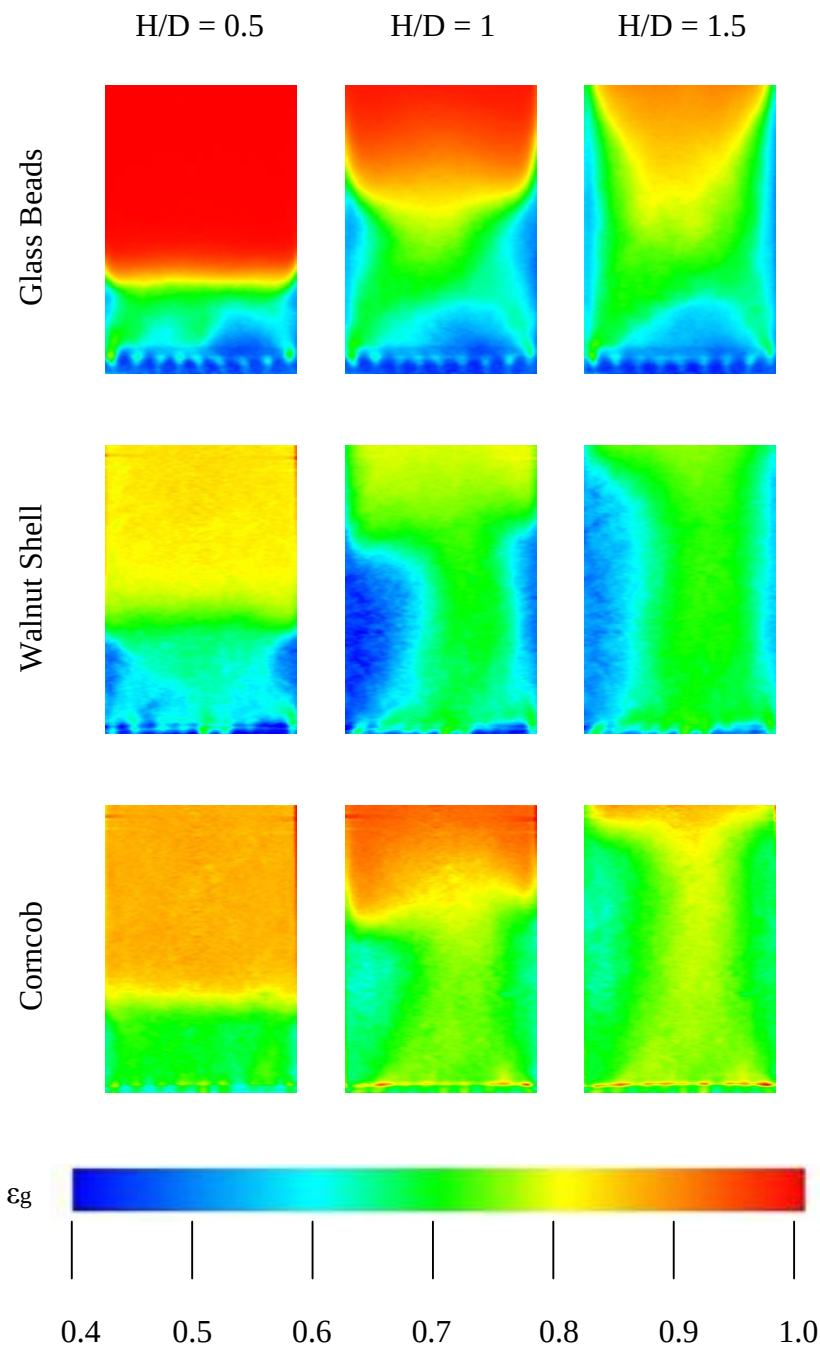

Figure 4.33: Gas holdup y-slice for all materials at $U_g = 3U_{mf}$ for different H/D ratio.

It can be observed in Figure 4.32, based on the color scale located at the bottom of the figure, that as material density decreases, gas holdup increases. Glass beads have lower gas holdup than both ground walnut shell and ground corncob, while ground corncob exhibit the largest gas holdup of all the three materials. Figure 4.32 also shows the

different fluidization patterns for each material. For an H/D ratio of 0.5, all materials exhibit a similar fluidization structure, with regions of higher gas holdup in the center and near the walls of the fluidized bed, while the bed surface is fairly uniform for all three materials. At H/D = 1 and 1.5, glass beads and ground walnut shell show similarities between their fluidization structures, low gas holdup regions near the walls of the bed and high gas holdup regions flow through the center of the bed, however ground corncob fluidization structure at these H/D ratios differ from the other two materials. Ground corncob appears to exhibit a better distribution of gas holdup along the entire bed, therefore providing a better and more uniform fluidization; however, this observation is influenced by the color scale used in the imaging.

As U_g increases, flow structures between materials show both similarities and differences. Figure 4.33 shows that when H/D = 0.5, glass beads and ground walnut shell exhibit a similar structure, however ground corncob shows a more uniform fluidization than both glass beads and ground walnut shell. As H/D increases, the structures differ more between the denser material (glass beads) and the less dense materials (ground corncob and ground walnut shell). All materials showed regions of lower gas holdup near the walls of the bed indicating recirculation of bed material at higher superficial gas velocities. Also, a region of high gas holdup exists in the center of all beds due to large bubbles leaving the bed along the center axis of the bed. One difference between the material hydrodynamics can be observed in Figure 4.33 at H/D ratios of 1 and 1.5, where the bottom region of low gas holdup present in the glass beads bed is not apparent in ground walnut shell and ground corncob. The absence of a low gas holdup region near the distribution plate is caused by the difference in the air penetration from the distributor plate. The air is evenly distributed for the glass bead bed as Figure 4.33 shows, while in ground walnut shell and ground corncob beds channeling appears near the bed base,

characterized by high gas holdup paths flowing from the aeration plate into the bed. Channeling is attributed to the reduction in the necessary force needed to move particles from the air stream and is more likely to occur as the bed material density decreases, therefore channels in ground corncob are more pronounced than in glass beads and ground walnut shell. Also, the effects observed in the figures, especially the ones where certain gas holdup zones disappeared between one material and other can be caused by the color resolution used for the different material. For example, gas holdup in ground corncob and ground walnut shell span from approximately 0.5 to 1.0, while gas holdup for glass beads spans from 0.4 to 1.0. If different color resolutions were used to obtain the y-slices for each material, some of the apparent differences in flow structure between materials will be reduced.

In order to corroborate the qualitative observations made between different bed material densities, quantitative comparisons between materials are also presented in this section. Figure 4.34 shows the horizontal-average and time-average gas holdup as a function of the axial height for the three materials at H/D of 1. As shown, as the density decreases the average gas holdup increases, confirming what was found and discussed earlier in previous figures.

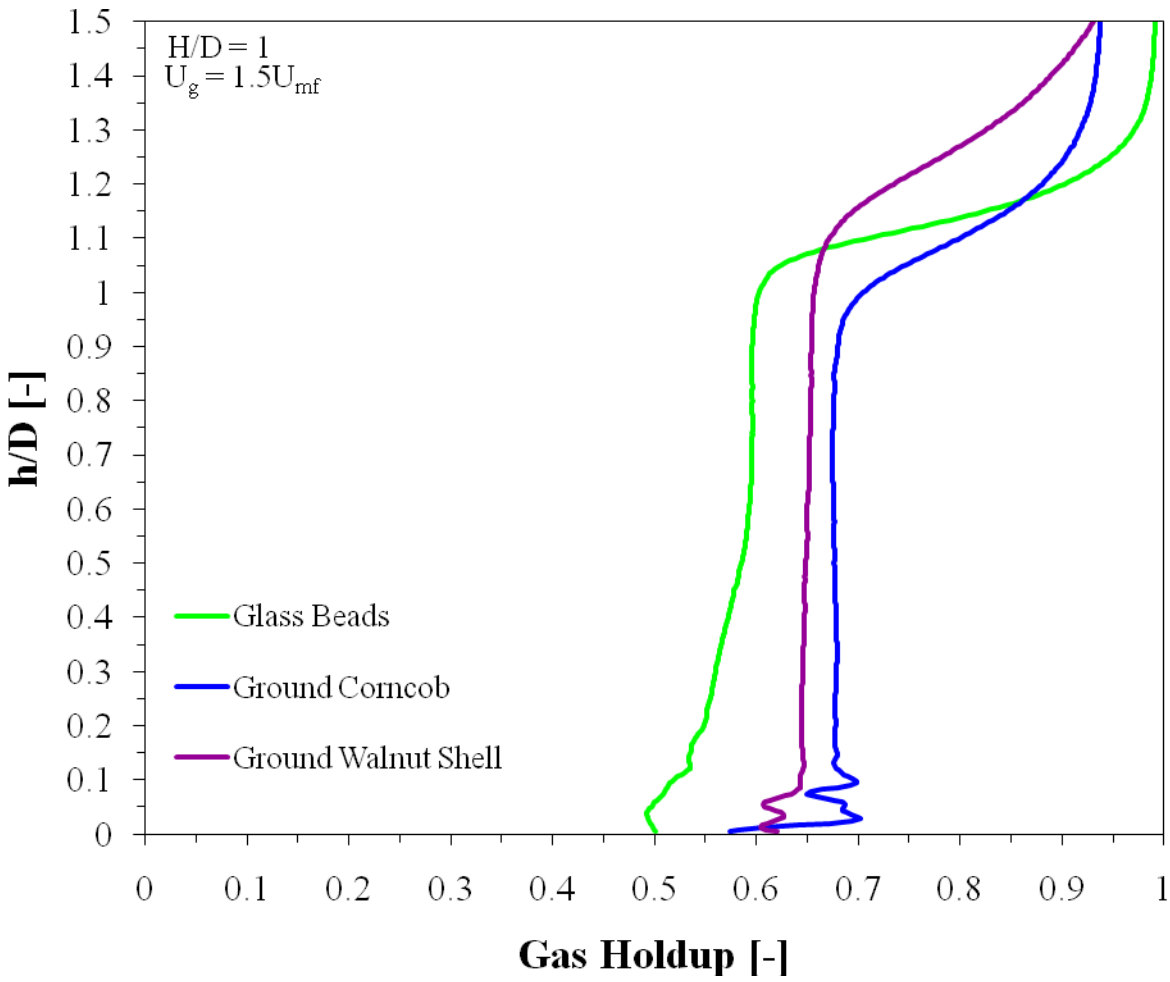

Figure 4.34: Gas holdup as a function of height for all materials at H/D = 1 and U_g = $1.5U_{mf}$.

Figure 4.34 also illustrates that horizontal-average and time-average gas holdup curves follow a similar shape for each material. Gas holdup is approximately constant in the bulk of the bed except near the surface of the bed where the average gas holdup has an abrupt change towards higher values. The lower gas holdup regions at the bottom of the beds indicate that air is less dispersed near the distributor plate, likely because of air jets from the distributor plate orifices. It can be observed also that ground walnut shell has a higher bed expansion than glass beads and ground corncob. This effect is attributed to experimental variation in the way the bed was filled, a process which can introduce

packing effects into the material, providing more expansion than expected when the bed is aerated.

4.3 Summary

In summary, results showed that bed height and material density have several effects in the fluidized bed hydrodynamics. Minimum fluidization velocity does not show any relevant change due to bed height. Furthermore, material density indeed changes the values of the minimum fluidization velocity. For the local time-average gas holdup, different effects produced by the change in bed height were encountered. For glass beads, as the H/D ratio increased the overall gas holdup decreased. Conversely, for ground corncob, as the H/D ratio increased, the horizontal-average gas holdup showed a slight increased. On the other hand, for ground walnut shell H/D ratio changes do not affect the overall average gas holdup at low superficial gas velocities, but as superficial gas velocity increases, there is an increase in the overall average gas holdup values as the H/D ratio increased. Finally, as material density decreased, gas holdup increased. Glass beads have lower gas holdup than both ground walnut shell and ground corncob, while ground corncob exhibit the largest gas holdup of all the three materials.

Chapter 5: Conclusions and Recommendations

5.1 Conclusions

This study provided important information and data to better understand fluidized bed hydrodynamics. The conclusive findings obtained from this study are related with the objectives described in Chapter 1, and are the following:

Objective 1: Review the literature regarding fluidization, bed height, and material density effects on fluidized beds hydrodynamics, and noninvasive X-ray techniques for visualization of multiphase flow systems.

Conclusion 1: In Chapter 2, fluidization, fluidized beds, as well as different fluidization regimes present in a multiphase flow system were reviewed. A review of the influence that bed height and bed material density has on important hydrodynamic parameters, such as gas holdup and minimum fluidization velocity, was also presented. Unique characteristics of biomass fluidization, thermochemical conversion processes, and methods to improve biomass fluidization were also explained in this chapter. Finally, different techniques used for the visualization and characterization of multiphase flow systems were described as well as the important role these invasive or noninvasive techniques, particularly noninvasive X-ray techniques, play in multiphase flow characterization.

Objective 2: Determine the effects of bed height on the minimum fluidization velocity.

Conclusion 2: Minimum fluidization velocity was determined for all the materials tested in this study (glass beads, ground corncob, and ground walnut shell) at different H/D ratio. Results showed that as H/D ratio increased, minimum fluidization velocity remained approximately constant. Thus, there is no correlation between minimum fluidization velocity and bed height for this type of fluidized bed. These findings

corroborated the information obtained in the literature about effects of bed height in minimum fluidization velocity for 3D cylindrical fluidized beds.

Objective 3: Compare the effects of material density on the minimum fluidization velocity.

Conclusion 3: In this study, minimum fluidization velocity was obtained for three different materials. Results showed that minimum fluidization was influenced by the change in the material density. As density increased minimum fluidization velocity increased. Since the volume of each material is constant, high density materials have more mass than low density materials. Therefore, in order to fluidize the material, a higher superficial gas velocity is required to overcome the bed weight. Consequently, a larger pressure drop is produced with high density materials, increasing U_{mf}.

Objective 4: Acquire X-ray CT images and determine time-average local gas holdup information of the fluidized bed.

Conclusion 4: X-ray computed tomography (CT) scans were captured for all three materials at different H/D ratios (0.5, 1, 1.5, 2, 3) and different superficial gas velocities (U_g = 1.25, 1.5, 1.75, 2, 3 U_{mf}). CT images allow for quantitative and qualitative analysis of the time-average local gas holdup. A series of 2D images as well as plots were used to identify present trends, fluidization structures, and variations in the gas holdup due to changes in both height-to-diameter ratio and material density.

Objective 5: Evaluate the effects of bed height on the time-average local gas holdup.

Conclusion 5: The effects of bed height observed in the time-average local gas holdup vary depending on the bed material tested. For glass beads, as H/D increased there is a decrease in the average gas holdup, this decrease is attributed to the presence of more material in the fluidized bed, hindering bed expansion. However, when the material changed to ground corncob and ground walnut shell. As H/D increased in ground corncob

fluidized beds, the overall average gas holdup increased slightly. On the other hand, for ground walnut shell filled beds, increasing H/D did not affect the overall average gas holdup at low superficial gas velocities, but as superficial gas velocity increased, there was an increase in the overall average gas holdup. Additionally, as H/D increased, the hydrodynamic-induced bed structures differed more in the denser material (glass beads) than the less dense materials (ground corncob and ground walnut shell). All materials showed regions of low gas holdup near the bed walls at higher superficial gas velocities, indicating bed material recirculation. Finally, a region of high gas holdup exists in the center of all beds due to large bubbles leaving the bed along the center axis of the bed.

Objective 6: Determine the material density effects on the time-average local gas holdup.

Conclusion 6: As material density decreased gas holdup increased. Glass beads had lower gas holdup than both ground walnut shell and ground corncob, while ground corncob exhibited the largest gas holdup of all three materials. The fluidization structure for the three materials was similar at H/D = 0.5, with regions of high gas holdup in the center and near the walls of the fluidized bed, and the bed surface was easily identified. At H/D = 1 and 1.5 glass beads and ground walnut shell showed similarities between their fluidization structures, including low gas holdup regions near the bed walls and high gas holdup regions in the bed center. Ground corncob, on the other hand, exhibited a better gas holdup distribution along the entire bed, providing a better and more uniform fluidization.

5.2 Recommendations

Future studies examining the same effects of bed material and bed height should be performed using a fluidized bed with a larger diameter to evaluate how fluidization and the hydrodynamics of the bed are influenced by the change in diameter; these results should be compared to those of this study. This comparison will help to identify scale-up issues.

Future experiments should be performed using material of different sizes and morphology to evaluate the fluidization and hydrodynamics dependency on the material properties. Comparing these new results to those of this study will help to identify unique fluidization characteristics of different materials, as well as, how the hydrodynamics change when material size changes. Thus, these future experiments will expand the work that has been done in this research.

The nuances of the CT system should also be further explored to understand intensity variations when the fluidized bed stand is moved vertically. This will improve reconstruction methods over larger axial regions.

References

Abdullah, M. Z., Husain, Z., and Yin Pong, S. L. (2003). "Analysis of cold flow fluidization test results for various biomass fuels." *Biomass and Bioenergy,* **24**(6): 487-494.

Boyer, C., Duquenne, A.-M., and Wild, G. (2002). "Measuring techniques in gas-liquid and gas-liquid-solid reactors." *Chemical Engineering Science,* **57**(16): 3185-3215.

Bridgwater, A. V., and Peacocke, G. V. C. (2000). "Fast pyrolysis processes for biomass." *Renewable and Sustainable Energy Reviews,* **4**(1): 1-73.

Brown, R. C. (2003). *Biorenewable resources: Engineering new products from agriculture*. Ames, IA, Iowa State Press.

Chaouki, J., Larachi, F., and Dudukovic, M. P. (1997). "Noninvasive tomographic and velocimetric monitoring of multiphase flows." *Industrial and Engineering Chemistry Research,* **36**(11): 4476-4503.

Cranfield, R. R., and Geldart, D. (1974). "Large particle fluidisation." *Chemical Engineering Science,* **29**(4): 935-947.

Crowe, C. T. (2006). *Multiphase flow handbook*. Boca Raton, FL, CRC Press.

Demirbas, A. (2007). "Combustion of biomass." *Energy Sources, Part A: Recovery, Utilization, and Environmental Effects,* **29**(6): 549 - 561.

Dos Santos, F. J., and Goldstein Jr, L. (2008). "Experimental aspects of biomass fuels in a bubbling fluidized bed combustor." *Chemical Engineering and Processing: Process Intensification,* **47**(9-10): 1541-1549.

Du, B., Warsito, W., and Fan, L.-S. (2003). "Bed nonhomogeneity in turbulent gas-solid fluidization." *AIChE Journal,* **49**(5): 1109-1126.

Franka, N. P. (2008). "Visualizing fluidized beds with x-rays". **MS Thesis**, *Department of Mechanical Engineering.* Iowa State University**,** Ames, IA.

Franka, N. P., and Heindel, T. J. (2009). "Local time-averaged gas holdup in a fluidized bed with side air injection using x-ray computed tomography." *Powder Technology,* **193**(1): 69-78.

Franka, N. P., Heindel, T. J., and Battaglia, F.(2007)."Visualizing cold-flow fluidized beds with x-rays". *ASME International Mechanical Engineering Congress and Exposition.* Seattle, Washington, ASME: IMECE2007-43073.

Geldart, D. (1973). "Types of gas fluidization." *Powder Technology,* **7**(5): 285-292.

Grassler, T., and Wirth, K. E. (2000). "X-ray computer tomography - potential and limitation for the measurement of local solids distribution in circulating fluidized beds." *Chemical Engineering Journal,* **77**(1): 65-72.

Gunn, D. J., and Hilal, N. (1997). "The expansion of gas-fluidised beds in bubbling fluidisation." *Chemical Engineering Science,* **52**(16): 2811-2822.

Hanping, C., Bin, L., Haiping, Y., Guolai, Y., and Shihong, Z. (2008). "Experimental investigation of biomass gasification in a fluidized bed reactor." *Energy & Fuels,* **22**(5): 3493-3498.

Heindel, T. J., Gray, J. N., and Jensen, T. C. (2008). "An x-ray system for visualizing fluid flows." *Flow Measurement and Instrumentation,* **19**(2): 67-78.

Hilal, N., Ghannam, M. T., and Anabtawi, M. Z. (2001). "Effect of bed diameter, distributor and inserts on minimum fluidization velocity." *Chemical Engineering and Technology,* **24**(2): 161-165.

Kantzas, A., Wright, I., and Kalogerakis, N. (1997). "Quantification of channelling in polyethylene resin fluid beds using x-ray computer assisted tomography (cat)." *Chemical Engineering Science,* **52**(13): 2023-2035.

Ketcham, R. A., and Carlson, W. D. (2001). "Acquisition, optimization and interpretation of x-ray computed tomographic imagery: Applications to the geosciences." *Computers & Geosciences,* **27**(4): 381-400.

Mena, P. C., Rocha, F. A., Teixeira, J. A., Sechet, P., and Cartellier, A. (2008). "Measurement of gas phase characteristics using a monofibre optical probe in a three-phase flow." *Chemical Engineering Science,* **63**(16): 4100-4115.

Mohan, D., Pittman, C. U., and Steele, P. H. (2006). "Pyrolysis of wood/biomass for bio-oil: A critical review." *Energy & Fuels,* **20**(3): 848-889.

Patel, A. K., Waje, S. S., Thorat, B. N., and Mujumdar, A. S. (2008). "Tomographic diagnosis of gas maldistribution in gas-solid fluidized beds." *Powder Technology,* **185**(3): 239-250.

Ramos, G., García Ruiz, M., Prieto Marqués, J. J., and Guardiola Soler, J. (2002). "Minimum fluidization velocities for gas-solid 2d beds." *Chemical Engineering and Processing,* **41**(9): 761-764.

Rao, T. R., and Bheemarasetti, J. V. R. (2001). "Minimum fluidization velocities of mixtures of biomass and sands." *Energy,* **26**(6): 633-644.

Sau, D. C., Mohanty, S., and Biswal, K. C. (2007). "Minimum fluidization velocities and maximum bed pressure drops for gas-solid tapered fluidized beds." *Chemical Engineering Journal,* **132**(1-3): 151-157.

Seeger, A., Kertzscher, U., Affeld, K., and Wellnhofer, E. (2003). "Measurement of the local velocity of the solid phase and the local solid hold-up in a three-phase flow by x-ray based particle tracking velocimetry (xptv)." *Chemical Engineering Science,* **58**(9): 1721-1729.

Si, C., and Guo, Q. (2008). "Fluidization characteristics of binary mixtures of biomass and quartz sand in an acoustic fluidized bed." *Industrial & Engineering Chemistry Research,* **47**(23): 9773-9782.

Yates, J. G., Cheesman, D. J., Lettieri, P., and Newton, D. (2002). "X-ray analysis of fluidized beds and other multiphase systems." *Kona,* **20**: 10.

Zhong, W., Chen, X., and Zhang, M. (2006). "Hydrodynamic characteristics of spout-fluid bed: Pressure drop and minimum spouting/spout-fluidizing velocity." *Chemical Engineering Journal,* **118**(1-2): 37-46.

Zhong, W., Jin, B., Zhang, Y., Wang, X., and Xiao, R. (2008). "Fluidization of biomass particles in a gas−solid fluidized bed." *Energy & Fuels,* **22**(6): 4170-4176.

Zhou, D., Dong, S., Wang, H., and Bi, H. T. (2008). "Minimum fluidization velocity of a three-phase conical fluidized bed in comparison to a cylindrical fluidized bed." *Industrial & Engineering Chemistry Research,* **48**(1): 27-36.

Zhu, H., Zhu, J., Li, G., and Li, F. (2008). "Detailed measurements of flow structure inside a dense gas-solids fluidized bed." *Powder Technology,* **180**(3): 339-349.